



3 4456 0276788 8

LACE TR-024
(ORNL/M-492)

ornl

**OAK RIDGE
NATIONAL
LABORATORY**

MARTIN MARIETTA

Summary of Posttest Aerosol Code-Comparison Results for LWR Aerosol Containment Experiment (LACE) LA3

A. L. Wright
P. C. Arwood

OAK RIDGE NATIONAL LABORATORY
CENTRAL RESEARCH LIBRARY
CIRCULATION SECTION
4500N ROOM 175
LIBRARY LOAN COPY
DO NOT TRANSFER TO ANOTHER PERSON
If you wish someone else to see this
report, send in name with report and
the library will arrange a loan.

OPERATED BY
MARTIN MARIETTA ENERGY SYSTEMS, INC.
FOR THE UNITED STATES
DEPARTMENT OF ENERGY

This report was prepared as an account of work sponsored by an agency of the United States Government. Neither the United States Government nor any agency thereof, nor any of their employees, makes any warranty, express or implied, or assumes any legal liability or responsibility for the accuracy, completeness, or usefulness of any information, apparatus, product, or process disclosed, or represents that its use would not infringe privately owned rights. Reference herein to any specific commercial product, process, or service by trade name, trademark, manufacturer, or otherwise, does not necessarily constitute or imply its endorsement, recommendation, or favoring by the United States Government or any agency thereof. The views and opinions of authors expressed herein do not necessarily state or reflect those of the United States Government or any agency thereof.

LACE TR-024
ORNL/M-492

Chemical Technology Division

SUMMARY OF POSTTEST AEROSOL CODE-COMPARISON RESULTS FOR
LWR AEROSOL CONTAINMENT EXPERIMENT (LACE) LA3

Principal Investigators

A. L. Wright
P. C. Arwood

Prepared for
ELECTRIC POWER RESEARCH INSTITUTE
3412 Hillview Avenue
Palo Alto, California 94303

EPRI Project No. 2135-18

Date Issued — June 1988

Prepared by the
OAK RIDGE NATIONAL LABORATORY
Oak Ridge, Tennessee 37831
operated by
MARTIN MARIETTA ENERGY SYSTEMS, INC.
for the
U.S. DEPARTMENT OF ENERGY
under contract DE-AC05-84OR21400



3 4456 0276788 8

NOTICE

This report was prepared by the organization(s) named below as an account of work sponsored by the Electric Power Research Institute, Inc. (EPRI). Neither EPRI, members of EPRI, the organization(s) named below, nor any person acting on behalf of any of them: (a) makes any warranty, express or implied, with respect to the use of any information, apparatus, method, or process disclosed in this report or that such use may not infringe privately owned rights; or (b) assumes any liabilities with respect to the use of, or for damages resulting from the use of, any information, apparatus, method or process disclosed in this report.

Prepared by

OAK RIDGE NATIONAL LABORATORY
Oak Ridge, Tennessee

[REDACTED]

[REDACTED]

1. The first part of the document discusses the importance of maintaining accurate records of all transactions.

2. It also emphasizes the need for regular audits to ensure the integrity of the financial data.

3. Finally, it highlights the role of transparency in building trust with stakeholders.

CONTENTS

	Page
ABSTRACT.....	vii
1. INTRODUCTION.....	1
2. SUMMARY OF CODE INPUTS AND REQUESTED CODE OUTPUTS FOR LA3 POSTTEST CALCULATIONS.....	2
3. PRESENTATION OF TEST AND CODE RESULTS FOR TEST LA3.....	14
4. DISCUSSION OF LA3 CODE-EXPERIMENT COMPARISON RESULTS.....	72
4.1 TEST LA3A	72
4.2 TEST LA3B	84
4.3 TEST LA3C	92
5. SUMMARY AND CONCLUSIONS	101
6. ACKNOWLEDGMENTS.....	109
7. REFERENCES.....	109
APPENDIX A: THE MODIFICATION OF THE TRAP MELT MASS MEDIAN DIAMETER CALCULATION.....	113

ABSTRACT

This report describes work performed as part of the LACE Code-Experiment Comparison Project, which is sponsored by the Electric Power Research Institute (EPRI Project No. 2135-18). The report presents and summarizes comparisons of test results and aerosol computer-code calculations for LACE LA3, which consists of three separate experiments denoted as LA3A, LA3B, and LA3C. All of the LACE tests were performed at the Westinghouse Hanford Engineering Development Laboratory (HEDL), which is operated by the Westinghouse Hanford Company for the U.S. Department of Energy (US/DOE). The LACE LA3 test series was performed to simulate "containment bypass" accident sequence conditions. In each test, measurements were made to characterize aerosol transport through a 0.063-m diameter, 28.8-m length steel pipe; variables in the experiments included the gas flow velocity through the pipe and the mass ratio of the cesium hydroxide (CsOH) and manganese oxide (MnO) aerosols input to the pipe. Results from calculations performed for each of the three experiments are presented and discussed in the report.

SUMMARY OF POSTTEST AEROSOL CODE-COMPARISON RESULTS FOR
LWR AEROSOL CONTAINMENT EXPERIMENT (LACE) LA3

A. L. Wright
P. C. Arwood

1. INTRODUCTION

The Light-Water Reactor (LWR) Aerosol Containment Experiments (LACE) have been performed to investigate, at large scale, the aerosol retention behavior in reactor coolant system piping and in containment under simulated severe LWR accident conditions. An additional, and equally important, objective of these tests is to provide a data base for validating aerosol behavior computer codes and related thermal-hydraulic computer codes. The LACE test project is internationally funded and has been performed at the Hanford Engineering Development Laboratory (HEDL) - operated by the Westinghouse Hanford Company - under the leadership of an overall project board and the Electric Power Research Institute (EPRI).

The overall LACE project has two components: (1) the experiments being performed at HEDL and (2) aerosol-transport and thermal-hydraulic code-comparison activities. The aerosol-transport code-comparison activities are being coordinated at the Oak Ridge National Laboratory, while the thermal-hydraulic code-comparison activities are being coordinated at Intermountain Technologies, Inc. (ITI) in Idaho Falls, Idaho. For each of the six LACE tests, pretest and posttest aerosol code calculations are being performed. The ORNL code-comparison activities include (1) providing guidance to participating aerosol code analysts to help them in performing calculations, (2) compiling the results from calculations, and (3) critically evaluating the code results and comparisons against the test data.

This report summarizes the results from the posttest calculations performed for test series LA3, which consisted of three experiments denoted as LA3A, LA3B, and LA3C. The LA3 test series was designed to simulate LWR "containment bypass" (V-sequence) accident conditions. The calculations were "blind" in that the code analysts did not have access

to the LA3 results when they performed their calculations. As defined in the LA3 test plan,¹ these three experiments addressed aerosol behavior during flow through an 0.063-m diameter, 28.8-m length pipe for simulated "containment bypass" accident sequence conditions. The tests were performed for varied flow velocities through the test pipe and for varied MnO/CsOH aerosol source mass ratios.

The next section (Section 2) of this report presents an overall description of the LACE LA3 test series. The section then summarizes the defined code inputs and requested code outputs for the LA3 posttest calculations. Section 3 of the report presents the test results and the results from the code calculations. Section 4 then presents an evaluation of the test and code-comparison results for each of the three LA3 tests. Finally, a summary of the results and insights gained from the LA3 post-test code-experiment comparisons is presented in the final section of the report.

2. SUMMARY OF CODE INPUTS AND REQUESTED CODE OUTPUTS FOR LA3 POSTTEST CALCULATIONS

Figure 1 illustrates the experimental set-up for the LA3 tests; additional details are presented in the LA3 test plan.¹ CsOH and MnO aerosols were injected into a 0.063-m-diam, 28.8-m-long test pipe which had six 90° bends. The aerosol injection period for each test was 60 min, and during that time period, airborne aerosol concentration and size measurements were made upstream and downstream of the 28.8-m long, constant-diameter section of the test pipe.

The major test parameters in the LA3 test series were (1) the gas flow velocity through the test pipe and (2) the MnO/CsOH aerosol mass ratio input to the test pipe. The approximate values of these parameters for the LA3 tests were:²

<u>Experiment</u>	<u>v(m/s)</u>	<u>MnO/CsOH mass ratio</u>
LA3A	77	5.0
LA3B	25	7.5
LA3C	24	1.4

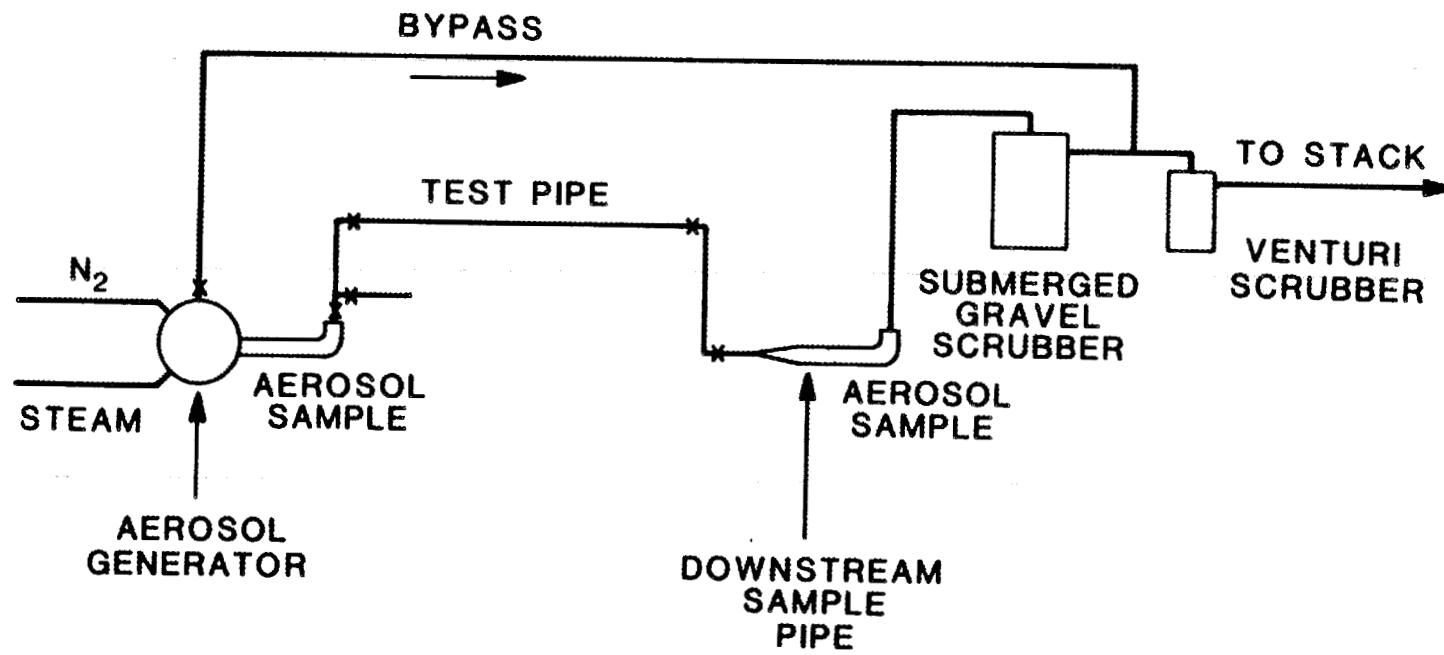


Fig. 1. LA3 experimental arrangement (Source: HEDL 8704-063.1).

As a point of reference, for test LA1 flow velocities varied from 100 m/s at the pipe inlet to 200 at the outlet, and the MnO/CsOH ratio was equal to 1.35 (based on mass balance data, as the LA3 values are). Note that the LA1 and LA3 velocities are higher than those expected in V-sequence accident conditions.

Two letters describing aerosol code inputs for the LA3 posttest calculations were sent to LACE program participants. The first letter³ provided the initial set of instructions for the LA3 calculations. The second letter⁴ provided corrected data for the aerosol source to the test pipe for each experiment. Table 1 describes the sources of data for use in the LA3 posttest calculations. Much of the data for these calculations was contained on IBM floppy disks - in the form of text files named LA3TH10.TXT, LA3TH10.DAT, LA3TH11.DAT, and LA3TH12.DAT - that were transmitted to the project participants.

Table 2 summarizes the test-pipe geometry for the LA3 series. Calculations were performed to model pipe sections 4 through 21 - the 28.8 m length of pipe with a constant diameter of 0.063 m. Note that there were six 90° bends in the portion of the test pipe that was modeled.

Aerosol source rate and size data for the LA3 calculations are presented in Tables 3-8. Aerosol analysts had their choice of using (1) time-averaged or (2) time-dependent aerosol source information for their calculations; this was an improvement over the situation for the previous LA1 calculations. Measurements of aerosol source rates and sizes were made at sampling station T5 which is located in the bend in pipe section 1b (see Table 2). However, significant aerosol deposition did occur in pipe sections 2 and 3; therefore, the measured aerosol sizes do not truly represent those that enter section 4 of the pipe (unfortunately, we cannot estimate the error in calculated aerosol deposition for the LA3 tests associated with the uncertainty in aerosol source sizes).

Table 9 presents a summary of the gas flow-rate data sources for the LA3 calculations. We see that for the LA3 tests gas flows through the test pipe were a sum of steam, nitrogen, helium, and argon flows. However, all aerosol transport codes do not include the capability to

Table 1. Summary of information needed for LA3
blind posttest pipe calculations

CODE INPUT DATA	WHERE INFORMATION FOUND ^a
1. Test pipe geometry, layout:	Tables 1,2 in LA3TH10.TXT and Table 2 in this report. Only pipe sections 4-21 to be used in calculations.
2. Aerosol source parameters:	Tables 3-5 in LA3TH10.TXT and Tables 3-8 in this report.
3. Aerosol agglomerate density and shape factors:	To be specified by code user. LA3A THEORETICAL SOLID DENSITY, based on source mass ratios = 4.9 g/cm ³ . LA3B THEORETICAL SOLID DENSITY, based on source mass ratios = 5.2 g/cm ³ . LA3C THEORETICAL SOLID DENSITY, based on source mass ratios = 4.5 g/cm ³ .
4. Test pipe temperatures:	LA3A: Table A.3, A.4 in LA3TH10.DAT. LA3B: Table B.3, B.4 in LA3TH11.DAT. LA3C: Table C.3, C.4 in LA3TH12.DAT. Locations of thermocouples in test pipe presented in Table 7 in LA3TH10.TXT.
5. Test pipe pressures:	LA3A: Table A.2 in LA3TH10.DAT. LA3B: Table B.2 in LA3TH11.DAT. LA3C: Table C.2 in LA3TH12.DAT. Locations of pressure gauges in test pipe presented in Table 7 in LA3TH10.TXT.
6. Test pipe flow rates:	LA3A: Table A.1 in LA3TH10.DAT and Section G in LA3TH10.TXT; also summarized in Table 9 of this report. LA3B: Table B.1 in LA3TH11.DAT and Section G in LA3TH10.TXT; also summarized in Table 9 of this report. LA3C: Table C.1 in LA3TH12.DAT and Section G in LA3TH10.TXT; also summarized in Table 9 of this report.

^aRefers to tables on IBM-format floppy disks supplied by HEDL staff.

Table 2. LA3 test pipe geometry^a

Section No.	Pipe Description	Flow Direction	Diameter (cm)	Length (m)
1a	Straight ^b	East	30	1.52
1b	90° Bend	_____	30	0.72
1c	Reducer	Up	30-10	0.28
2	Ball Valve	Up	10	0.23
3	Reducer	Up	10-6.3	0.28
4	Straight ^c	Up	6.3	2.26
5	90° Bend ^d	_____	6.3	0.38
6	Ball Valve	West	6.3	0.19
7	Straight	West	6.3	4.20
8	90° Bend ^d	_____	6.3	0.38
9	Straight	South	6.3	2.58
10	Straight	South	6.3	4.32
11	90° Bend ^d	_____	6.3	0.38
12	Straight	East	6.3	4.32
13	Straight	East	6.3	3.17
14	90° Bend ^d	_____	6.3	0.38
15	Straight	North	6.3	1.84
16	Ball Valve	North	6.3	0.19
17	90° Bend ^d	_____	6.3	0.38
18	Straight ^c	Down	6.3	2.15
19	90° Bend ^c	_____	6.3	0.38
20	Ball Valve	West	6.3	0.19
21	Straight	West	6.3	1.09
22	Transition	West	6.3-30	1.17
23 ^a	Straight ^b	West	30	1.95
23 ^b	90° Bend	Up	30	0.58

^aFor LA3 posttest calculations, ONLY Sections 4 through 21 were modeled. The overall length of Sections 4-21 is 28.78 m.

^bAerosol samples taken at downstream end of each 30-cm pipe section.

^cWall scoops located at downstream ends of vertical pipe sections.

^dRadius of pipe bends in 6.3-cm pipe is 95 mm.

Table 3. Aerosol source rate data for test LA3A^a

Time (min)	CsOH source rate (g/s)	MnO source rate (g/s)	Total source rate (g/s)
0 ^b	0.105	0.774	0.879
1.3	0.105	0.774	0.879
4.3	0.080	0.702	0.783
10.3	0.078	0.614	0.691
19.3	0.108	0.096	0.204
26.3	0.108	0.132	0.240
29.3	0.136	0.093	0.229
32.3	0.097	1.051	1.147
35.5	0.101	0.882	0.982
41.7	0.097	0.807	0.904
44.3	0.101	0.680	0.781
47.3	0.083	0.594	0.677
50.3	0.108	0.439	0.547
56.3	0.101	0.239	0.340
59.3	0.103	0.127	0.230
60 ^b	0.103	0.127	0.230

CsOH average source rate from mass balance = 0.0992 g/s
MnO average source rate from mass balance = 0.4933 g/s
Total average source rate from mass balance = 0.5925 g/s

Duration of aerosol source = 0 to 60 min

^aAerosol source rate vs time values presented above obtained by normalizing measured source rate data so that the integrated average source rate equals the average source rate determined from the mass balance data.

^bSource rate values at 0 and 60 min assumed the same as the values at the nearest measurement times.

Table 4. Aerosol source rate data for test LA3B^a

Time (min)	CsOH source rate (g/s)	MnO source rate (g/s)	Total source rate (g/s)
0 ^b	0.275	0.979	1.254
1.3	0.275	0.979	1.254
4.3	0.110	0.985	1.094
10.2	0.068	0.934	1.003
19.2	0.132	0.254	0.386
26.3	0.091	0.716	0.807
29.2	0.102	0.677	0.779
32.2	0.084	0.662	0.746
35.2	0.089	0.565	0.654
41.4	0.068	0.749	0.817
44.3	0.077	0.785	0.862
50.2	0.072	0.925	0.997
56.3	0.079	0.976	1.055
59.2	0.077	0.933	1.010
60 ^b	0.077	0.933	1.010

CsOH average source rate from mass balance = 0.0975 g/s

MnO average source rate from mass balance = 0.7533 g/s

Total average source rate from mass balance = 0.8508 g/s

Duration of aerosol source = 0 to 60 min

^aAerosol source rate vs time values presented above obtained by normalizing measured source rate data so that the integrated average source rate equals the average source rate determined from the mass balance data.

^bSource rate values at 0 and 60 min assumed the same as the values at the nearest measurement times.

Table 5. Aerosol source rate data for test LA3C^a

Time (min)	CsOH source rate (g/s)	MnO source rate (g/s)	Total source rate (g/s)
0 ^b	0.187	0.349	0.536
1.3	0.187	0.349	0.536
4.3	0.175	0.347	0.522
10.5	0.254	0.425	0.679
19.1	0.314	0.384	0.698
26.2	0.310	0.266	0.577
29.3	0.324	0.062	0.386
32.0	0.291	0.315	0.607
35.2	0.323	0.464	0.787
41.2	0.311	0.495	0.807
44.2	0.282	0.434	0.716
50.2	0.267	0.434	0.701
56.2	0.205	0.468	0.673
59.2	0.268	0.433	0.701
60 ^b	0.268	0.433	0.701

CsOH average source rate from mass balance = 0.2726 g/s

MnO average source rate from mass balance = 0.3870 g/s

Total average source rate from mass balance = 0.6596 g/s

Duration of aerosol source = 0 to 60 min

^aAerosol source rate vs time values presented above obtained by normalizing measured source rate data so that the integrated average source rate equals the average source rate determined from the mass balance data.

^bSource rate values at 0 and 60 min assumed the same as the values at the nearest measurement times.

Table 6. Aerosol source size-distribution data for test LA3A

Time (min)	CsOH AMMD (μm)	CsOH standard deviation	CsOH d_{50} (μm)	CsOH d_g (μm)	MnO AMMD (μm)	MnO standard deviation	MnO d_{50} (μm)	MnO d_g (μm)	Mixed AMMD (μm)	Mixed standard deviation	Mixed d_{50} (μm)	Mixed d_g (μm)
Using solid material-density values ^a :												
7.25	3.00	3.33	1.564	0.020	0.90	2.09	0.386	0.076	1.20	2.25	0.542	0.075
23.25	1.30	1.62	0.678	0.337	0.62	2.11	0.266	0.050	0.92	1.85	0.416	0.134
39.75	1.91	1.97	0.996	0.251	2.62	1.83	1.123	0.376	2.50	1.84	1.129	0.370
53.25	1.30	1.67	0.678	0.308	0.56	2.32	0.240	0.029	0.87	1.95	0.393	0.103
Mean	1.88	2.15	0.980	0.169	1.18	2.09	0.506	0.099	1.37	1.97	0.619	0.156
Using one-half of solid material-density values ^a :												
7.25	3.00	3.33	2.212	0.029	0.90	2.09	0.546	0.107	1.20	2.25	0.767	0.107
23.25	1.30	1.62	0.958	0.477	0.62	2.11	0.376	0.071	0.92	1.85	0.588	0.189
39.75	1.91	1.97	1.408	0.355	2.62	1.83	1.589	0.531	2.50	1.84	1.597	0.524
53.25	1.30	1.67	0.958	0.435	0.56	0.43	0.340	0.040	0.87	1.95	0.556	0.146
Mean	1.88	2.15	1.386	0.239	1.18	1.62	0.715	0.356	1.37	1.97	0.875	0.220

^aThe published CsOH solid density is 3.68 g/cm³; the published MnO solid density is 5.44 g/cm³. Based on the average aerosol source rates presented in Table 3, the mixture solid density is 4.9 g/cm³. In the table above, the mass-median diameter is d_{50} ; and the geometric mean diameter, d_g , was calculated using the formula: $\ln(d_g) = \ln(d_{50}) - 3 \cdot [\ln(\sigma_g)]^2$, where σ_g is the geometric standard deviation.

Table 7. Aerosol source size-distribution data for test LA3B

Time (min)	CsOH AMMD (μm)	CsOH standard deviation	CsOH d_{50} (μm)	CsOH d_g (μm)	MnO AMMD (μm)	MnO standard deviation	MnO d_{50} (μm)	MnO d_g (μm)	Mixed AMMD (μm)	Mixed standard deviation	Mixed d_{50} (μm)	Mixed d_g (μm)
Using solid material-density values ^a :												
7.25	2.81	1.78	1.465	0.540	2.64	1.82	1.132	0.386	2.66	1.81	1.166	0.406
23.25	2.41	1.79	1.256	0.454	2.63	1.86	1.128	0.355	2.28	1.89	1.000	0.296
38.25	2.50	1.82	1.303	0.444	2.19	1.90	0.939	0.273	2.23	1.88	0.978	0.296
53.25	2.50	2.48	1.303	0.110	2.50	2.48	1.072	0.090	2.50	2.48	1.096	0.092
Mean	2.56	1.97	1.334	0.336	2.39	2.02	1.025	0.233	2.42	2.01	1.061	0.246
Using one-half of solid material-density values ^a :												
7.25	2.81	1.78	2.072	0.764	2.64	1.82	1.601	0.546	2.66	1.81	1.650	0.574
23.25	2.41	1.79	1.777	0.643	2.63	1.86	1.595	0.502	2.28	1.89	1.414	0.419
38.25	2.50	1.82	1.843	0.629	2.19	1.90	1.328	0.386	2.23	1.88	1.383	0.418
53.25	2.50	2.48	1.843	0.155	2.50	2.48	1.516	0.128	2.50	2.48	1.550	0.131
Mean	2.56	1.97	1.887	0.475	2.39	2.02	1.449	0.329	2.42	2.01	1.501	0.348

^aThe published CsOH solid density is 3.68 g/cm³; the published MnO solid density is 5.44 g/cm³. Based on the average aerosol source rates presented in Table 3, the mixture solid density is 5.2 g/cm³. In the table above, the mass-median diameter is d_{50} ; and the geometric mean diameter, d_g was formulated using the formula: $\ln(d_g) = \ln(d_{50}) - 3 \cdot [\ln(\sigma_g)]^2$, where σ_g is the geometric standard deviation.

Table 8. Aerosol source size-distribution data for test LA3C

Time (min)	CsOH AMMD (μm)	CsOH standard deviation	CsOH d_{50} (μm)	CsOH d_g (μm)	MnO AMMD (μm)	MnO standard deviation	MnO d_{50} (μm)	MnO d_g (μm)	Mixed AMMD (μm)	Mixed standard deviation	Mixed d_{50} (μm)	Mixed d_g (μm)
Using solid material-density values ^a :												
7.04	2.17	2.17	1.131	0.187	1.76	2.44	0.755	0.069	1.85	2.32	0.872	0.104
23.18	1.92	2.06	1.001	0.209	1.37	2.55	0.587	0.042	1.70	2.20	0.801	0.124
38.04	2.38	1.80	1.241	0.440	1.83	2.00	0.785	0.186	2.10	1.91	0.990	0.282
53.06	2.30	1.78	1.199	0.442	1.71	2.23	0.733	0.106	1.95	2.08	0.919	0.184
Mean	2.19	1.95	1.142	0.300	1.67	2.30	0.716	0.089	1.90	2.13	0.896	0.161
Using one-half of solid material-density values ^a :												
7.04	2.17	2.17	1.600	0.264	1.76	2.44	1.067	0.098	1.85	2.32	1.233	0.147
23.18	1.92	2.06	1.415	0.295	1.37	2.55	0.831	0.060	1.70	2.20	1.133	0.176
38.04	2.38	1.80	1.755	0.622	1.83	2.00	1.110	0.263	2.10	1.91	1.400	0.399
53.06	2.30	1.78	1.696	0.625	1.71	2.23	1.037	0.151	1.95	2.08	1.300	0.260
Mean	2.19	1.95	1.614	0.424	1.67	2.30	1.013	0.126	1.90	2.13	1.267	0.228

^aThe published CsOH solid density is 3.68 g/cm³; the published MnO solid density is 5.44 g/cm³. Based on the average aerosol source rates presented in Table 3, the mixture solid density is 4.5 g/cm³. In the table above, the mass-median diameter is d_{50} ; and the geometric mean diameter, d_g , was calculated using the formula: $\ln(d_g) = \ln(d_{50}) - 3 \cdot [\ln(\sigma_g)]^2$, where σ_g is the geometric standard deviation.

Table 9. Summary of LA3 gas flow-rate data

Gas flow	Experiment		
	<u>LA3A</u>	<u>LA3B</u>	<u>LA3C</u>
Steam and nitrogen	Table A.1, LA3TH10.DAT	Table B.1, LA3TH11.DAT	Table C.1, LA3TH12.DAT
Cesium system nitrogen	0.0030 kg/s	0.0024 kg/s	0.0024 kg/s
Helium	0.0006 kg/s	0.0006 kg/s	0.0006 kg/s
Argon	0.0008 kg/s	0.0008 kg/s	0.0008 kg/s

calculate the properties of the gas mixtures used in the LA3 tests (the United Kingdom and Italian TRAP-MELT2 versions do include this capability).

Finally, Table 10 summarizes the requested code output parameters for the LA3 blind calculations. Note that, as for the LA1 calculations, the code analysts were requested to provide information for each "control volume" modeled in their calculations, and also that they were free to choose how they wanted to nodalize the test pipe. We asked each analyst to provide information on the amount of calculated deposition and the deposition velocities for each important deposition mechanism in their calculations. As shown in Table 9, we requested code output data for four times. However, since the actual deposition data could only be obtained by a posttest mass balance, for the most part we only used the data provided for $t=3,600$ s.

3. PRESENTATION OF TEST AND CODE RESULTS FOR TEST LA3

The LA3 blind posttest pipe calculations were performed by eight investigators. The codes used and the affiliations of the code analysts are listed in Table 11. Five "TRAP-MELT" calculations were performed including (1) three TRAP-MELT2 calculations (the UK and IT versions of TRAP-MELT2 have enhanced capabilities over the reference version), (2) one calculation with the MCT-2 code (which includes TRAP-MELT2 as a module), and (3) one calculation using TRAP-MELT2.2, an updated version of the original TRAP-MELT2 code. The AEROSIM-M code is actually a containment aerosol transport code; but, as it was applied in LA1 calculations and in LA3 pretest calculations, it was used in a "Lagrangian" mode (following an aerosol/gas packet moving down the pipe) for the LA3 post test calculations. The RAFT code, which was developed at Argonne National Laboratories, was developed to predict the formation and transport of fission-product aerosols in LWR reactor coolant systems; this was the first time that it was applied to predict LACE results. The HAA4 code was the only log-normal code used for the LA3 calculations (all other codes were discrete particle-size distribution codes). HAA4 was originally a containment aerosol transport code. However, it was modified so that it could be used to calculate the length-wise variation of aerosol deposition in pipes, under the assumption that no aerosol

Table 10. Summary of requested code output parameters for
LA3 blind posttest calculations

OUTPUT TIMES (s): 600, 1200, 2400, 3600

OUTPUT PARAMETERS AND UNITS:

A. FOR EACH PIPE CONTROL VOLUME^a, AT EACH OUTPUT TIME:

1. Aerosol mass deposited in EACH control volume - for MIXED aerosol and for EACH species - in grams. PLEASE PROVIDE THIS FOR EACH DEPOSITION MECHANISM THAT WAS IMPORTANT - turbulent deposition, deposition in bends, settling, thermophoresis, etc.
2. Calculated deposition velocities for turbulent deposition, deposition in bends, deposition by settling, and thermophoretic deposition - in EACH control volume - in cm/s.
3. Airborne aerosol size in EACH control volume - for MIXED aerosol and for EACH species (if possible): provide the aerodynamic mass-median diameter - in μm - and the geometric standard deviation - dimensionless.

B. AT THE PIPE OUTLET, FOR EACH OUTPUT TIME:

1. Cumulative aerosol mass - for MIXED aerosol and for EACH species - transported out of the test pipe.
 2. Airborne aerosol size transported out of the test pipe - for MIXED aerosol and for EACH species (if possible): provide the aerodynamic mass-median diameter - in μm - and the geometric standard deviation - dimensionless.
-

^aCode analysts were to determine, based on their own judgement, the number of control volumes needed to model the test pipe for each calculation. We asked, however, that they provide us with the requested information for EACH of the assumed control volumes.

Table 11. Summary of codes used for LA3 calculations

Code ^a	Code analyst	Affiliation
AEROSIM-M (UK)	M. Kissane	United Kingdom, Atomic Energy Authority, Safety and Reliability Directorate
HAA4 (RI)	E. Vaughan	United States, Rockwell International
MCT-2 (NYPA)	P. Bieniarz	United States, New York Power Authority, Risk Management Associates
RAFT (FN)	J. Jokiniemi	Finland, Technical Research Centre
TRAP-MELT2 (IT)	F. Parozzi	Italy, ENEL-Thermal and Nuclear Research Centre
TRAP-MELT2 (JN)	H. Tateoka	Japan, Atomic Energy Research Institute
TRAP-MELT2 (UK) ^b	D. Williams	United Kingdom, Atomic Energy Authority, AEE Winfrith
TRAP-MELT2.2 (BCL)	V. Kogan	United States, Battelle Columbus Laboratories

^aInitials in parentheses indicate country or organization.

^bTwo sets of calculations were performed: one with time-averaged aerosol source size and one with time-dependent aerosol source size. Most of the results presented in this report are for the case with time-averaged source size.

agglomeration occurred as aerosol moved through the pipe. Finally, it should be noted that the AEROSIM-M, HAA4, RAFT, and TRAP-MELT2.2 codes included models for aerosol deposition in pipe bends. More will be discussed about these models later.

For each of the three LA3 tests, the HEDL staff measured (1) the masses of CsOH and MnO aerosol deposited in each section of the pipe, (2) the amounts of each aerosol transported out of the pipe, and (3) the airborne aerosol size distribution at the pipe inlet and pipe outlet as a function of time. The measured aerosol deposition and transport data for each aerosol species and for the total is presented in Tables 12 through 14. Tables 15 through 17 present the measured pipe inlet and outlet aerosol size distribution data.

The code-comparison results from each of the three tests will be discussed separately in the next section of the report. Figures 2 through 15 and Tables 18 and 19 present results for test LA3A. Figures 16 through 29 and Tables 20 and 21 present results for test LA3B, and Figs. 30 through 43 and Tables 22 and 23 present results for test LA3C.

For each test, the data in the figures consist of the following:

1. Six figures containing comparisons of measured and calculated CsOH, MnO, and total aerosol deposition profiles, and a table with comparisons of measured and calculated overall aerosol deposition in the pipe;
2. three figures containing comparisons (in the form of bar charts) of measured and calculated aerosol deposition in bends for CsOH, MnO, and the total aerosol;
3. a bar chart and a table with comparisons of measured and calculated aerosol transport out of the pipe; and
4. four figures with calculated profiles of the AMMD and GSD as a function of distance from the pipe inlet (pipe section 4).

Table 12. Summary of measured aerosol deposition and aerosol transport data for LACE LA3A

Pipe Section	CsOH Deposited (g)	MnO Deposited (g)	CsOH+MnO Deposited (g)
4	47.33	193.43	240.76
5 ^a	60.00	184.83	244.83
6	8.06	41.55	49.61
7	31.01	141.85	172.86
8 ^a	37.25	163.34	200.59
9	16.18	80.24	96.42
10	14.02	63.76	77.78
11 ^a	14.21	83.82	98.03
12	13.34	65.19	78.53
13	7.06	37.25	44.31
14 ^a	6.67	42.27	48.94
15	2.93	14.33	17.26
16	0.67	3.58	4.25
17 ^a	4.75	27.94	32.69
18	3.50	15.76	19.26
19 ^a	4.51	30.81	35.32
20	1.63	8.60	10.23
21	1.44	5.01	6.45
Total:	<u>274.56</u>	<u>1203.56</u>	<u>1478.12</u>
Deposited in joints:	14.88	78.80	93.68
Miscellaneous deposition:	3.36	64.48	67.84
Total deposition:	292.8	1346.84	1639.64
Aerosol transport out of pipe:	64.42	424.11	488.53
Total aerosol recovered:	357.22	1770.95	2128.17

^aPipe bend.

Table 13. Summary of measured aerosol deposition and transport data for LACE LA3B

Pipe Section	CsOH Deposited (g)	MnO Deposited (g)	CsOH+MnO Deposited (g)
4	4.74	14.04	18.78
5 ^a	35.19	265.19	300.38
6	2.23	13.30	15.53
7	4.16	9.60	13.76
8 ^a	24.88	195.76	220.64
9	1.74	2.95	4.69
10	3.05	9.60	12.65
11 ^a	25.85	200.19	226.04
12	2.42	5.91	8.33
13	2.03	7.39	9.42
14 ^a	22.46	186.15	208.61
15	1.11	3.69	4.80
16	0.44	2.95	3.39
17 ^a	15.39	125.58	140.97
18	2.08	12.56	14.64
19 ^a	14.23	113.02	127.25
20	1.26	9.60	10.86
21	0.48	1.48	1.96
Total:	<u>163.74</u>	<u>1178.96</u>	<u>1342.70</u>
Deposited in joints:	13.55	73.87	87.42
Miscellaneous deposition:	12.10	110.81	122.91
Total deposition:	189.39	1363.64	1553.03
Aerosol transport out of pipe:	152.99	1355.51	1508.50
Total aerosol recovered:	342.38	2719.15	3061.53

^aPipe bend.

Table 14. Summary of measured aerosol deposition
and aerosol transport data for LACE LA3C

Pipe Section	CsOH Deposited (g)	MnO Deposited (g)	CsOH+MnO Deposited (g)
4	334.26	343.68	677.94
5 ^a	148.81	216.52	365.33
6	27.48	49.26	76.74
7	37.88	24.06	61.94
8 ^a	39.37	72.17	111.54
9	10.15	9.74	19.89
10	35.16	44.68	79.84
11 ^a	29.22	58.43	87.65
12	5.94	6.87	12.81
13	2.48	2.86	5.34
14 ^a	14.11	34.37	48.48
15	3.96	5.73	9.69
16	1.49	3.44	4.93
17 ^a	10.40	26.35	36.75
18	4.95	7.45	12.40
19 ^a	10.65	25.20	35.85
20	7.18	12.60	19.78
21	1.24	1.72	2.96
Total:	<u>724.73</u>	<u>945.13</u>	<u>1669.86</u>
Deposited in joints:	30.70	73.22	103.92
Miscellaneous deposition:	32.19	68.74	100.93
Total deposition:	787.62	1087.09	1874.71
Aerosol transport out of pipe:	194.62	310.46	505.08
Total aerosol recovered:	982.24	1397.55	2379.79

^aPipe bend.

Table 15. Summary of measured test pipe inlet and outlet AMMD and GSD data for test LA3A

Measurement time (min)	Inlet AMMD (μm)	Outlet AMMD (μm)	Inlet GSD	Outlet GSD
<u>CsOH Aerosol:</u>				
7.25	3.00	1.42	3.33	2.64
23.25	1.30	0.97	1.62	3.64
39.75	1.91	0.89	1.97	4.08
53.25	<u>1.30</u>	<u>1.86</u>	<u>1.67</u>	<u>2.45</u>
Mean:	1.88	1.28	2.15	3.16
<u>MnO Aerosol:</u>				
7.25	0.90	1.38	2.09	2.17
23.25	0.62	0.78	2.11	3.72
39.75	2.62	1.00	1.83	3.00
53.25	<u>0.56</u>	<u>1.07</u>	<u>2.32</u>	<u>3.36</u>
Mean:	1.18	1.06	2.09	3.06
<u>Mixed Aerosol:</u>				
7.25	1.20	1.40	2.25	2.21
23.25	0.92	0.79	1.85	4.05
39.75	2.50	1.02	1.84	2.70
53.25	<u>0.87</u>	<u>1.00</u>	<u>1.95</u>	<u>3.60</u>
Mean:	1.37	1.05	1.97	3.14

Table 16. Summary of measured test pipe inlet and outlet AMMD and GSD data for test LA3B

Measurement time (min)	Inlet AMMD (μm)	Outlet AMMD (μm)	Inlet GSD	Outlet GSD
<u>CsOH Aerosol:</u>				
7.25	2.81	1.76	1.78	1.70
23.25	2.41	2.05	1.79	1.85
38.25	2.50	1.70	1.82	1.83
53.25	<u>2.50</u>	<u>2.10</u>	<u>2.48</u>	<u>1.95</u>
Mean:	2.56	1.90	1.97	1.83
<u>MnO Aerosol:</u>				
7.25	2.64	1.61	1.82	1.77
23.25	2.63	1.81	1.86	1.88
38.25	2.19	1.50	1.90	1.84
53.25	<u>2.50</u>	<u>1.96</u>	<u>2.48</u>	<u>1.84</u>
Mean:	2.39	1.72	2.02	1.83
<u>Mixed Aerosol:</u>				
7.25	2.66	1.65	1.81	1.74
23.25	2.28	1.80	1.89	1.81
38.25	2.23	1.54	1.88	1.77
53.25	<u>2.50</u>	<u>2.08</u>	<u>2.48</u>	<u>1.97</u>
Mean:	2.42	1.77	2.01	1.82

Table 17. Summary of measured test pipe inlet and outlet AMMD and GSD data for test LA3C

Measurement time (min)	Inlet AMMD (μm)	Outlet AMMD (μm)	Inlet GSD	Outlet GSD
<u>CsOH Aerosol:</u>				
7.04	2.17	0.70	2.17	2.00
23.15 ^a	1.92	1.00	2.06	1.70
38.04	2.38	0.47	1.80	1.87
53.06	<u>2.30</u>	<u>0.40</u>	<u>1.78</u>	<u>2.30</u>
Mean:	2.19	0.64	1.95	1.97
<u>MnO Aerosol:</u>				
7.04	1.76	0.65	2.44	1.89
23.15 ^a	1.37	1.00	2.55	1.70
38.04	1.83	0.41	2.00	1.93
53.06	<u>1.71</u>	<u>0.43</u>	<u>2.23</u>	<u>1.91</u>
Mean:	1.67	0.62	2.30	1.86
<u>Mixed Aerosol:</u>				
7.04	1.85	0.65	2.32	1.83
23.15 ^a	1.70	1.02	2.20	1.48
38.04	2.10	0.43	1.91	1.93
53.06	<u>1.95</u>	<u>0.46</u>	<u>2.08</u>	<u>1.85</u>
Mean:	1.90	0.64	2.13	1.77

^aAverage of inlet sampling time of 23.13 min and outlet sampling time of 23.18 min.

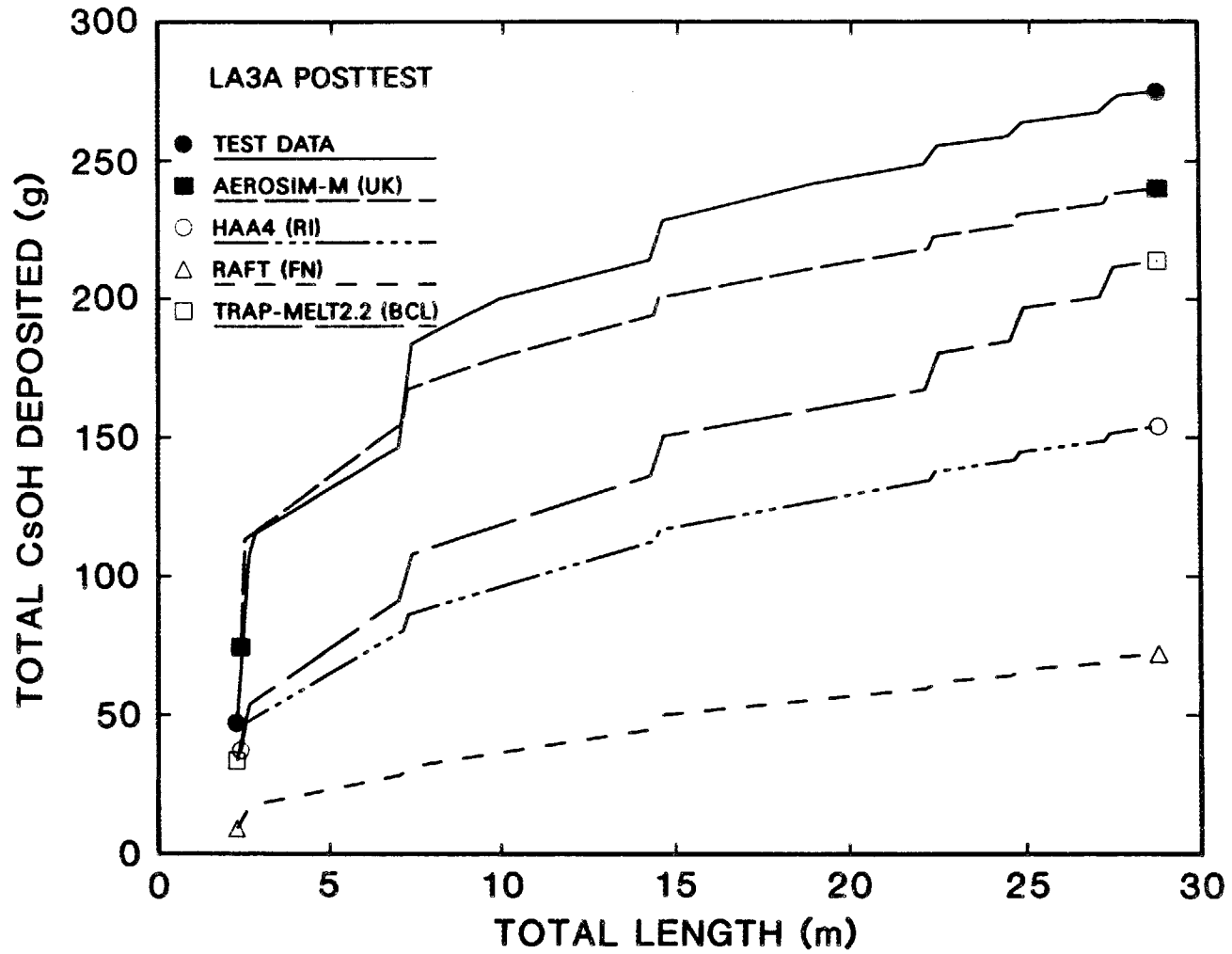


Fig. 2. LA3A posttest results: CsOH aerosol deposited in pipe vs distance from pipe inlet at end of test (3,600 s), for codes including bend deposition models.

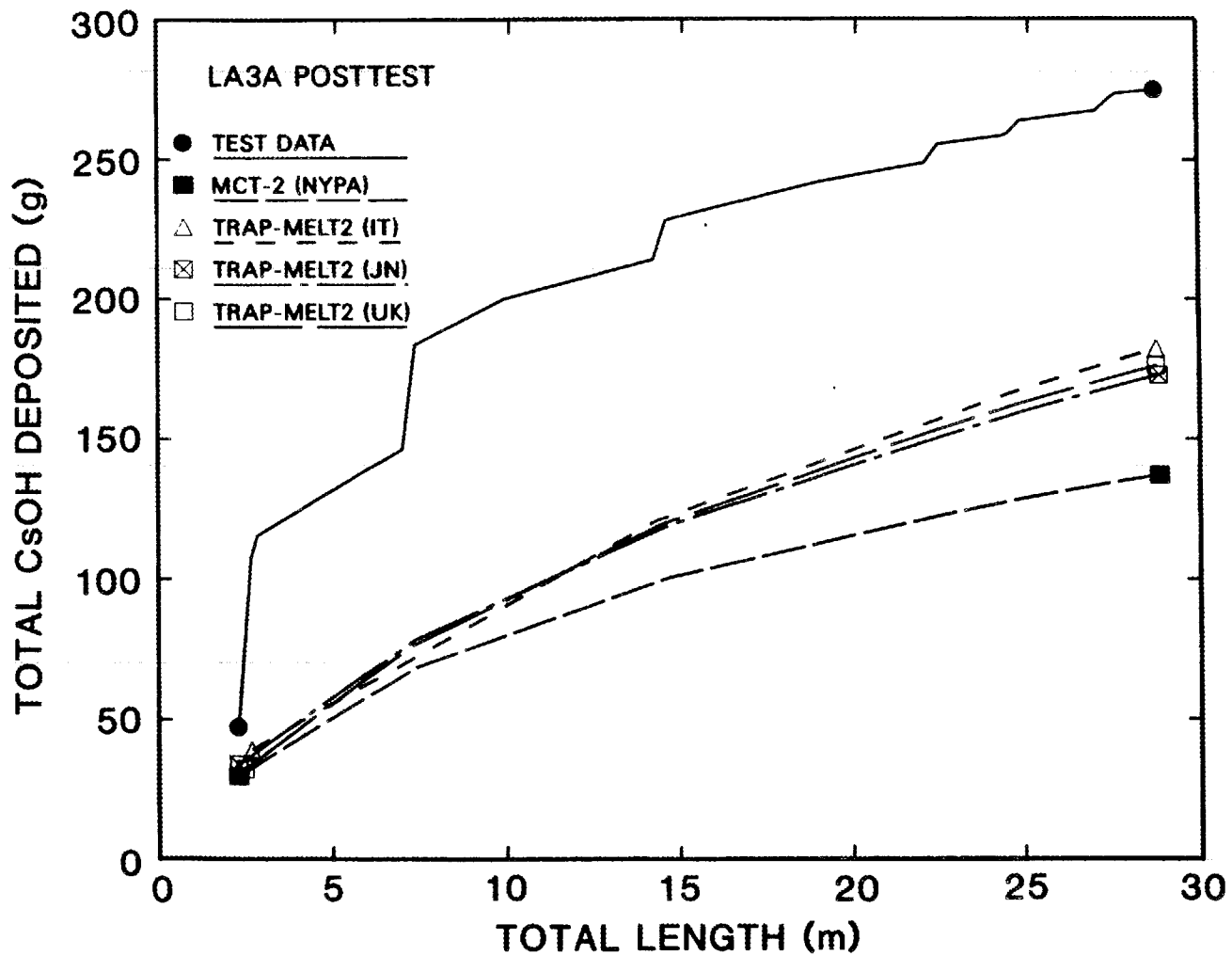


Fig. 3. LA3A posttest results: CsOH aerosol deposited in pipe vs distance from pipe inlet at end of test (3,600 s), for codes without bend deposition models.

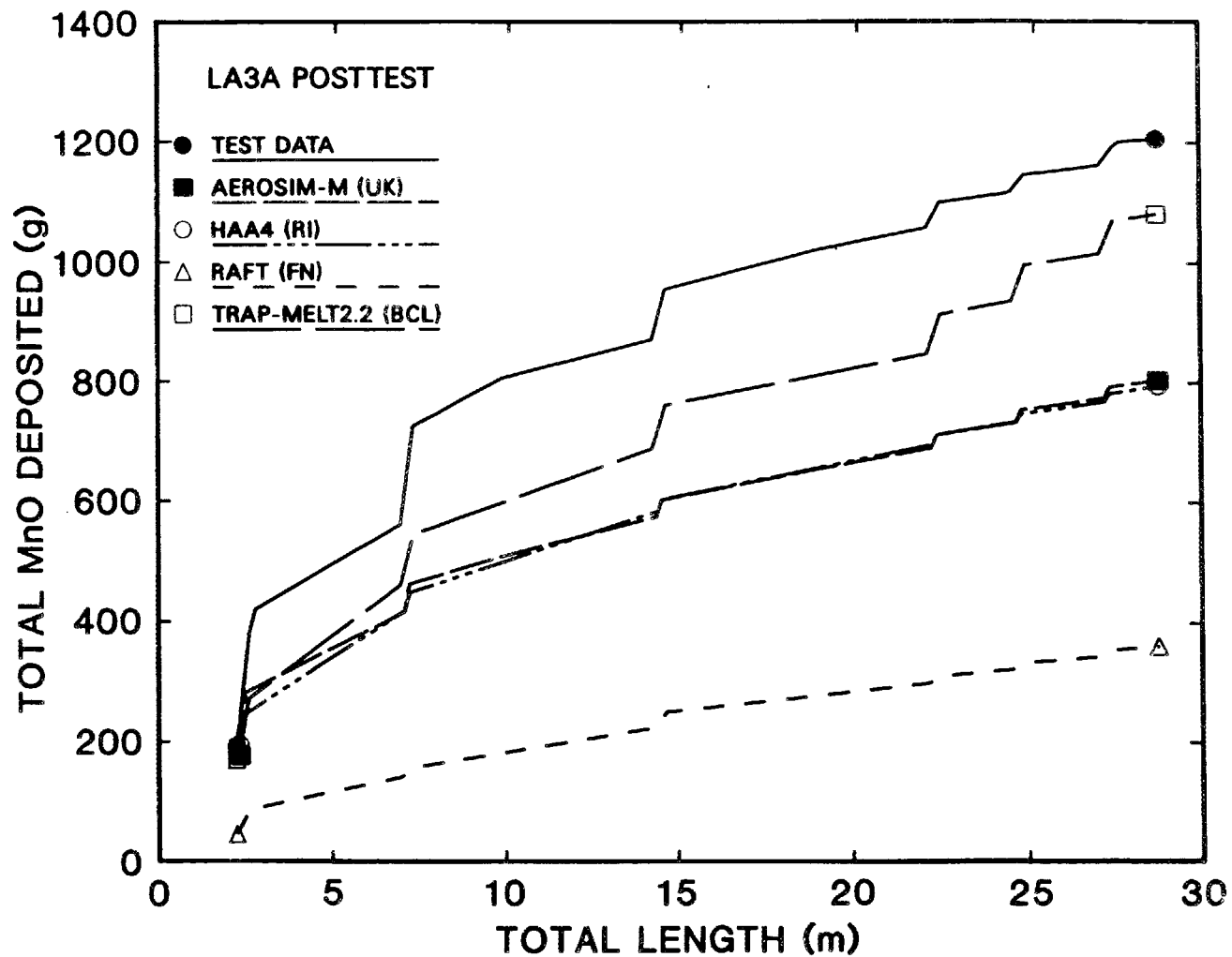


Fig. 4. LA3A posttest results: MnO aerosol deposited in pipe vs distance from pipe inlet at end of test (3,600 s), for codes including bend deposition models.

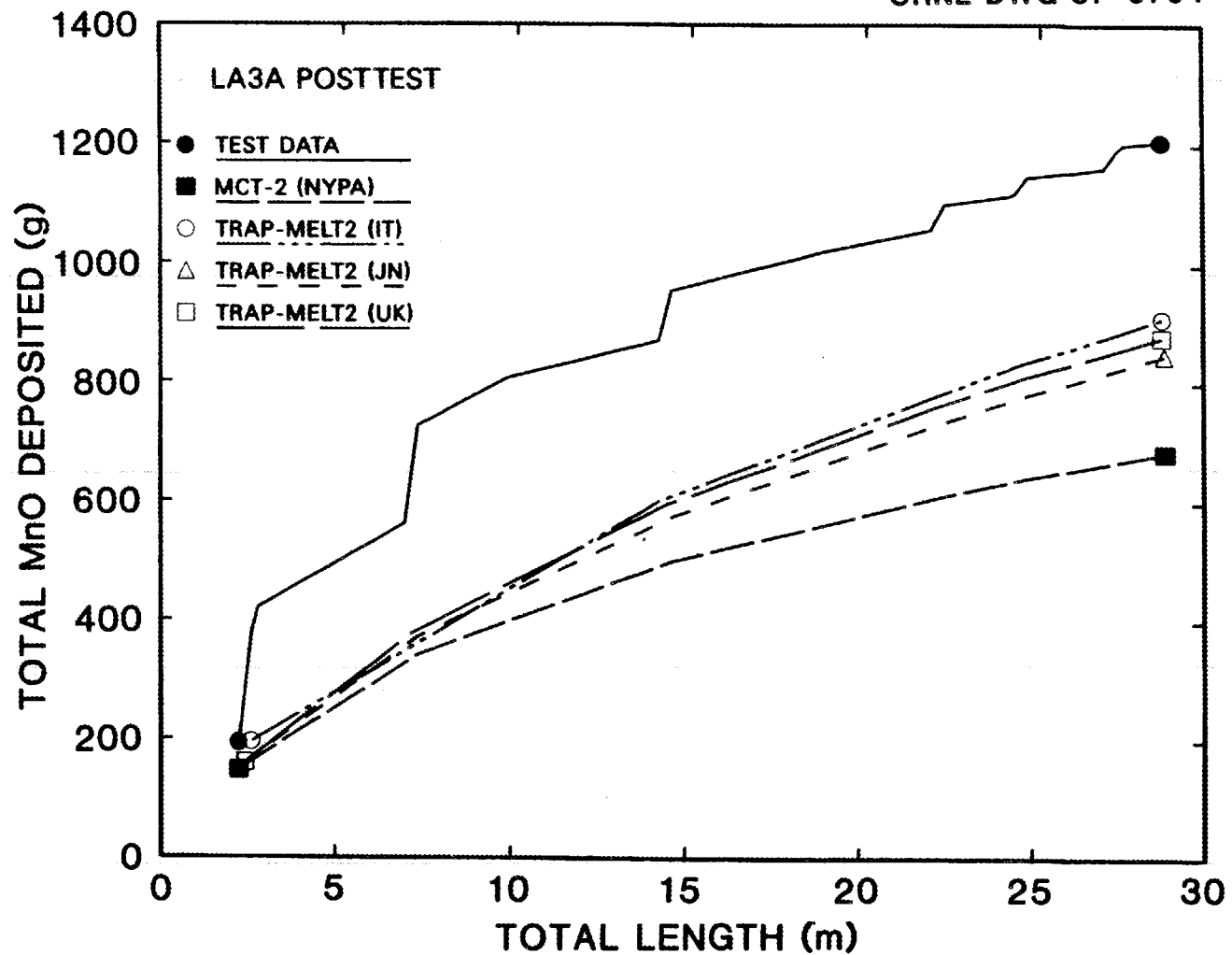


Fig. 5. LA3A posttest results: MnO aerosol deposited in pipe vs distance from pipe inlet at end of test (3,600 s), for codes without bend deposition models.

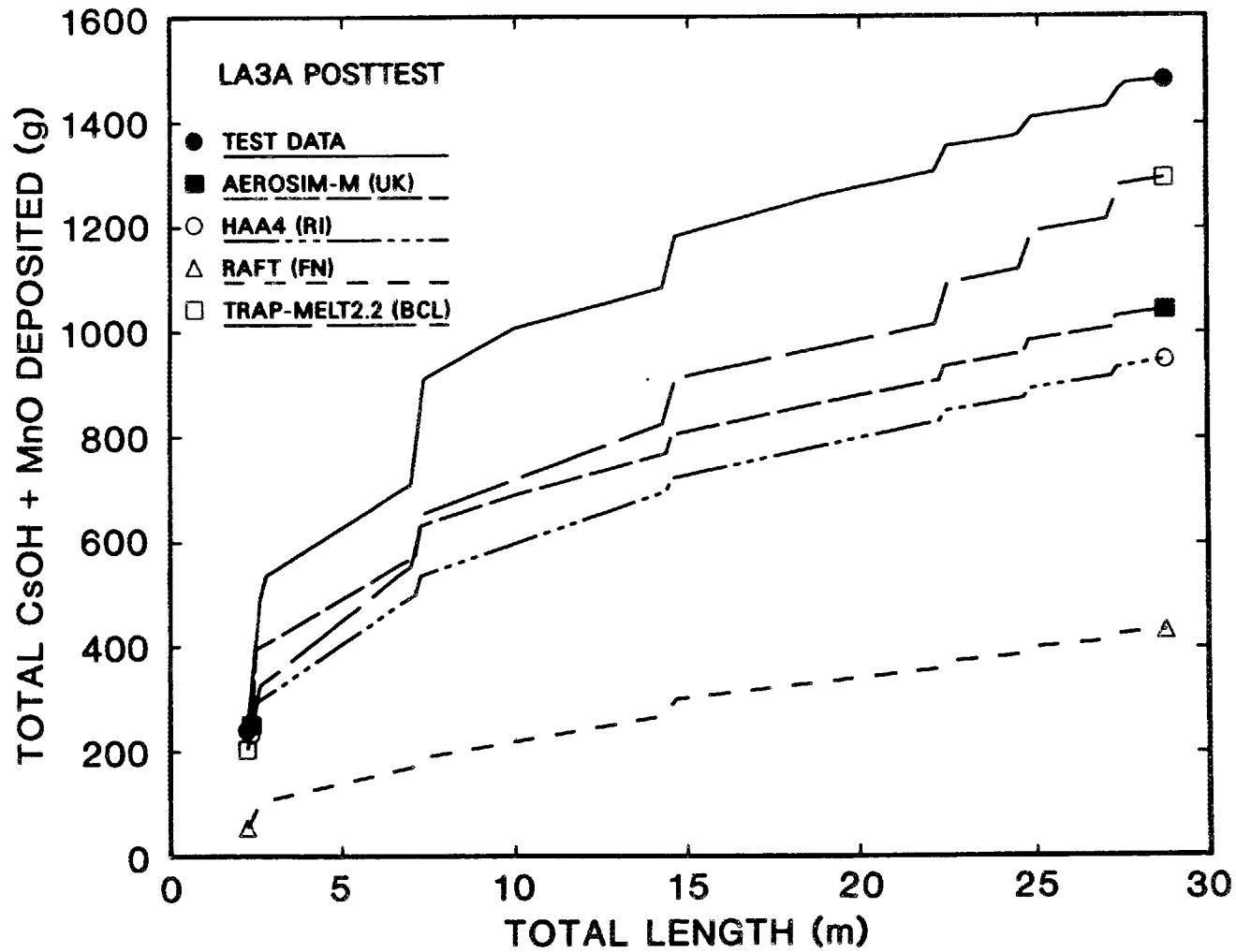


Fig. 6. LA3A posttest results: total (CsOH + MnO) aerosol deposited in pipe vs distance from pipe inlet at end of test (3,600 s), for codes including bend deposition models.

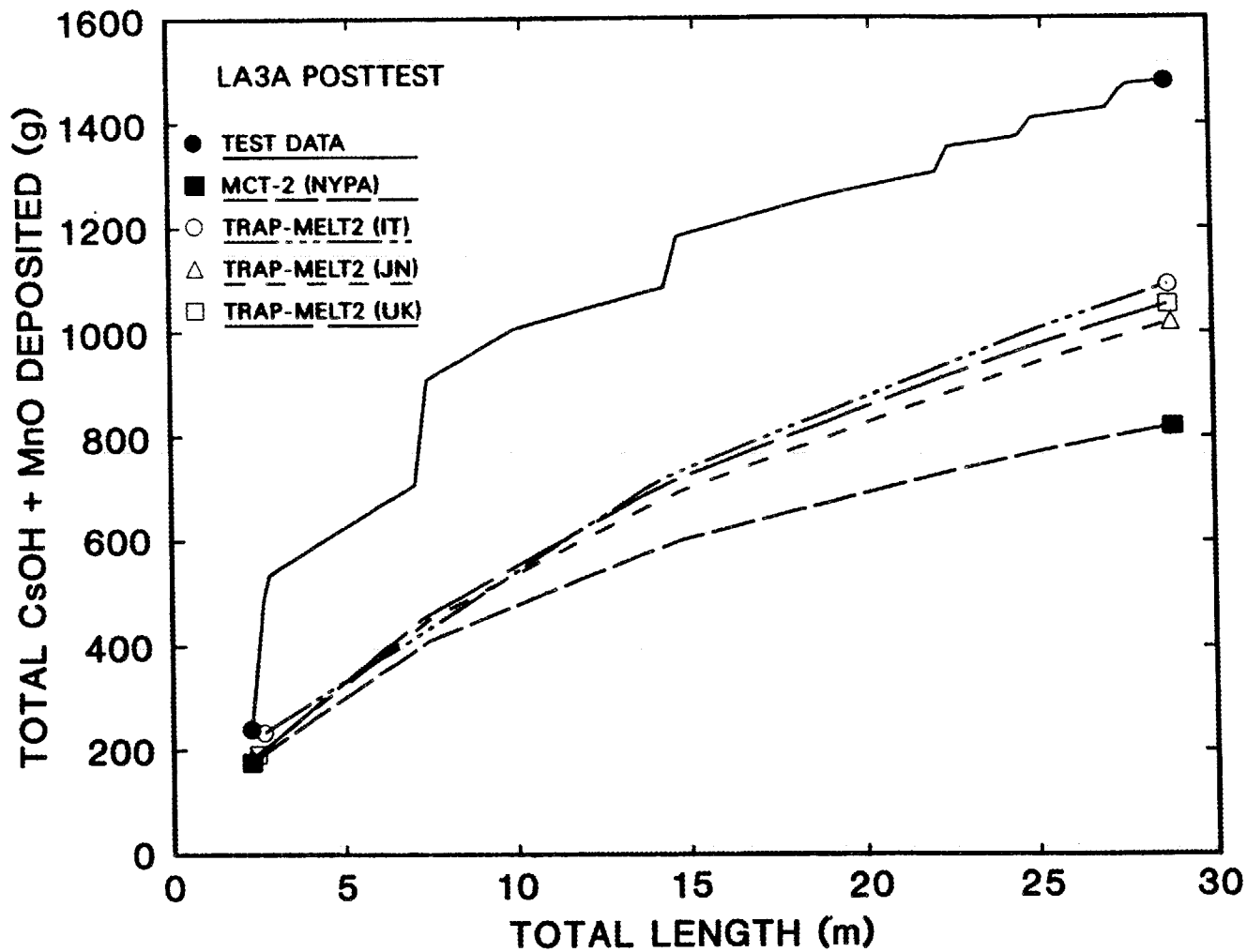


Fig. 7. LA3A posttest results: total (CsOH + MnO) aerosol deposited in pipe vs distance from pipe inlet at end of test (3,600 s), for codes without bend deposition models.

Table 18. Comparisons of measured and calculated aerosol deposition in pipe for test LA3A^a

Method	Total CsOH deposited (g)	Total MnO deposited (g)	Total aerosol deposited (g)
TEST DATA	274.6	1203.6	1478.1
AEROSIM-M (UK)	239.6	801.1	1040.7
HAA4 (RI)	153.9	791.7	945.6
RAFT (FN)	72.0	357.9	429.9
MCT-2 (NYPA)	137.0	681.2	818.2
TRAP-MELT2 (IT):	182.1	906.7	1088.8
TRAP-MELT2 (JN)	172.7	844.8	1017.5
TRAP-MELT2 (UK):			
time-averaged source size	16.0	875.2	1051.2
time dependent source size	176.3	877.0	1053.3
TRAP-MELT2.2 (BCL)	213.5	1078.0	1291.4

^aIn test LA3A, 87.6% of the Cs and 98.9% of the Mn input to the test equipment was recovered. This suggests that the uncertainties in the measured LA3A aerosol deposition data were ~12% for Cs and ~1% for Mn.

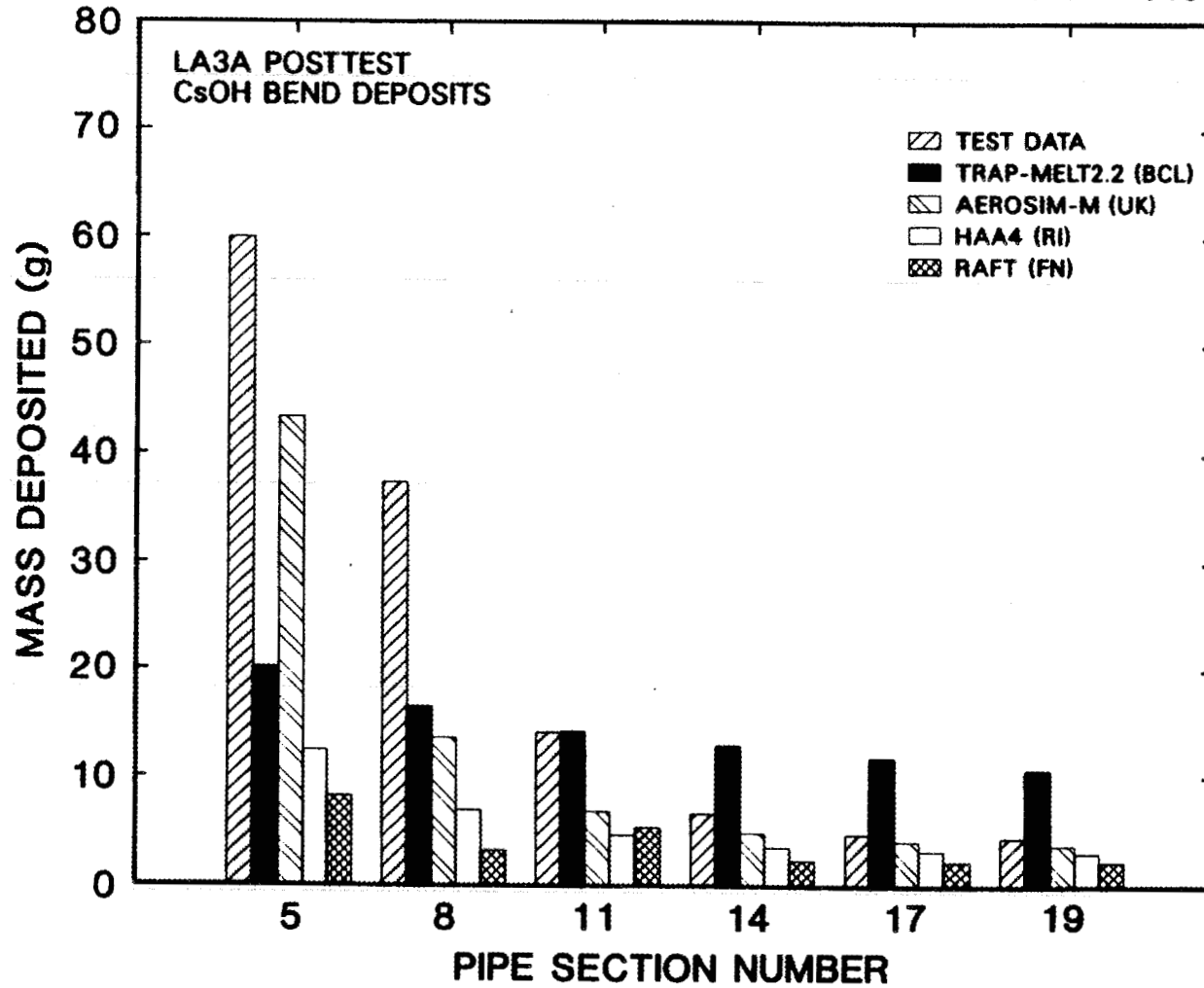


Fig. 8. LA3A posttest results: CsOH aerosol deposition in pipe bends at end of test (3,600 s).

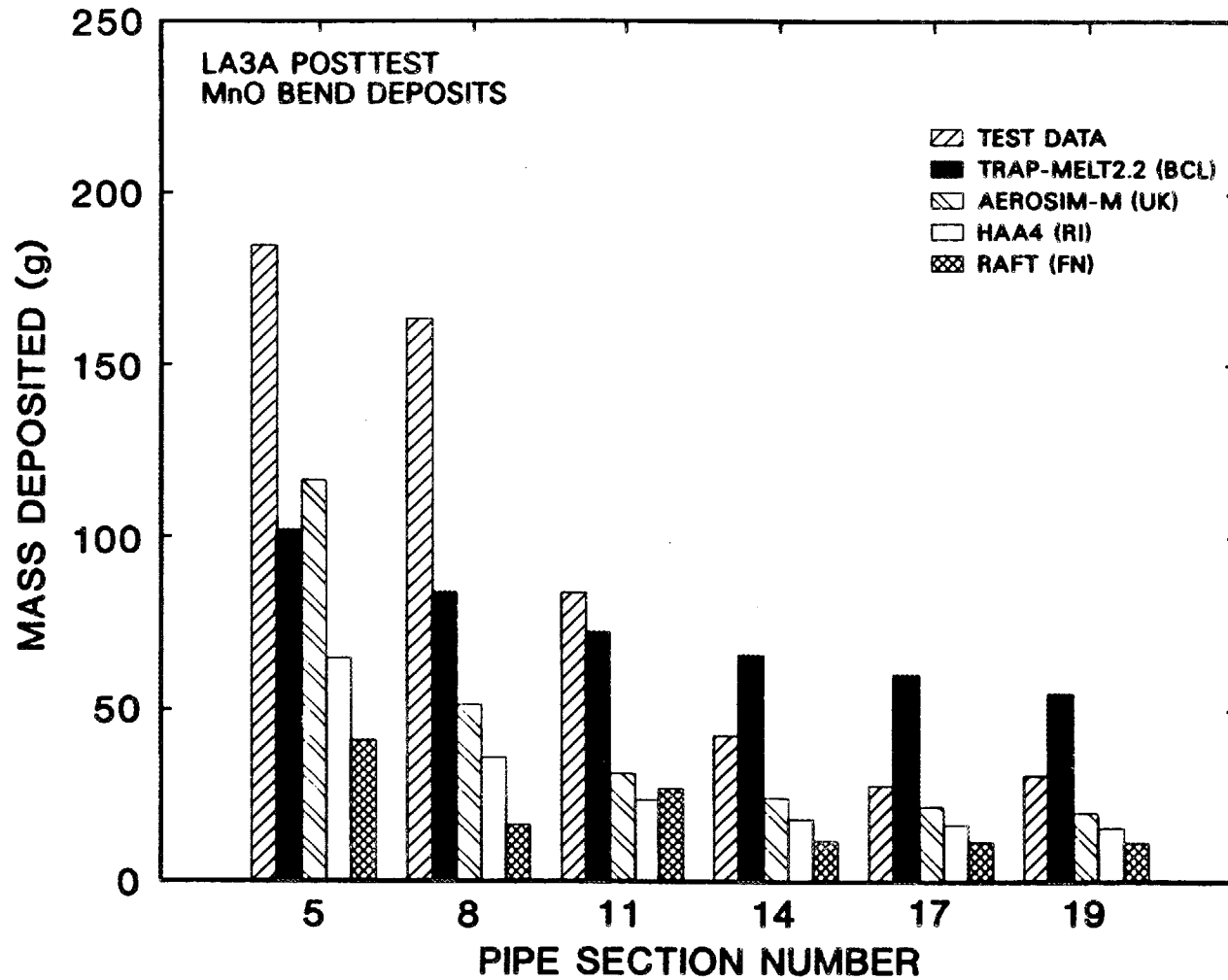


Fig. 9. LA3A posttest results: MnO aerosol deposition in pipe bends at end of test (3,600 s).

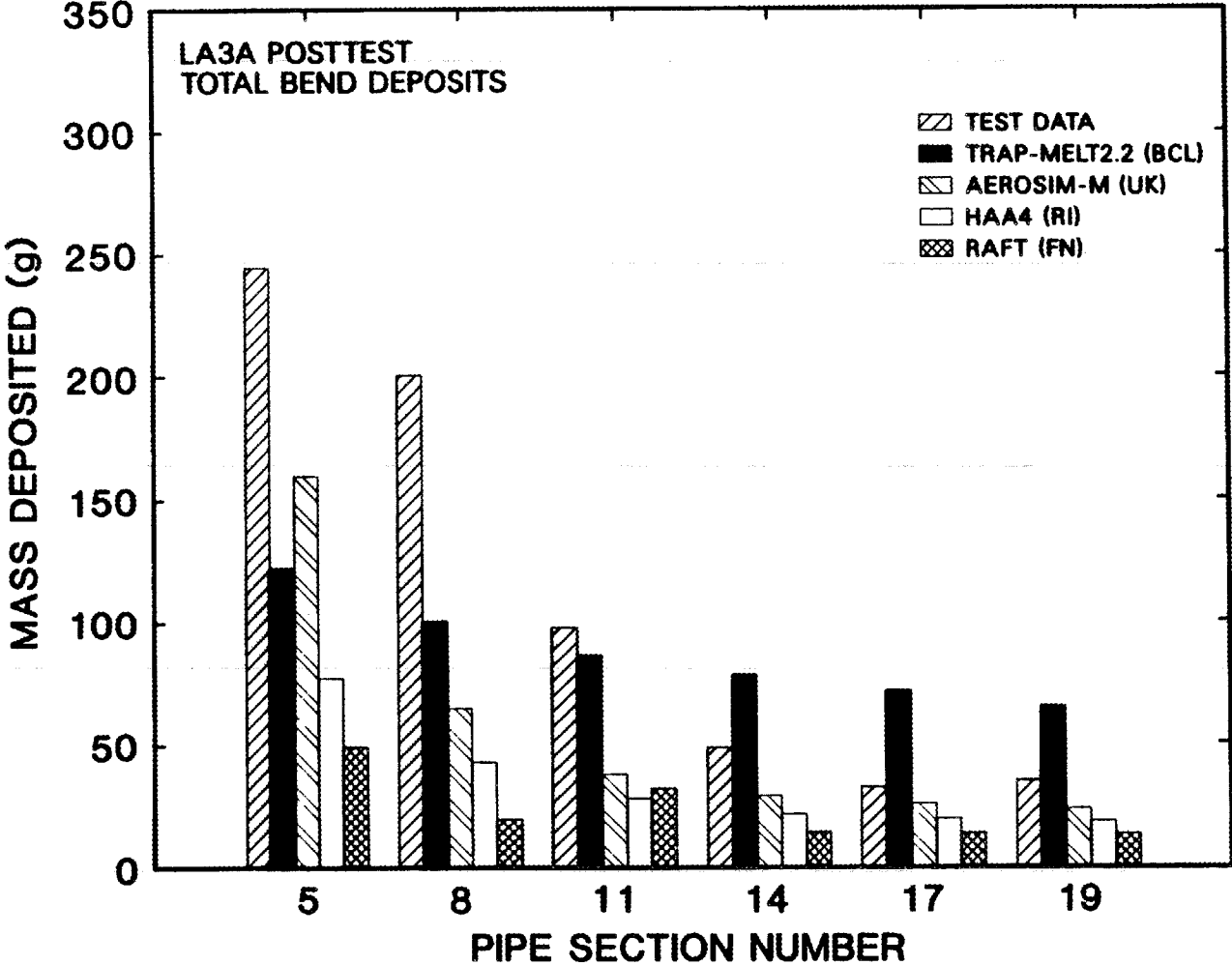


Fig. 10. LA3A posttest results: total (CsOH + MnO) aerosol deposition in pipe bends at end of test (3,600 s).

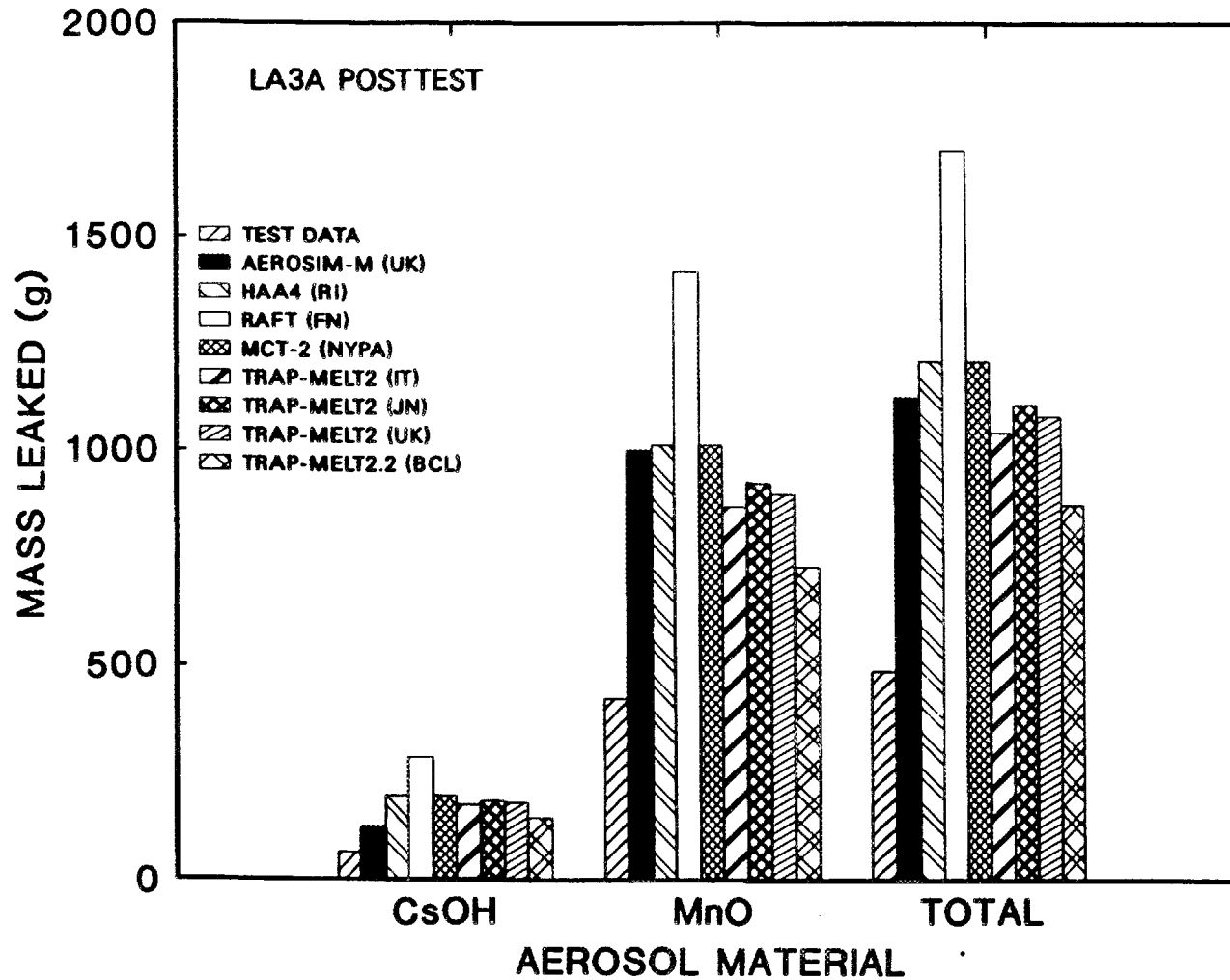


Fig. 11. LA3A posttest results: aerosol transport out of pipe at end of test (3,600 s).

Table 19. Comparisons of measured and calculated aerosol transport from pipe for test LA3A^a

Method	Total CsOH transported (g)	Total MnO transported (g)	Total aerosol transported (g)
TEST DATA	64.4	424.1	488.5
AEROSIM-M (UK)	123.8	1002.4	1126.3
HAA4 (RI)	195.8	1014.0	1210.0
RAFT (FN)	285.1	1418.0	1703.1
MCT-2 (NYPA)	195.8	1014.0	1210.0
TRAP-MELT2 (IT):	174.6	869.8	1044.4
TRAP-MELT2 (JN)	183.5	926.5	1109.9
TRAP-MELT2 (UK):			
time-averaged source size	181.1	900.7	1081.8
time-dependent source size	180.8	898.9	1079.7
TRAP-MELT2.2 (BCL)	144.9	731.1	876.0

^aIn test LA3A, 87.6% of the Cs and 98.9% of the Mn input to the test equipment was recovered. This suggests that the uncertainties in the measured LA3A aerosol transport data were ~12% for Cs and ~1% for Mn.

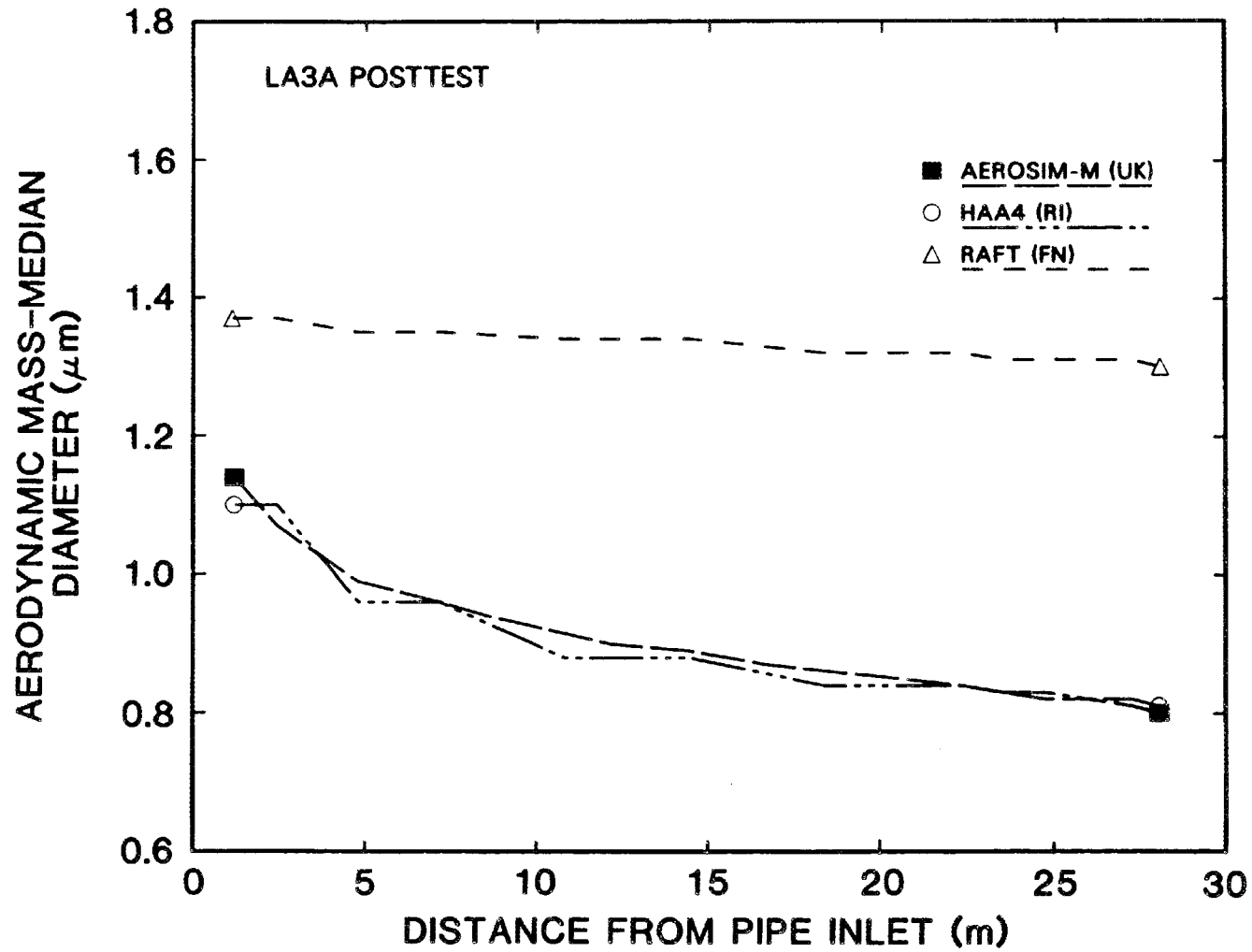


Fig. 12. LA3A posttest results: calculated aerodynamic mass-median diameter (AMMD) vs distance from pipe inlet at end of test (3,600 s), for codes that do not include TRAP-MELT modeling.

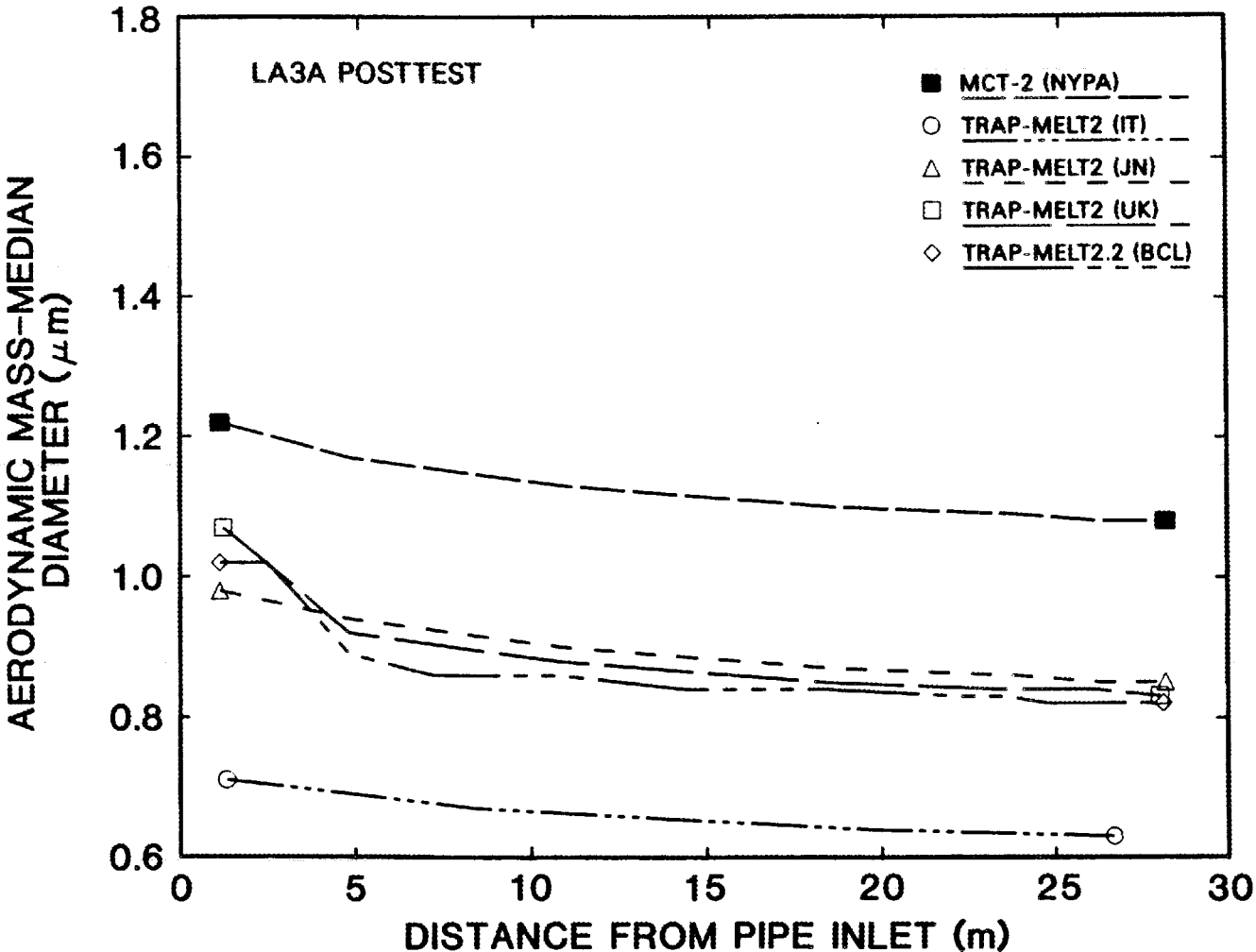


Fig. 13. LA3A posttest results: calculated aerodynamic mass-median diameter (AMMD) vs distance from pipe inlet at end of test (3,600 s), for codes that do include TRAP-MELT modeling.

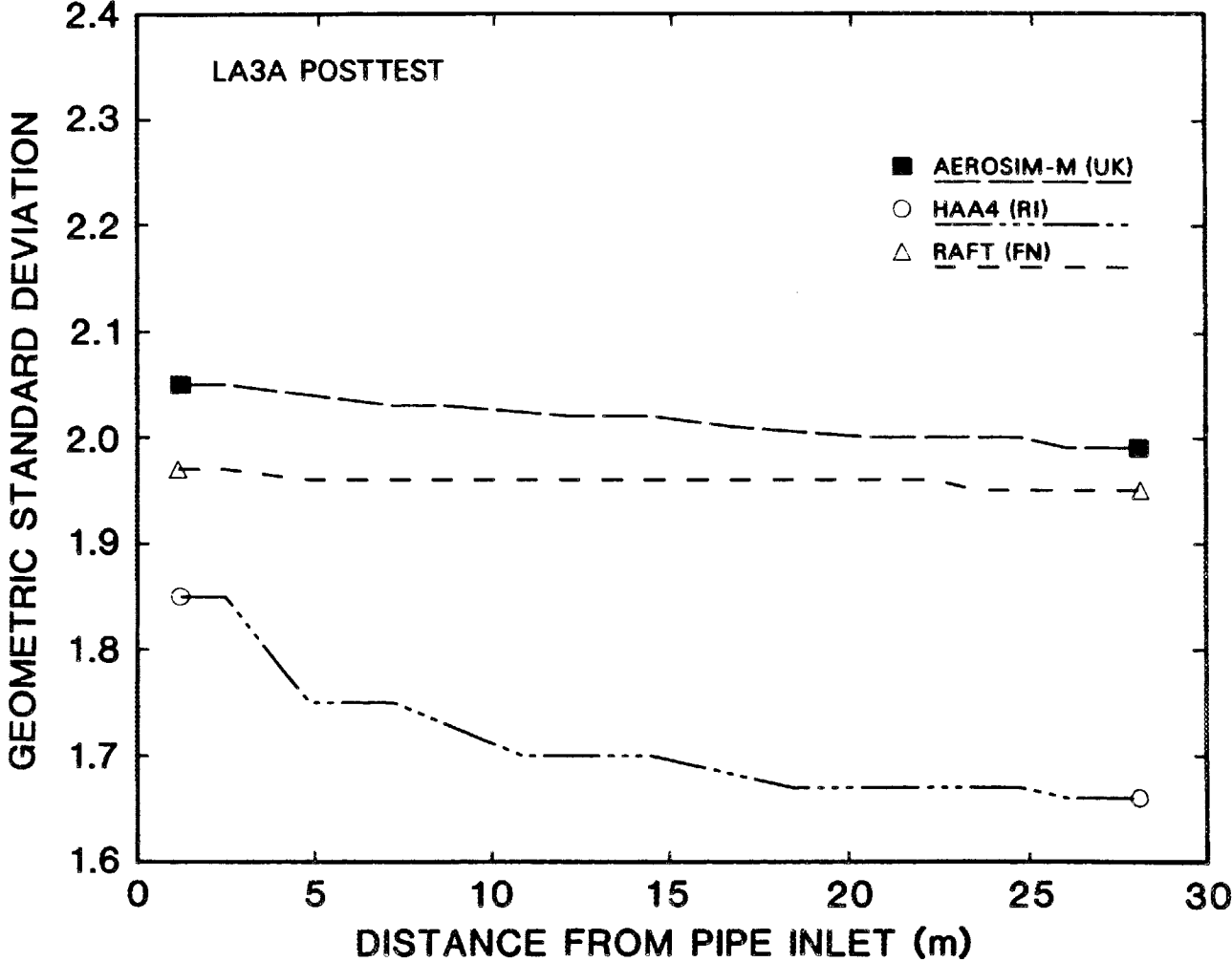


Fig. 14. LA3A posttest results: calculated geometric standard deviation (GSD) vs distance from pipe inlet at end of test (3,600 s), for codes that do not include TRAP-MELT modeling.

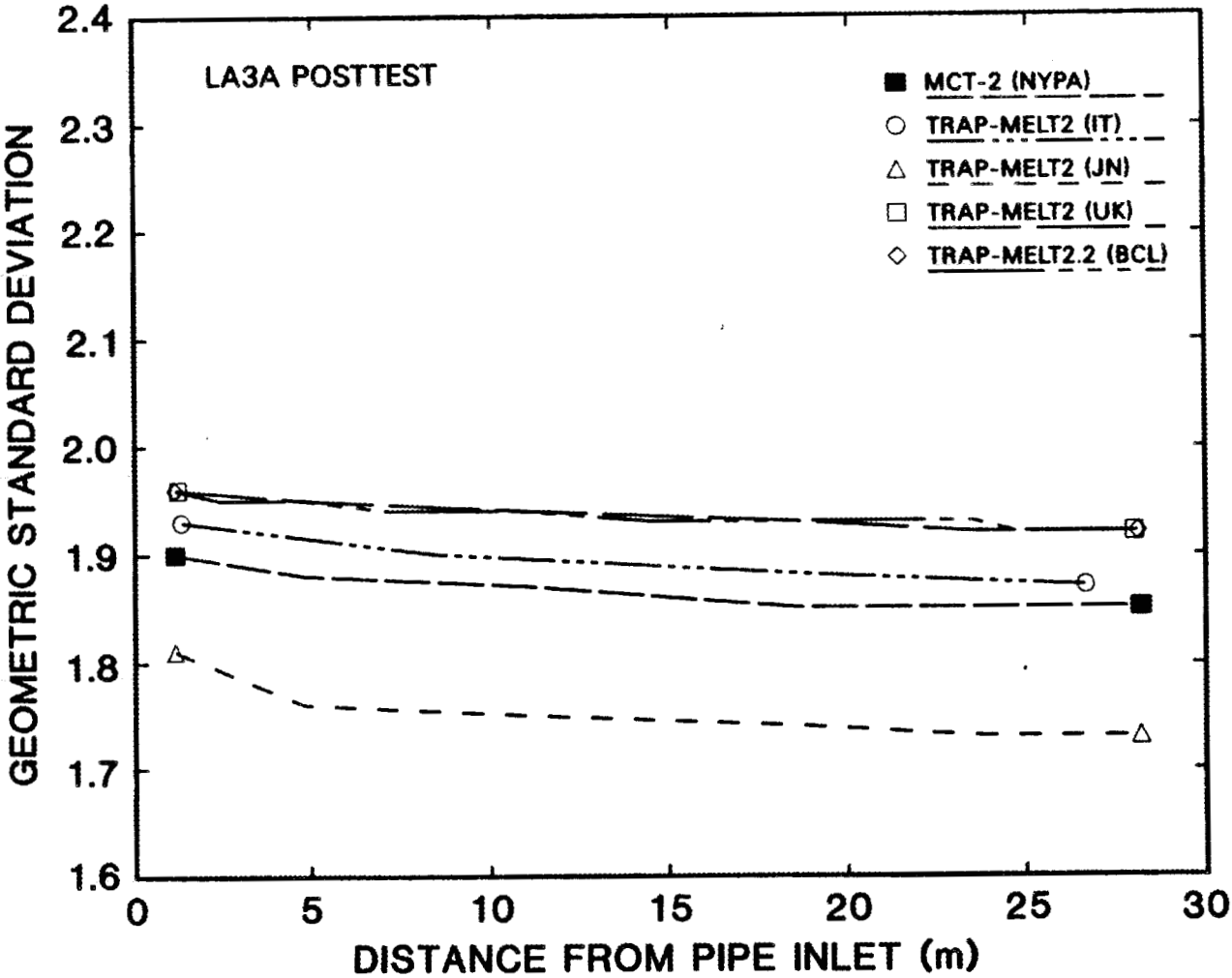


Fig. 15. LA3A posttest results: calculated geometric standard deviation (GSD) vs distance from pipe inlet at end of test (3,600 s), for codes that do include TRAP-MELT modeling.

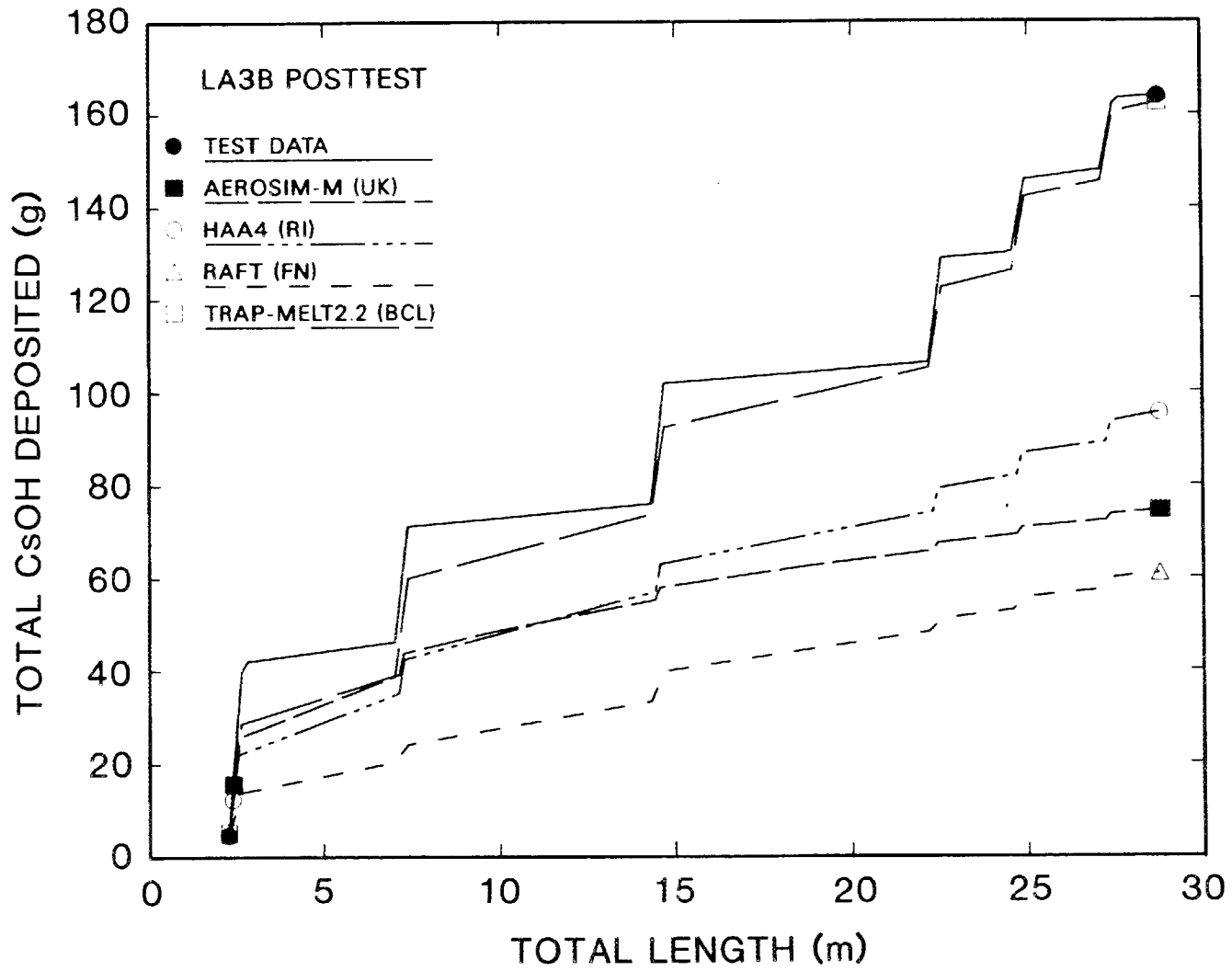


Fig. 16. LA3B posttest results: CsOH aerosol deposited in pipe vs distance from pipe inlet at end of test (3,600 s), for codes including bend deposition models.

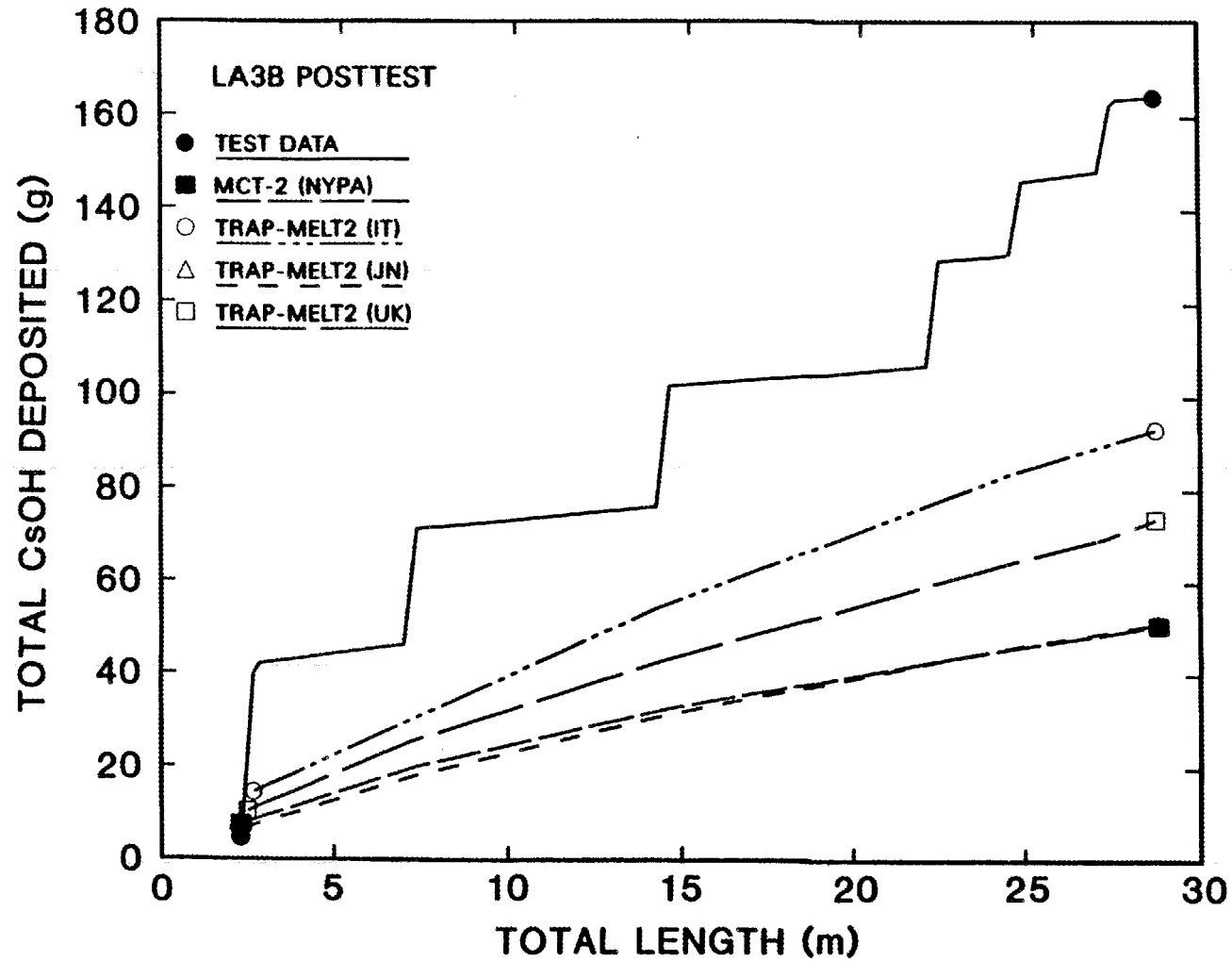


Fig. 17. LA3B posttest results: CsOH aerosol deposited in pipe vs distance from pipe inlet at end of test (3,600 s), for codes without bend deposition models.

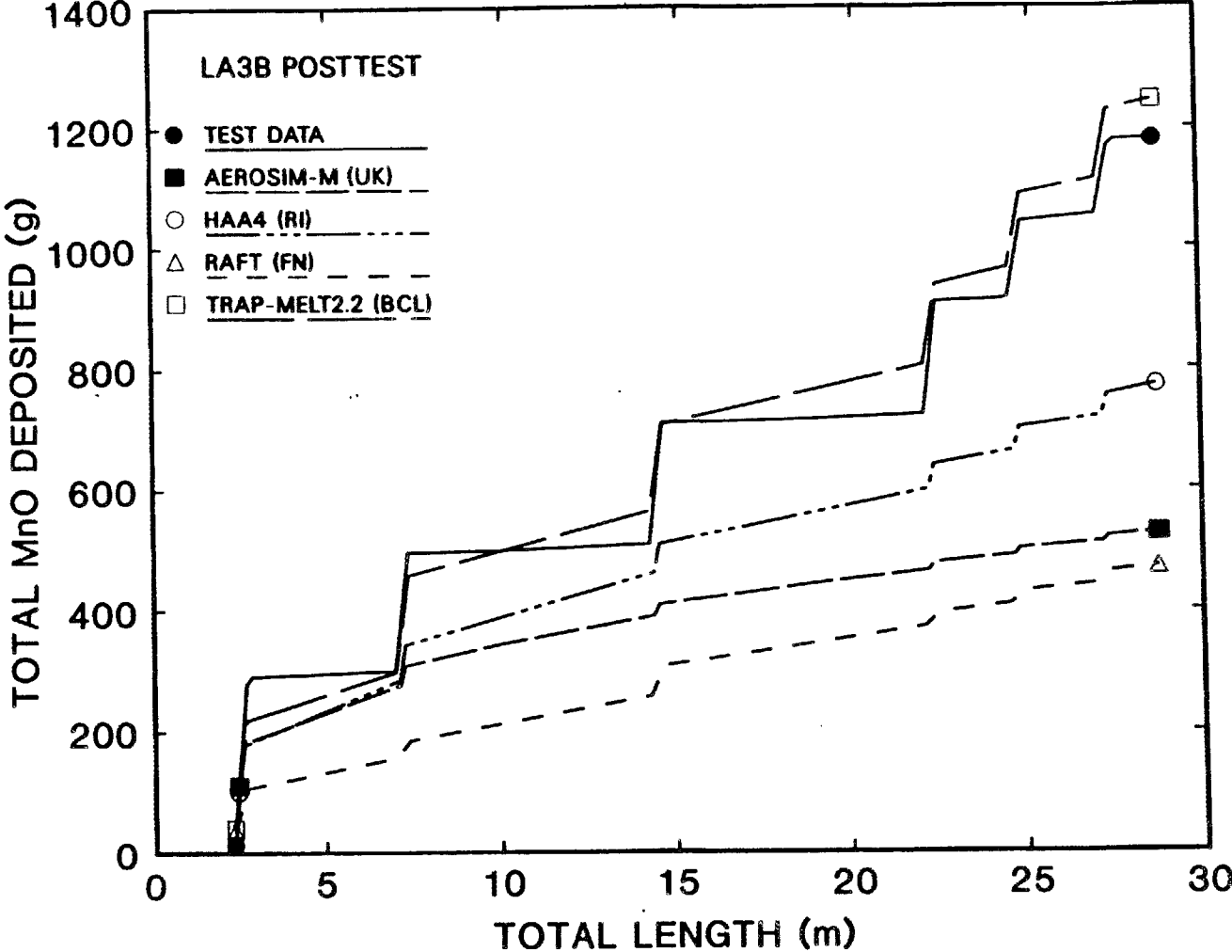


Fig. 18. LA3B posttest results: MnO aerosol deposited in pipe vs distance from pipe inlet at end of test (3,600 s), for codes including bend deposition models.

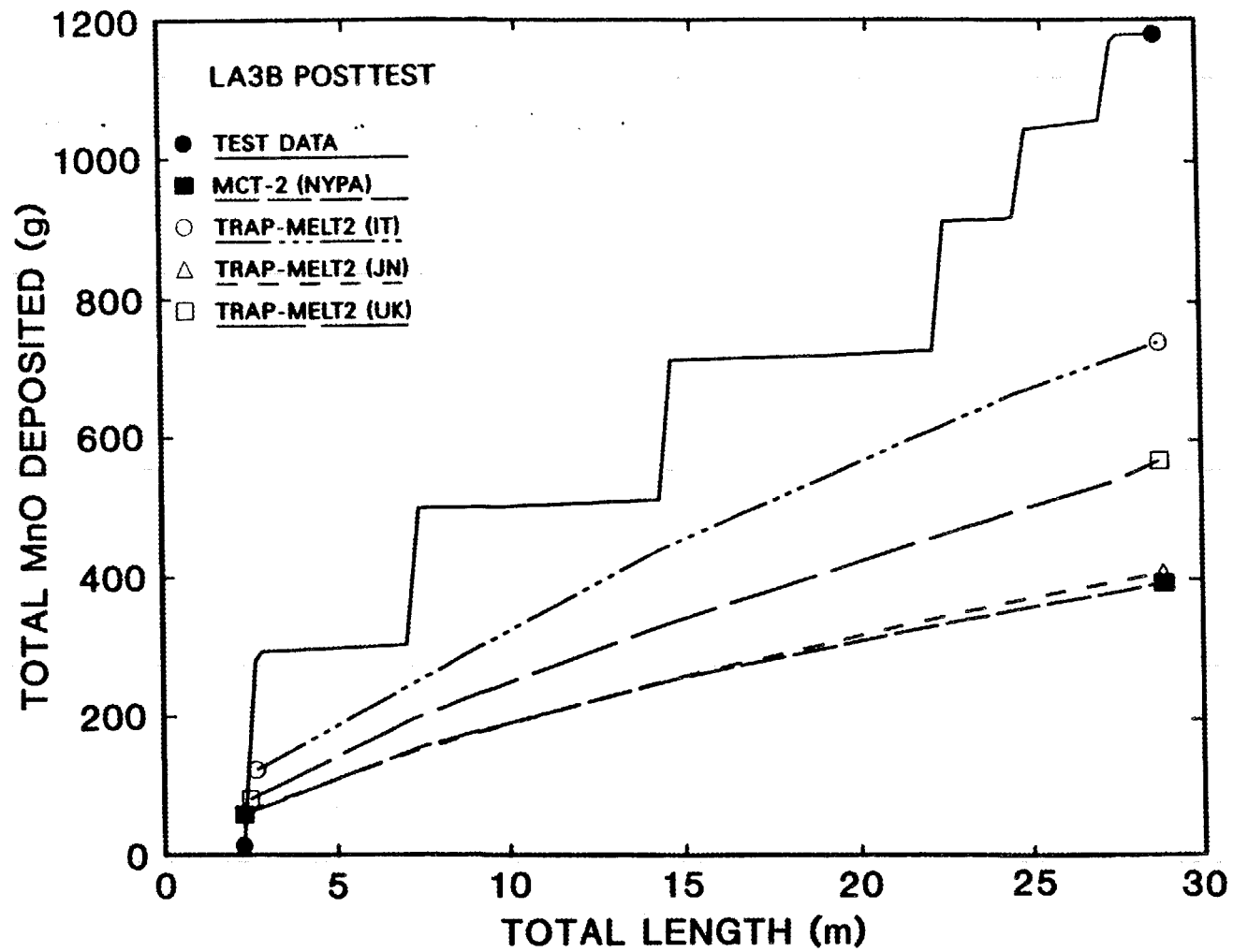


Fig. 19. LA3B posttest results: MnO aerosol deposited in pipe vs distance from pipe inlet at end of test (3,600 s), for codes without bend deposition models.

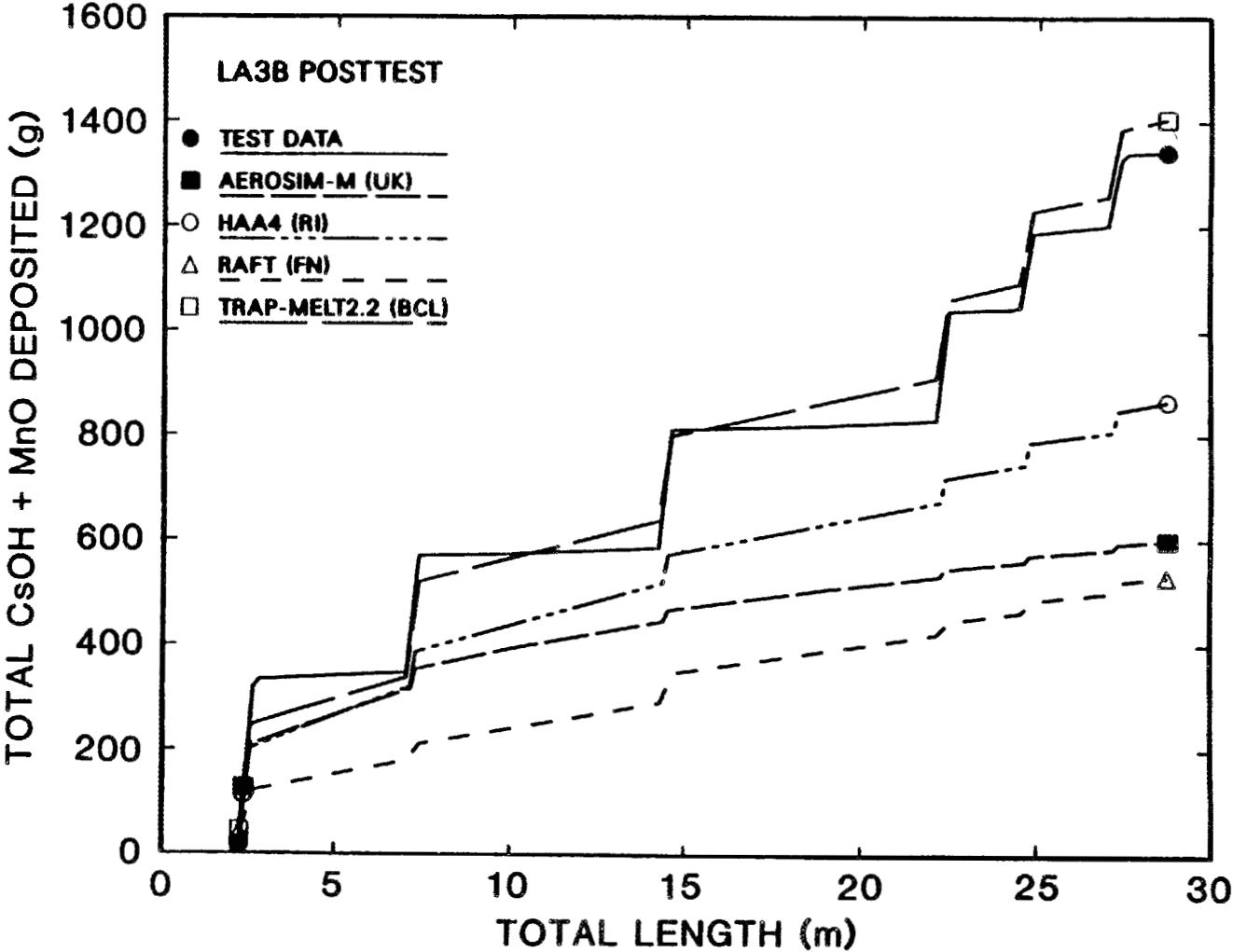


Fig. 20. LA3B posttest results: total (CsOH + MnO) aerosol deposited in pipe vs distance from pipe inlet at end of test (3,600 s), for codes including bend deposition models.

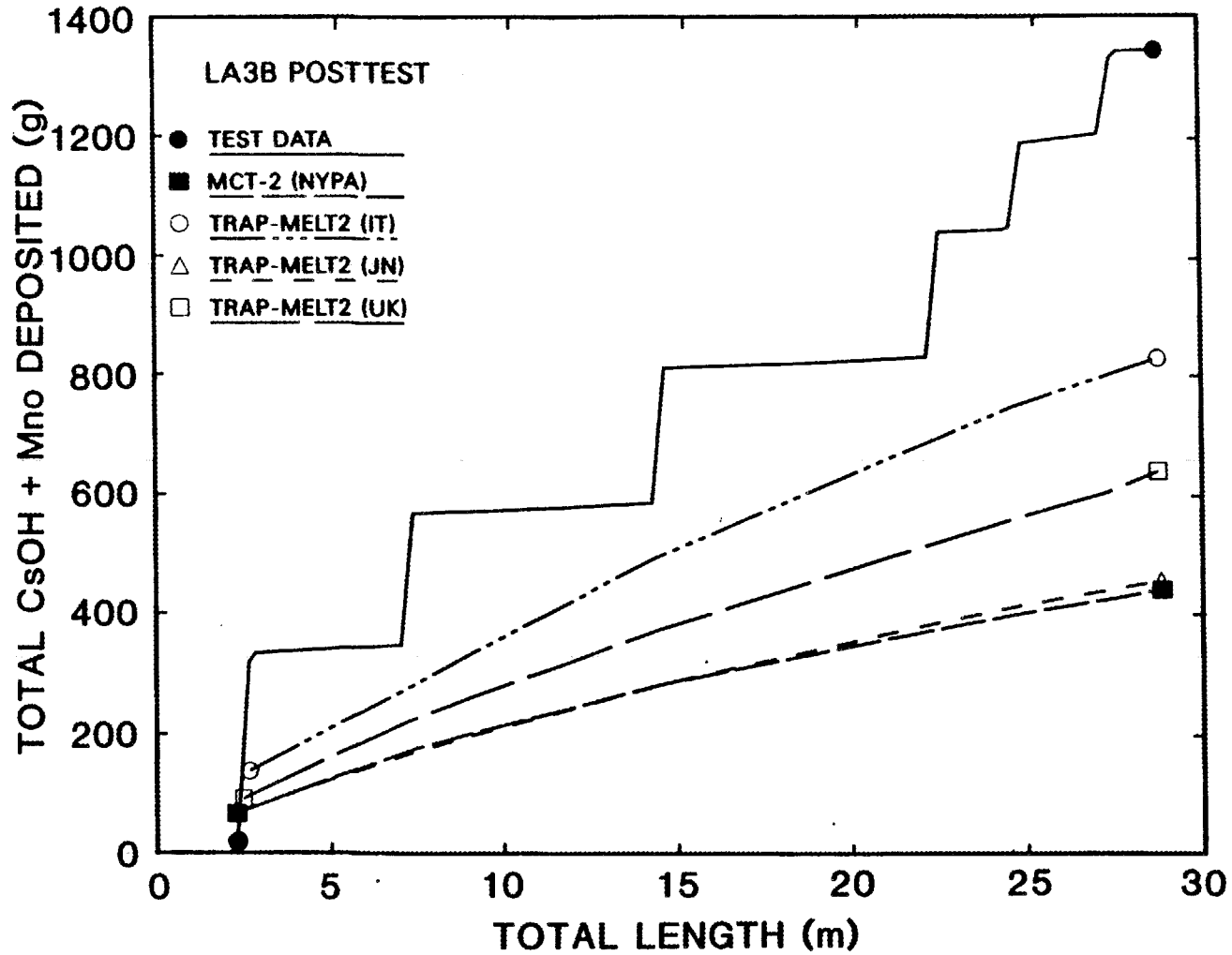


Fig. 21. LA3B posttest results: total (CsOH + MnO) aerosol deposited in pipe vs distance from pipe inlet at end of test (3,600 s), for codes without bend deposition models.

Table 20. Comparisons of measured and calculated aerosol deposition in pipe for test LA3B^a

Method	Total CsOH deposited (g)	Total MnO deposited (g)	Total aerosol deposited (g)
TEST DATA	163.7	1179.0	1342.7
AEROSIM-M (UK)	74.5	527.8	602.3
HAA4 (RI)	95.5	771.9	867.4
RAFT (FN)	61.0	471.1	532.1
MCT-2 (NYPA)	50.6	391.2	441.9
TRAP-MELT2 (IT):	92.5	736.0	828.5
TRAP-MELT2 (JN)	51.0	405.7	456.6
TRAP-MELT2 (UK):			
time-averaged source size	73.3	566.3	639.6
time-dependent source size	76.2	588.5	664.7
TRAP-MELT2.2 (BCL)	162.3	1243.2	1405.5

^aIn test LA3B, 93.8% of the Cs and 89.7% of the Mn input to the test equipment was recovered. This suggests that the uncertainties in the measured LA3B aerosol deposition data were ~6% for Cs and ~10% for Mn.

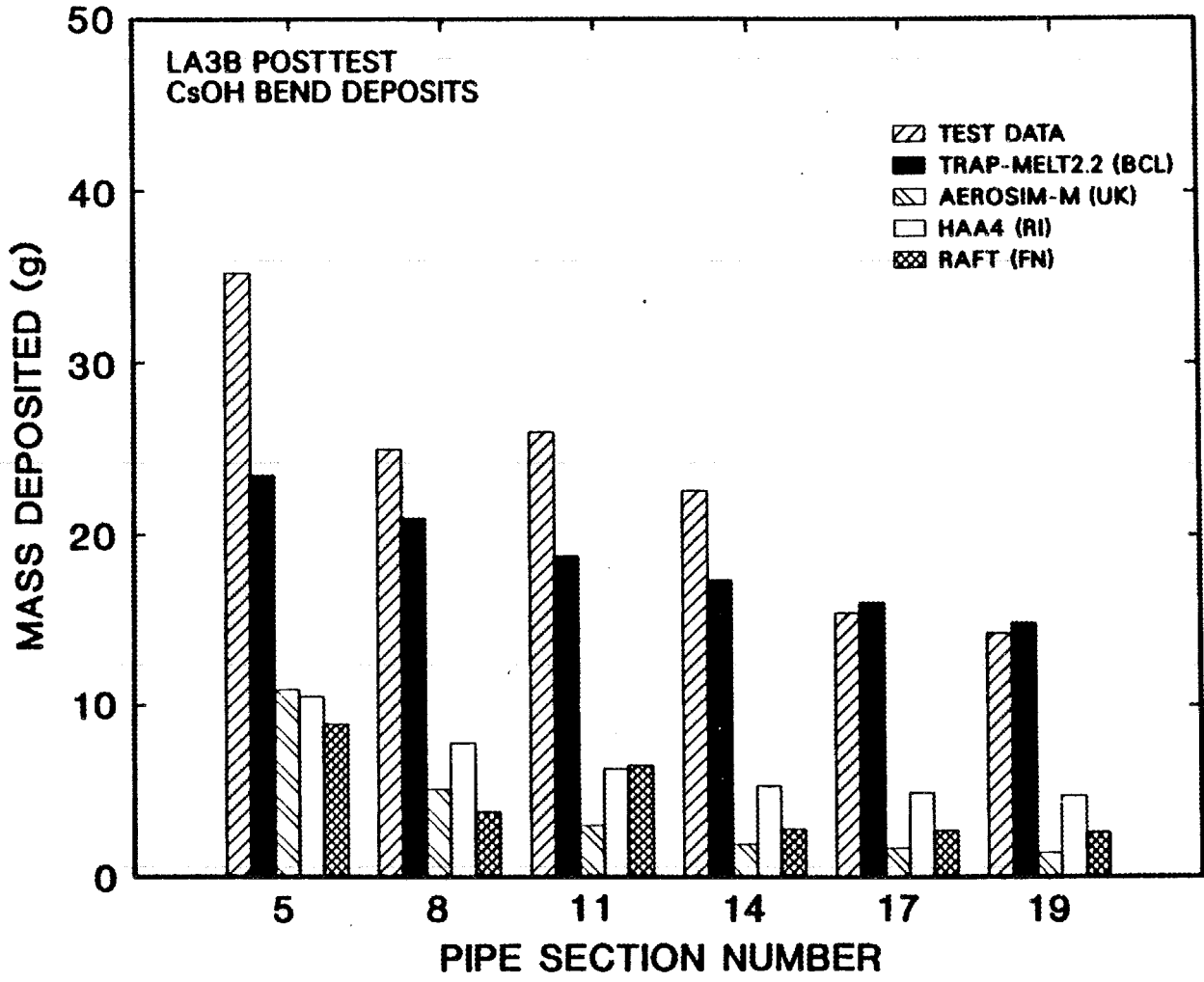


Fig. 22. LA3B posttest results: CsOH aerosol deposition in pipe bends at end of test (3,600 s).

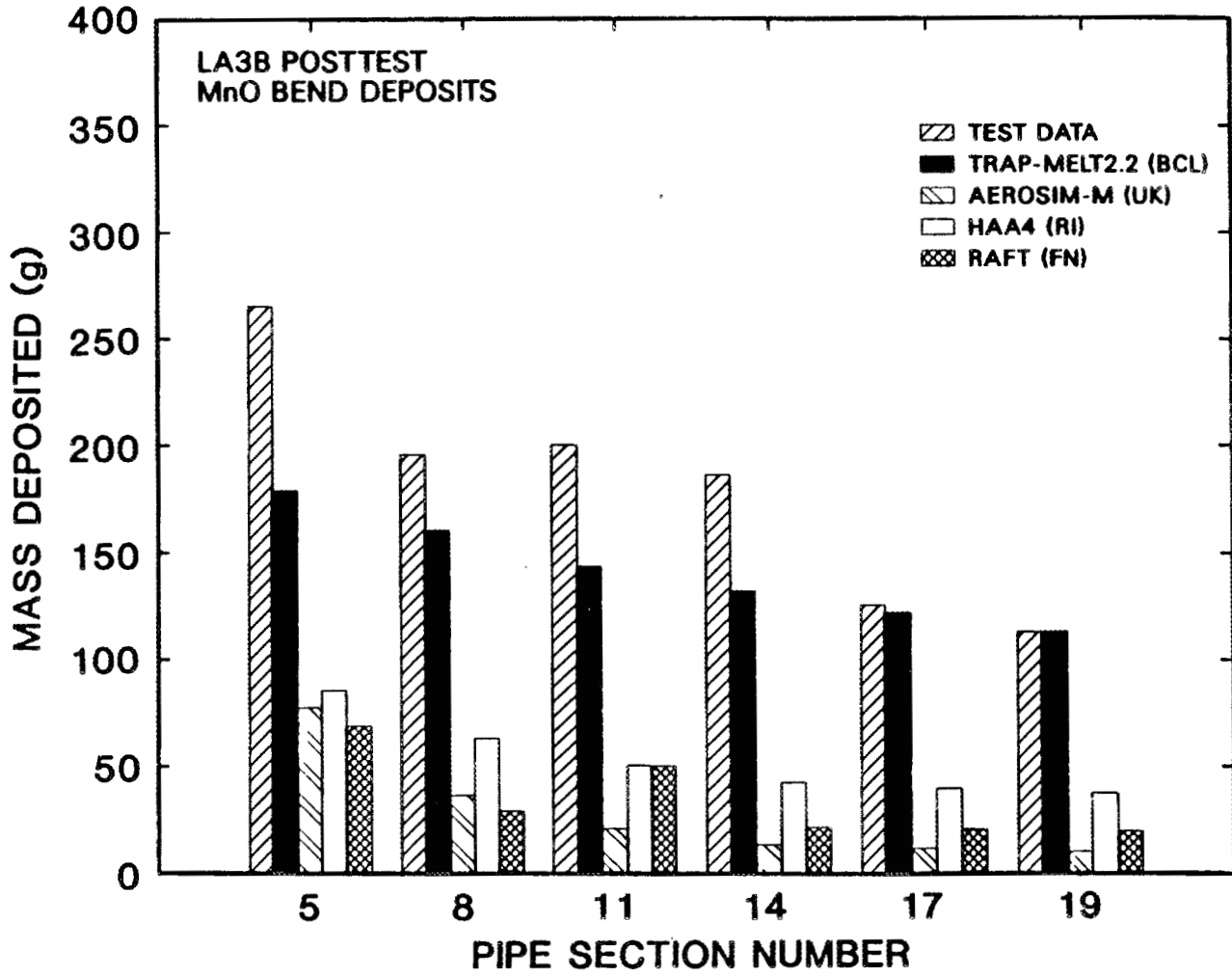


Fig. 23. LA3B posttest results: MnO aerosol deposition in pipe bends at end of test (3,600 s).

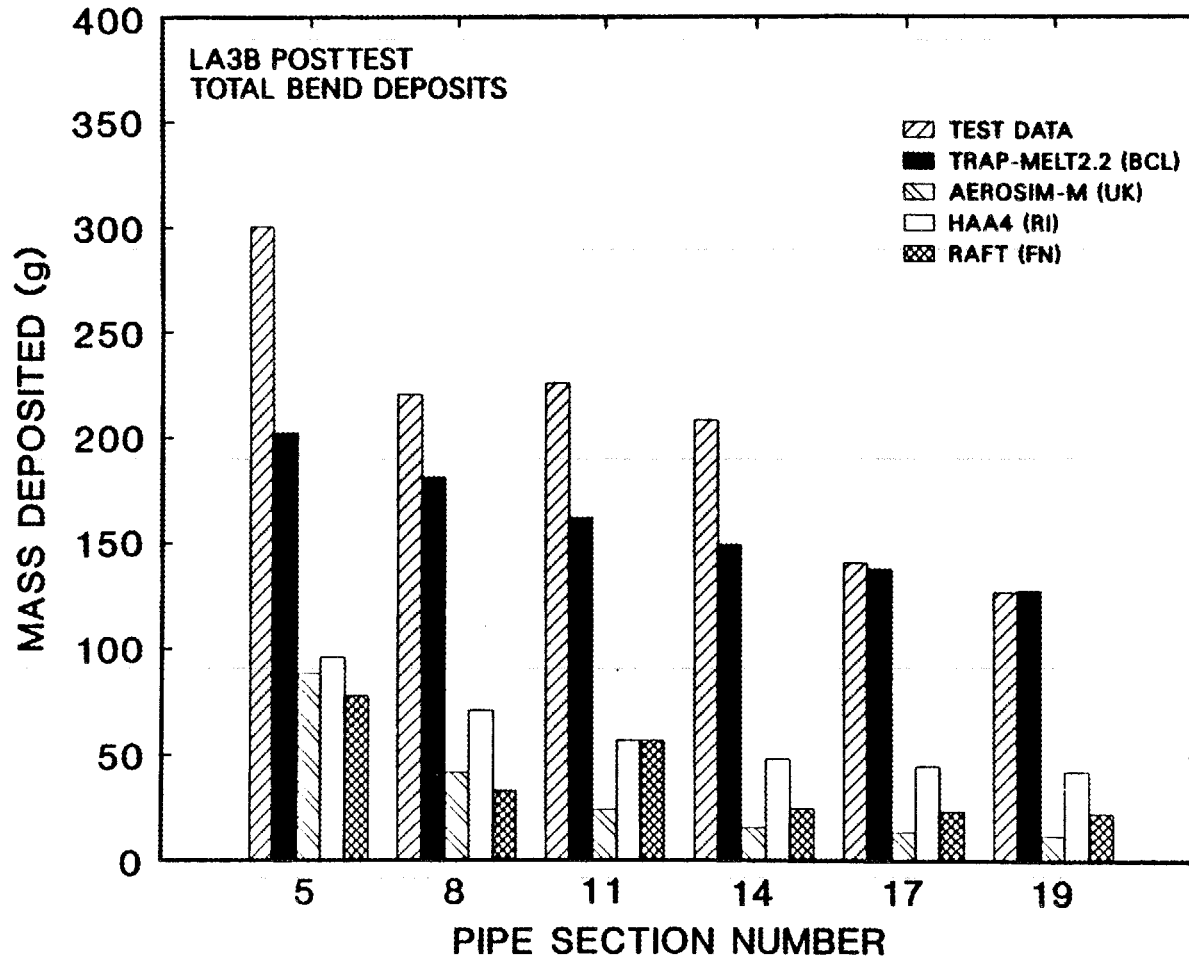


Fig. 24. LA3B posttest results: total (CsOH + MnO) aerosol deposition in pipe bends at end of test (3,600 s).

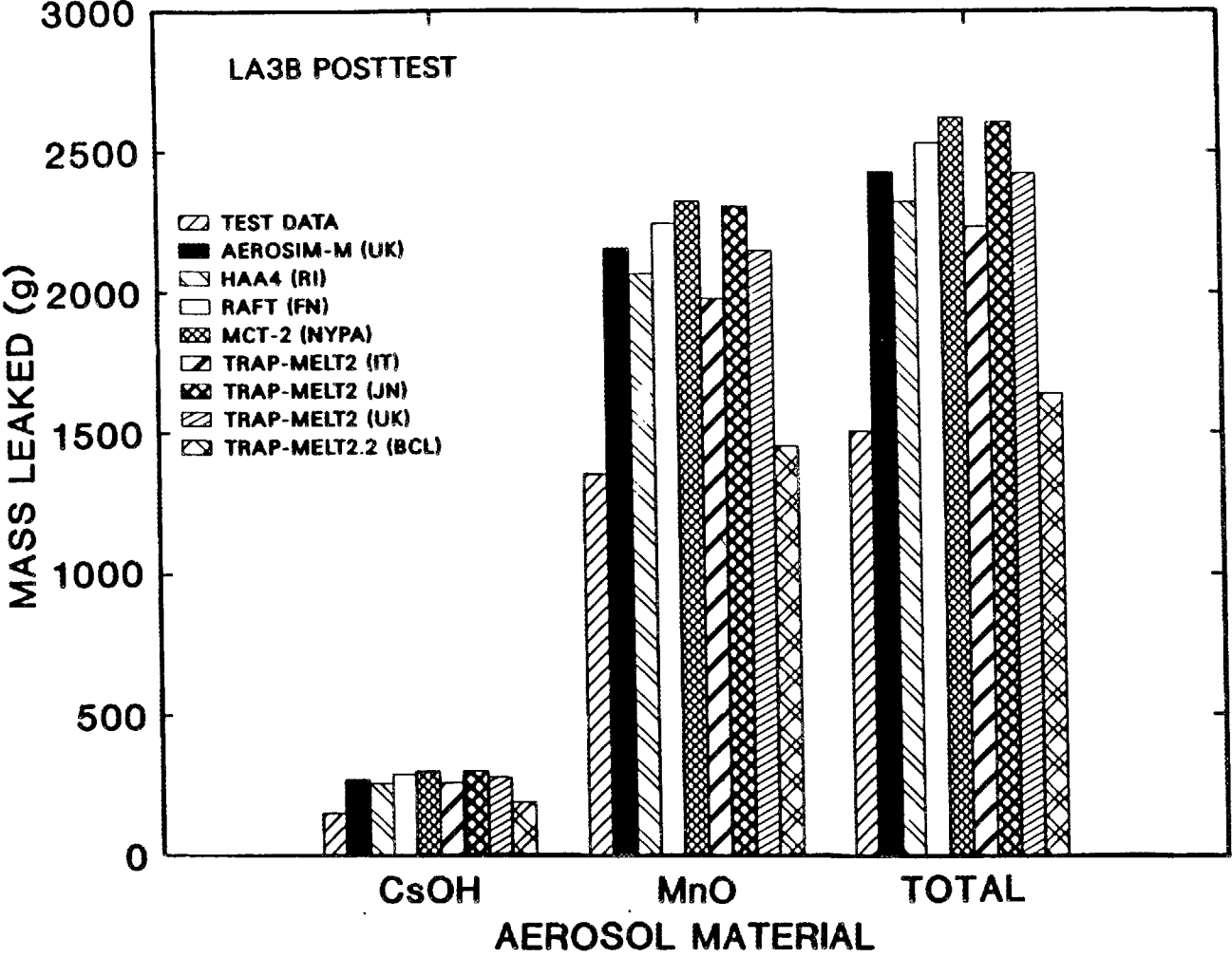


Fig. 25. LA3B posttest results: aerosol transport out of pipe at end of test (3,600 s).

Table 21. Comparisons of measured and calculated aerosol transport from pipe for test LA3B^a

Method	Total CsOH transported (g)	Total MnO transported (g)	Total aerosol transported (g)
TEST DATA	153.0	1355.5	1508.5
AEROSIM-M (UK)	272.5	2155.8	2428.2
HAA4 (RI)	258.5	2063.8	2322.3
RAFT (FN)	290.0	2240.8	2530.8
MCT-2 (NYPA)	300.4	2320.6	2621.0
TRAP-MELT2 (IT)	258.7	1975.6	2234.3
TRAP-MELT2 (JN)	300.2	2304.6	2604.8
TRAP-MELT2 (UK):			
time-averaged source size	277.7	2145.6	2423.3
time dependent source size	274.8	2123.4	2398.2
TRAP-MELT2.2 (BCL)	189.6	1452.1	1641.7

^aIn test LA3B, 93.8% of the Cs and 89.7% of the Mn input to the test equipment was recovered. This suggests that the uncertainties in the measured LA3B aerosol transport data were ~6% for Cs and ~10% for Mn.

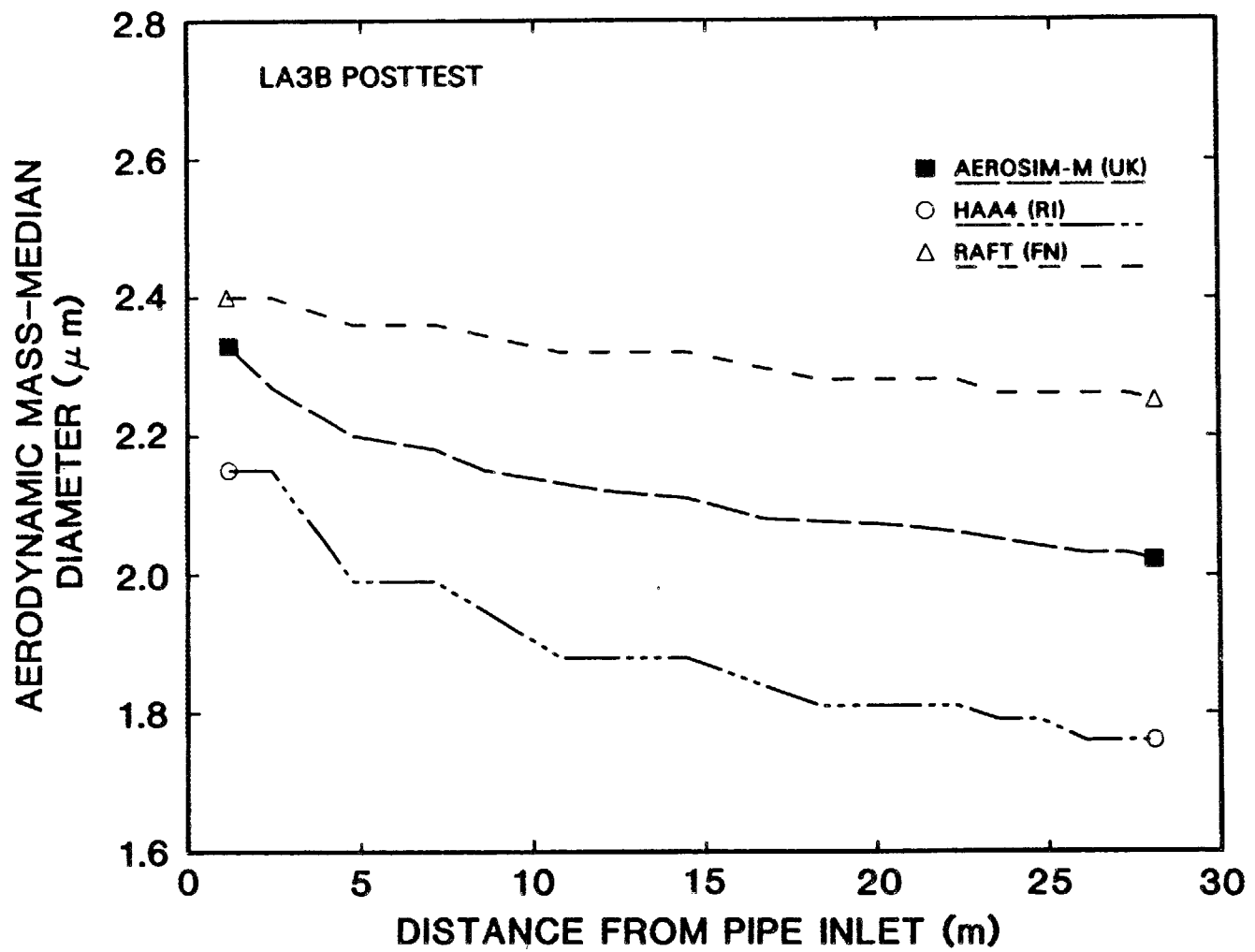


Fig. 26. LA3B posttest results: calculated aerodynamic mass-median diameter (AMMD) vs distance from pipe inlet at end of test (3,600 s), for codes that do not include TRAP-MELT modeling.

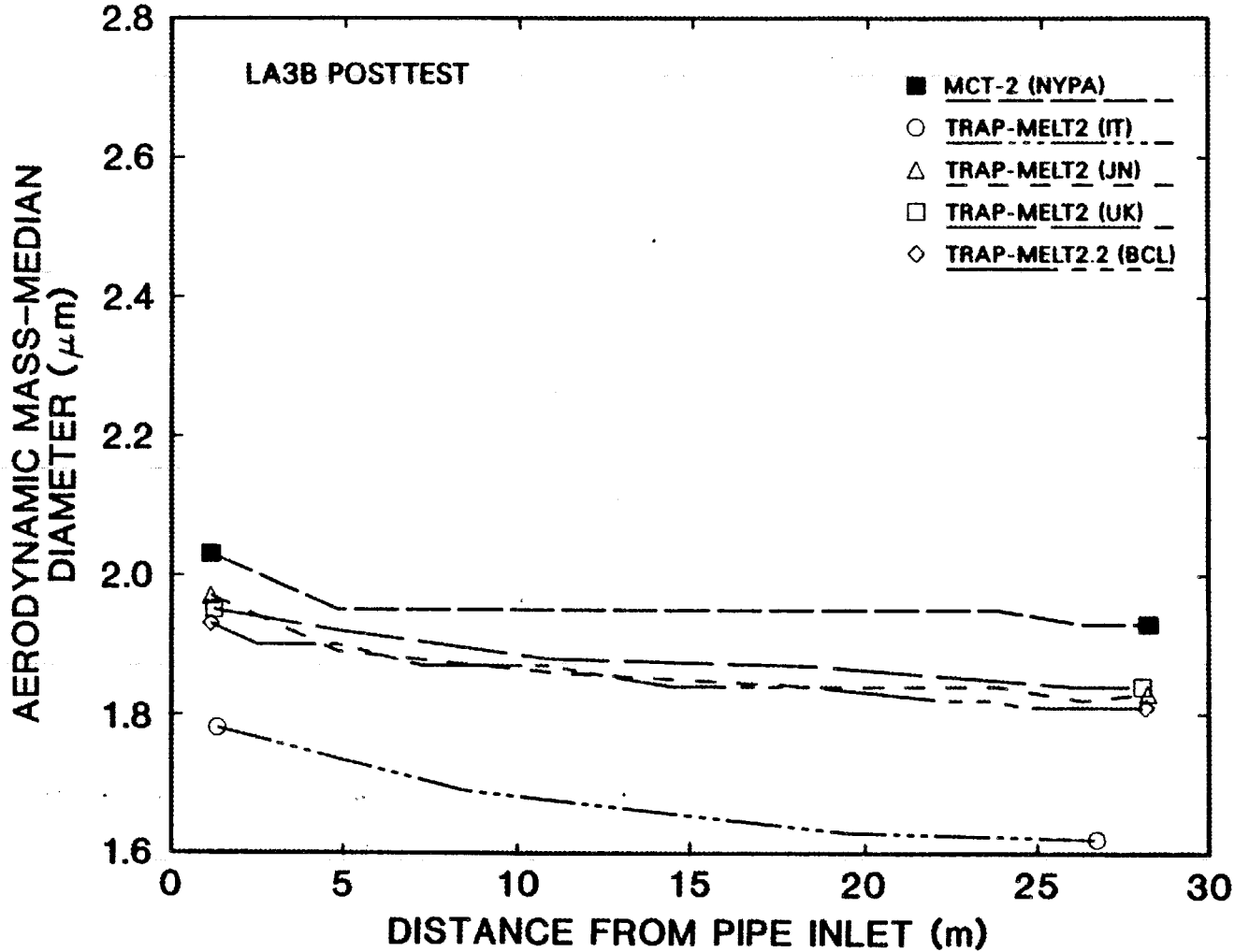


Fig. 27. LA3B posttest results: calculated aerodynamic mass-median diameter (AMMD) vs distance from pipe inlet at end of test (3,600 s), for codes that do include TRAP-MELT modeling.

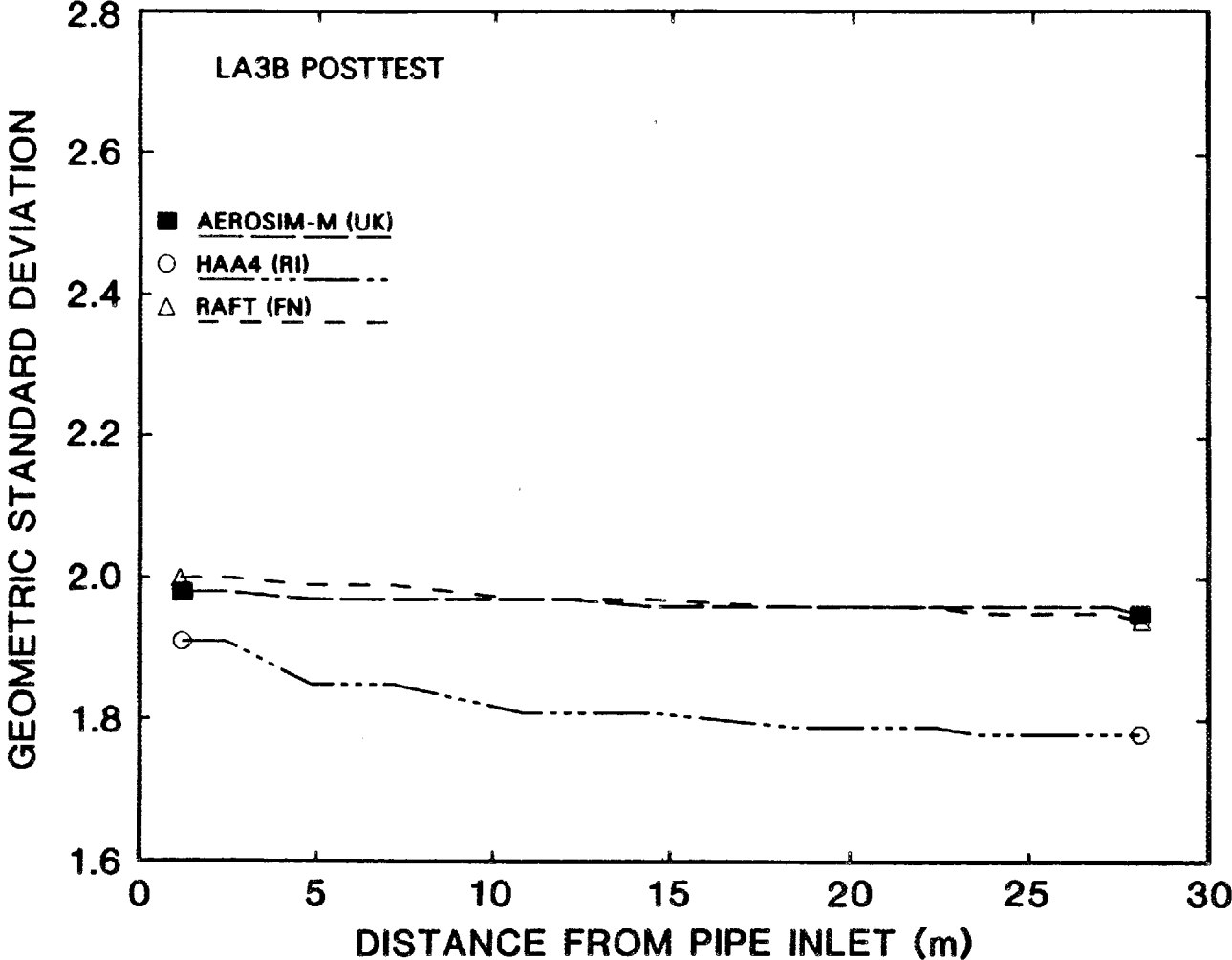


Fig. 28. LA3B posttest results: calculated geometric standard deviation (GSD) vs distance from pipe inlet at end of test (3,600 S), for codes that do not include TRAP-MELT modeling.

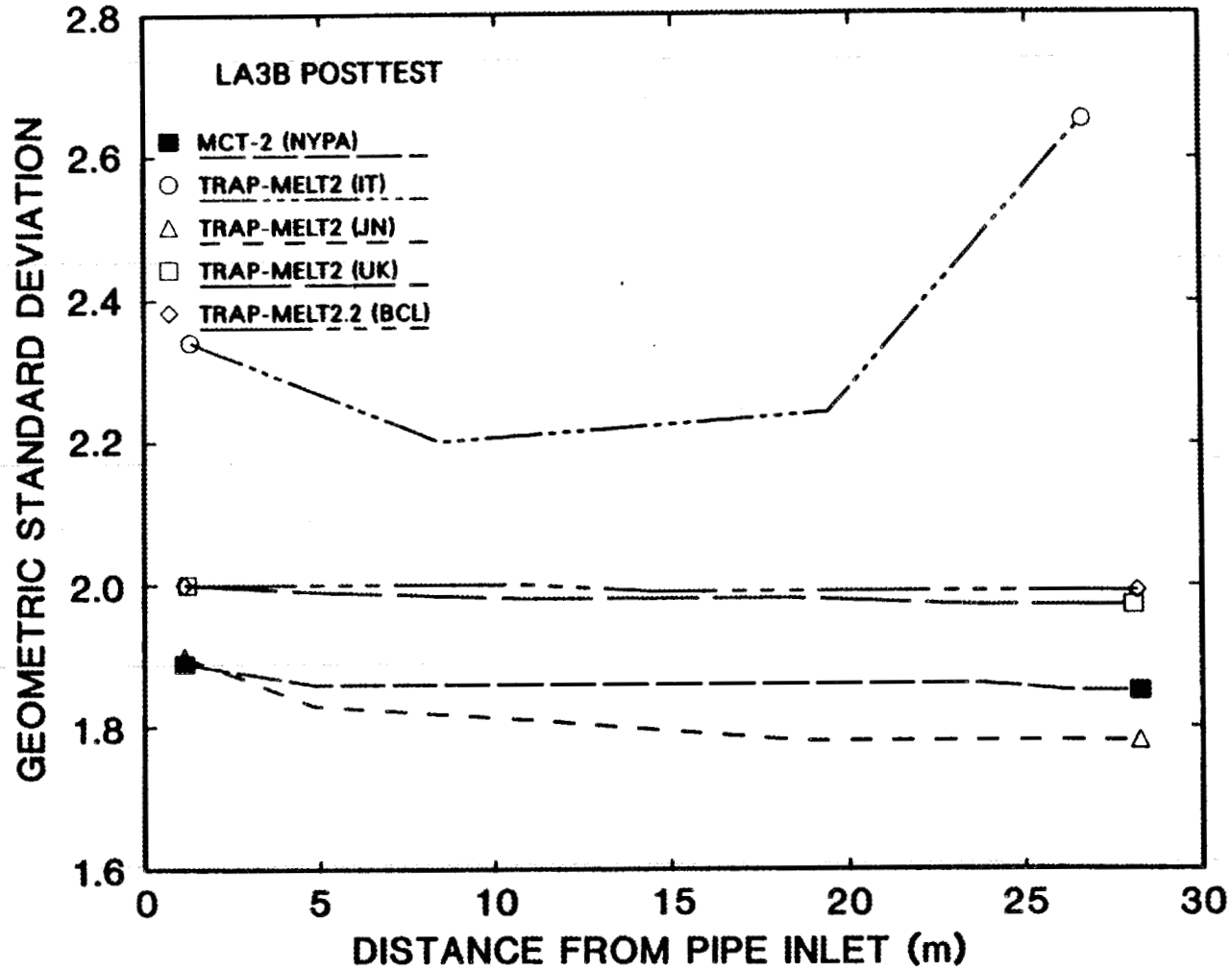


Fig. 29. LA3B posttest results: calculated geometric standard deviation (GSD) vs distance from pipe inlet at end of test (3,600 s), for codes that do include TRAP-MELT modeling.

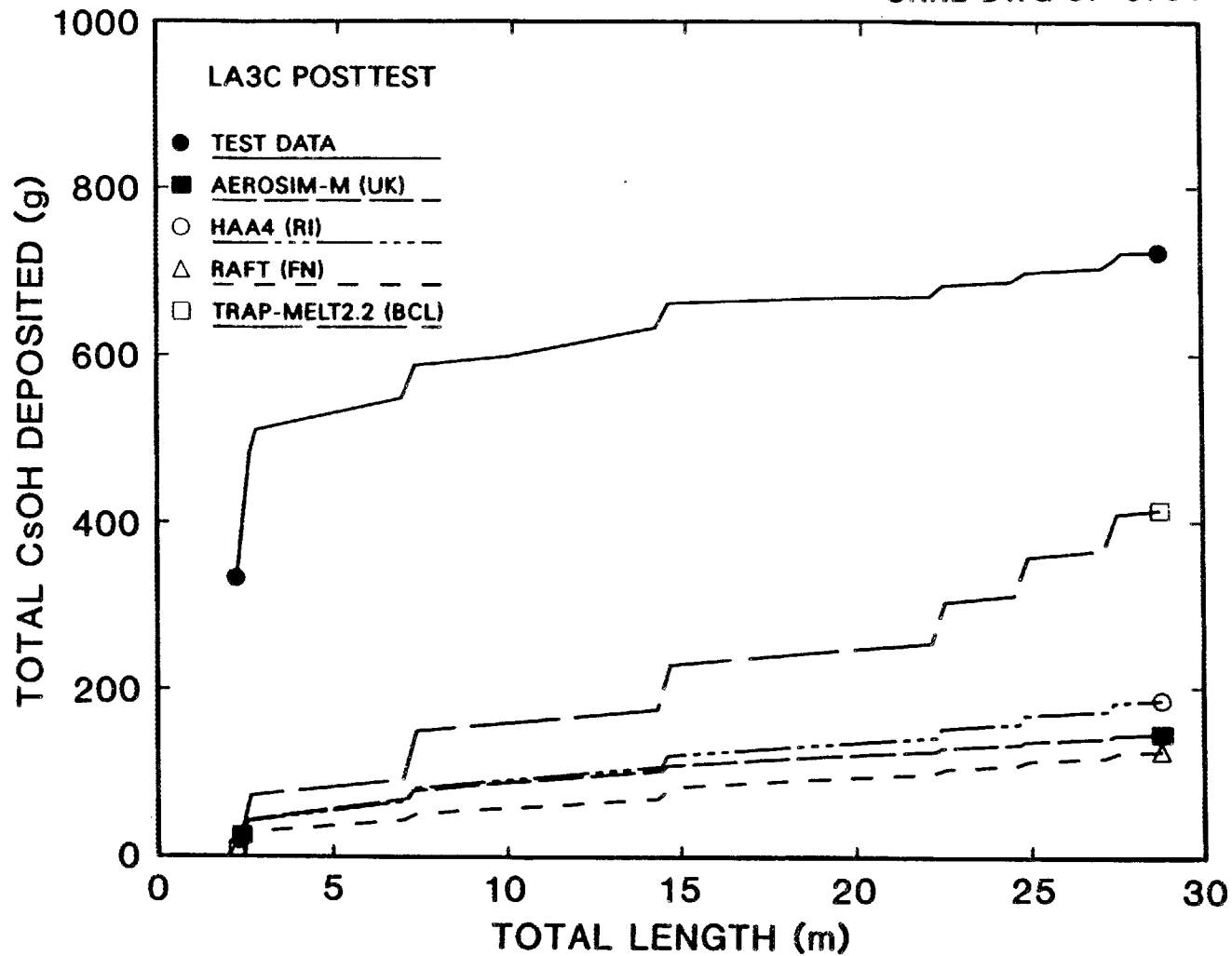


Fig. 30. LA3C posttest results: CsOH aerosol deposited in pipe vs distance from pipe inlet at end of test (3,600 s), for codes including bend deposition models.

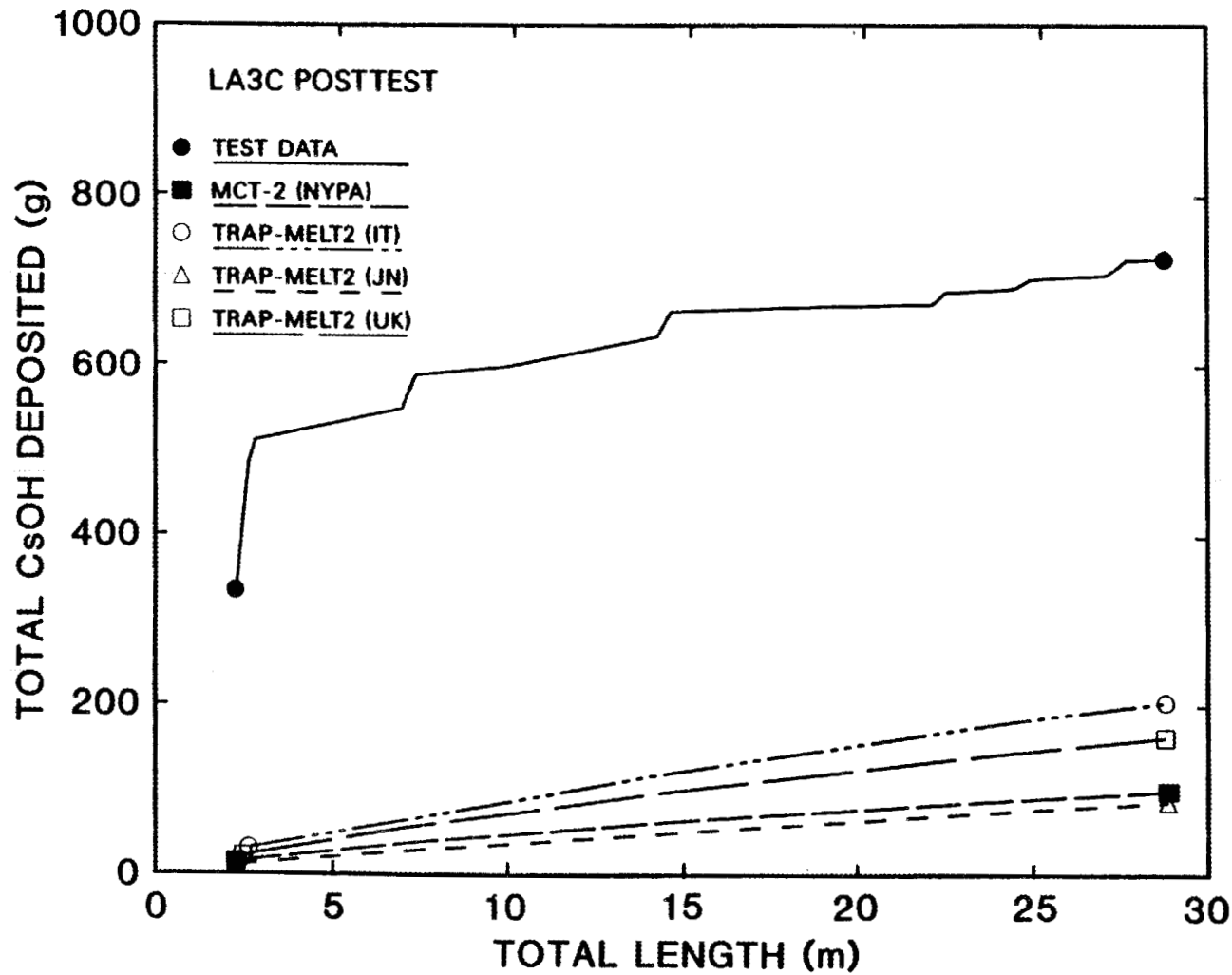


Fig. 31. LA3C posttest results: CsOH aerosol deposited in pipe vs distance from pipe inlet at end of test (3,600 s), for codes without bend

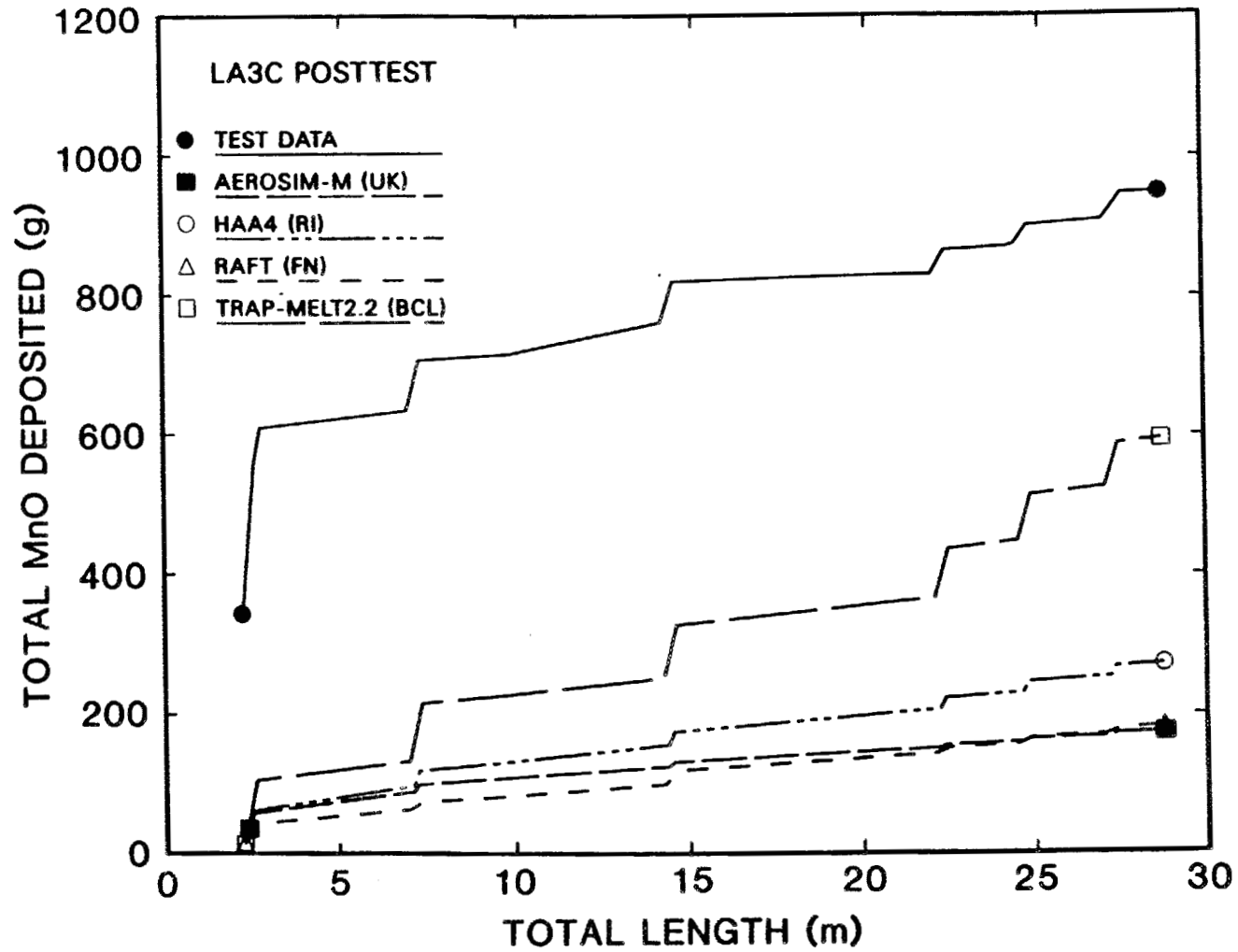


Fig. 32. LA3C posttest results: MnO aerosol deposited in pipe vs distance from pipe inlet at end of test (3,600 s), for codes including bend deposition models.

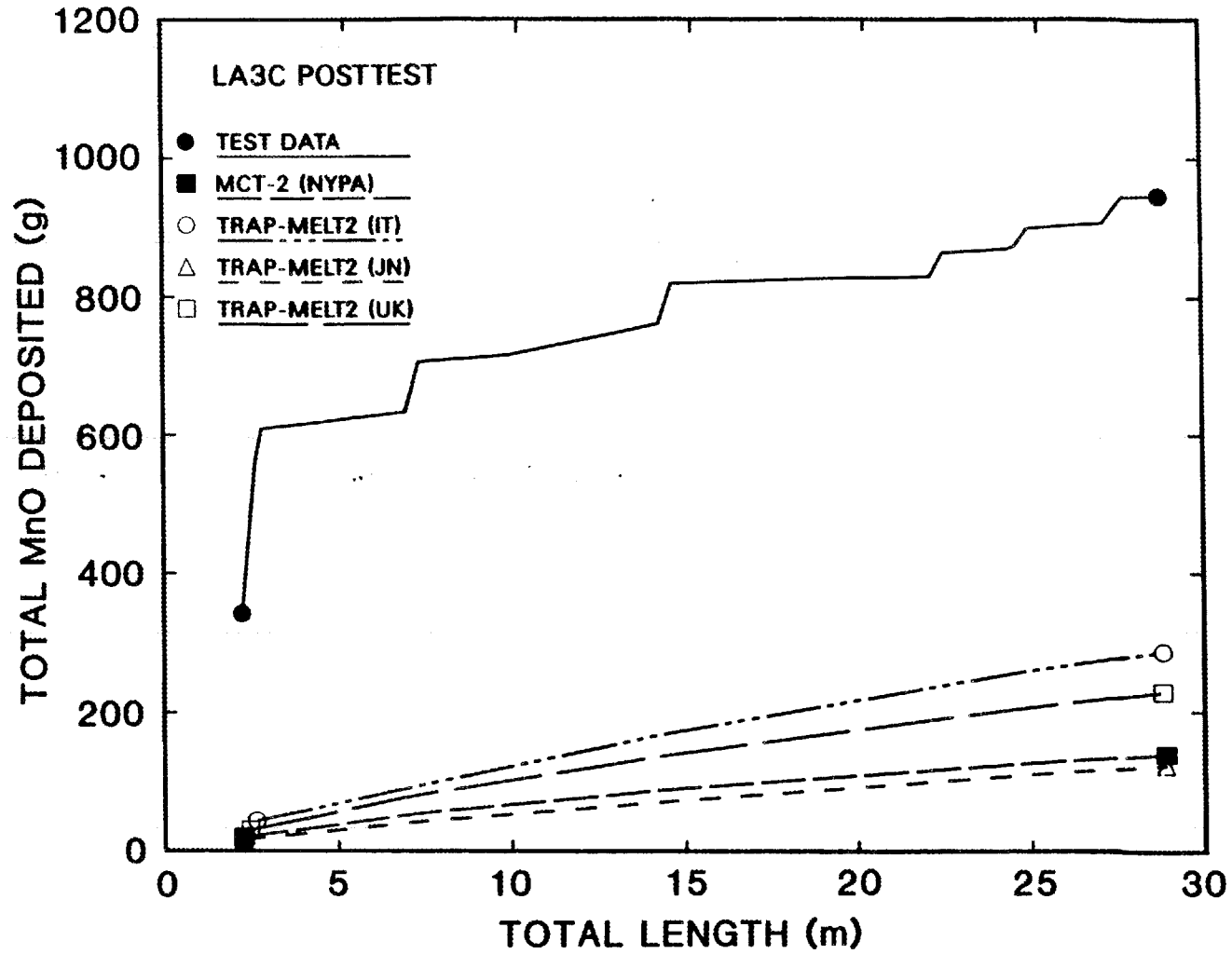


Fig. 33. LA3C posttest results: MnO aerosol deposited in pipe vs distance from pipe inlet at end of test (3,600 s), for codes without bend deposition models.

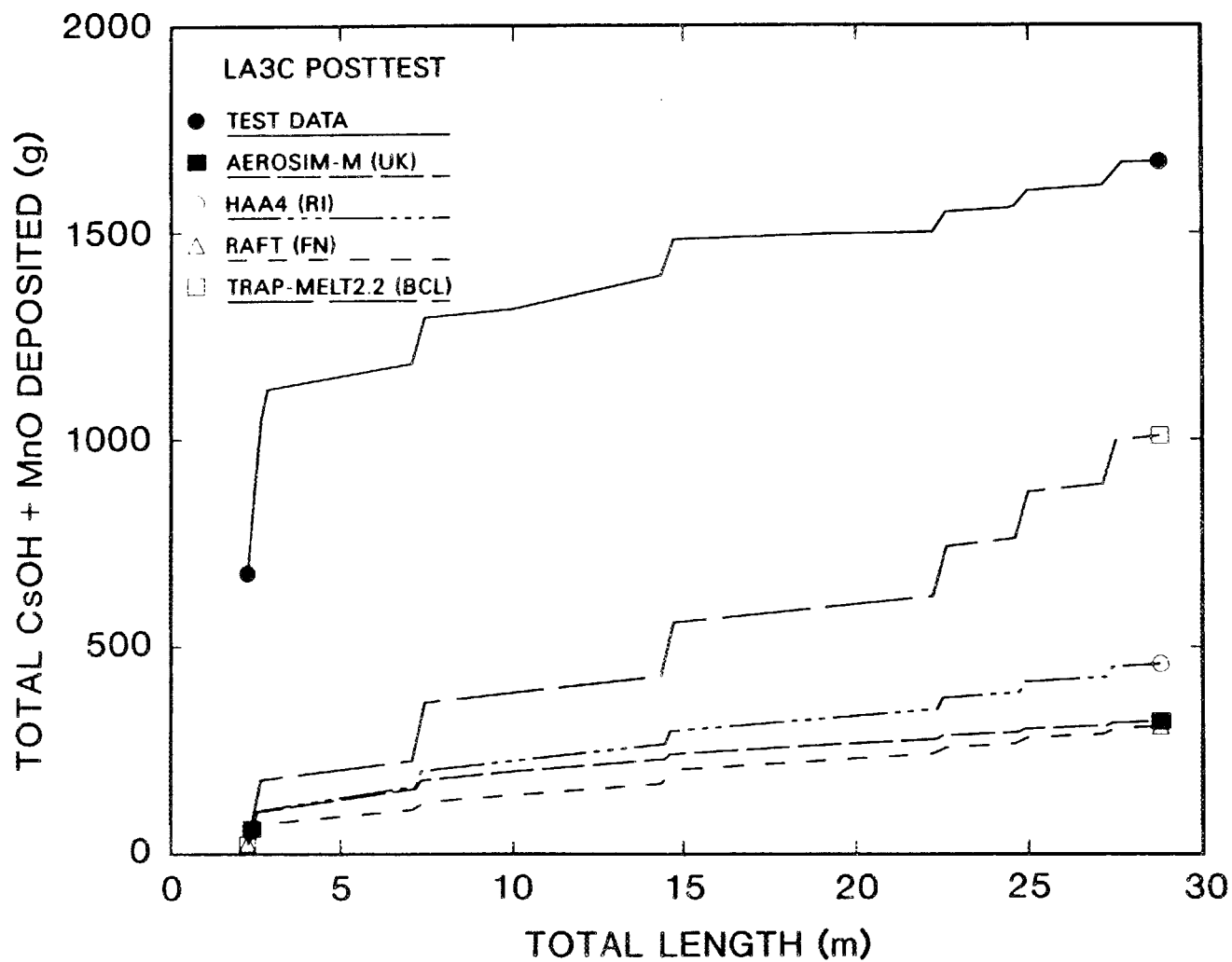


Fig. 34. LA3C posttest results: total (CsOH + MnO) aerosol deposited in pipe vs distance from pipe inlet at end of test (3,600 s), for codes including bend deposition models.

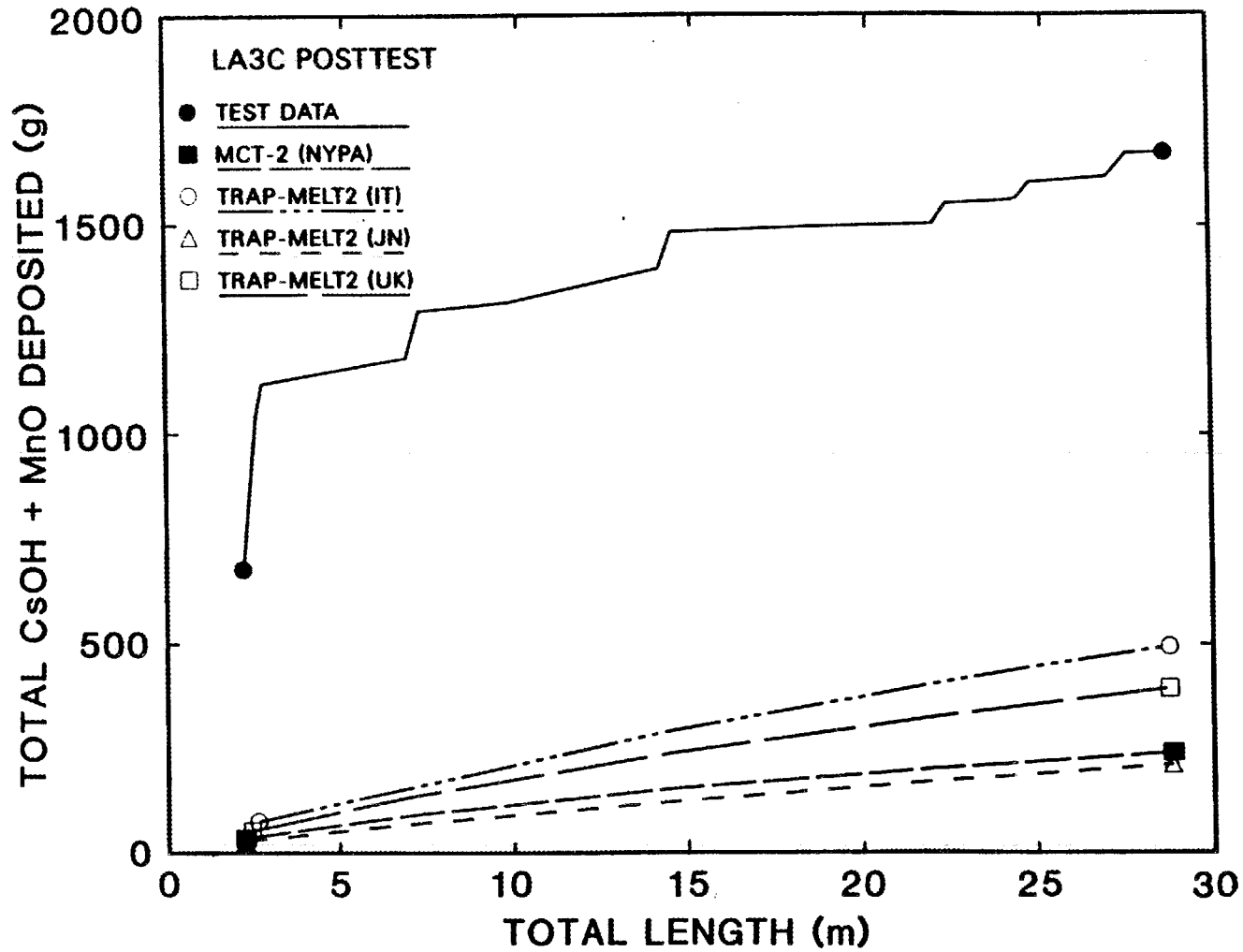


Fig. 35. LA3C posttest results: total (CsOH + MnO) aerosol deposited in pipe vs distance from pipe inlet at end of test (3,600 s), for codes without bend deposition models.

Table 22. Comparisons of measured and calculated aerosol deposition in pipe for test LA3C

Method	Total CsOH deposited (g)	Total MnO deposited (g)	Total aerosol deposited (g)
TEST DATA	724.7	945.1	1669.9
AEROSIM-M (UK)	148.3	172.3	320.6
HAA4 (RI)	188.4	269.7	458.2
RAFT (FN)	127.2	180.6	307.9
MCT-2 (NYPA)	188.4	269.7	458.2
TRAP-MELT2 (IT)	203.4	288.6	492.0
TRAP-MELT2 (JN)	86.0	124.2	210.2
TRAP-MELT2 (UK):			
time-averaged source size	162.0	230.1	392.1
time-dependent source size	160.8	228.3	389.1
TRAP-MELT2.2 (BCL)	416.0	591.8	1007.8

^aIn test LA3C, 87.8% of the Cs and 85.6% of the Mn input to the test equipment was recovered. This suggests that the uncertainties in the measured LA3C aerosol deposition data were ~12% for Cs and ~14% for Mn.

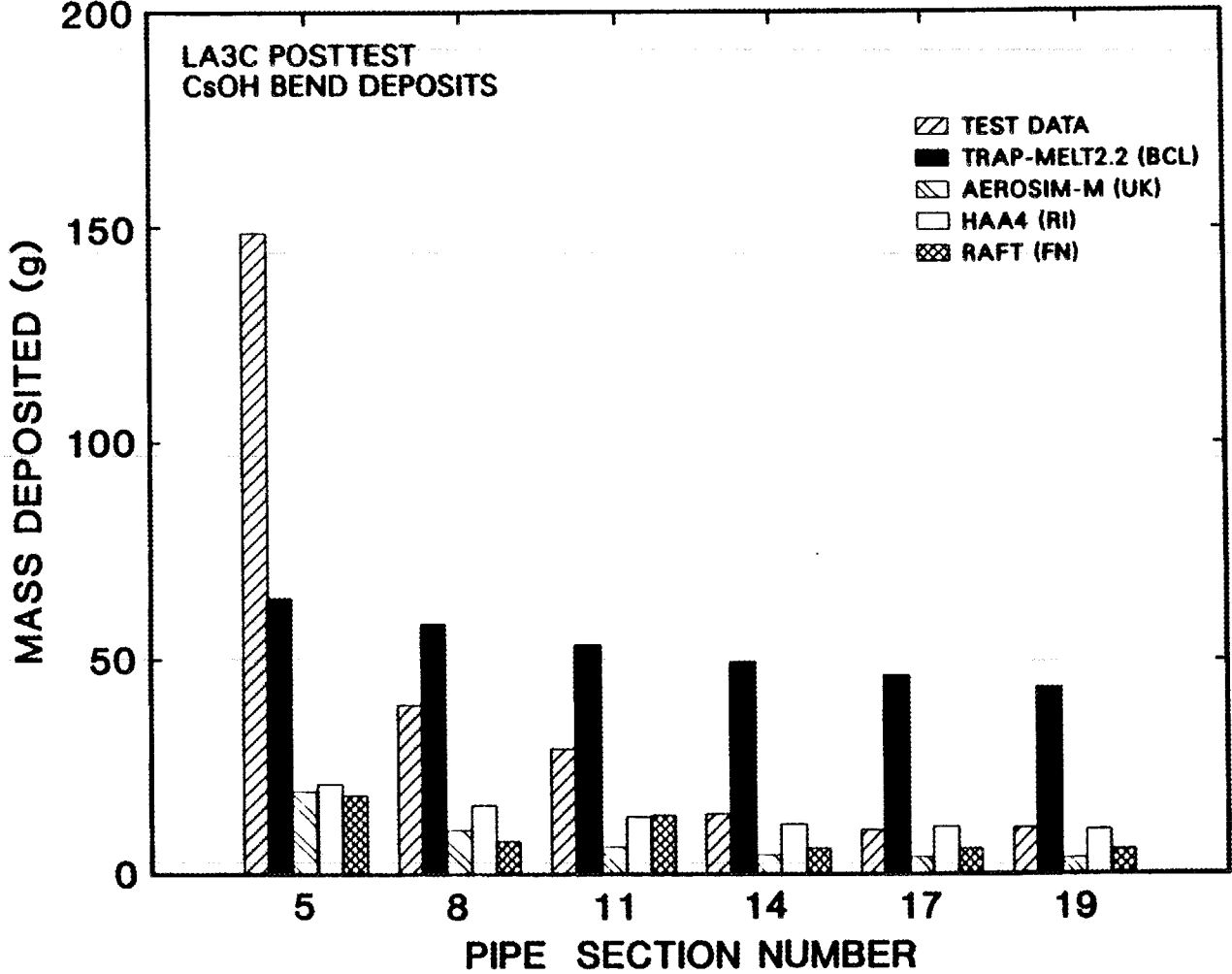


Fig. 36. LA3C posttest results: CsOH aerosol deposition in pipe bends at end of test (3,600 s).

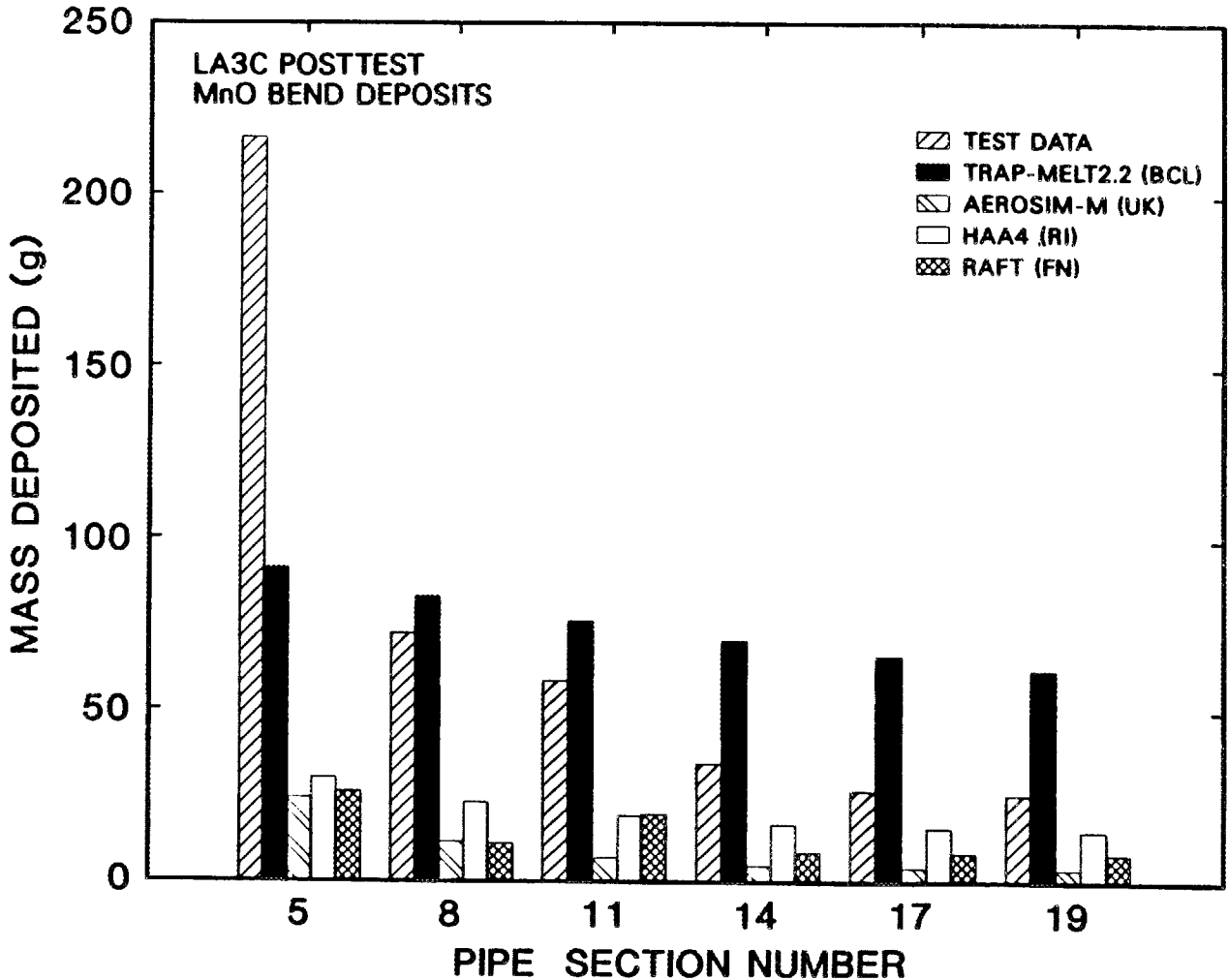


Fig. 37. LA3C posttest results: MnO aerosol deposition in pipe bends at end of test (3,600 s).

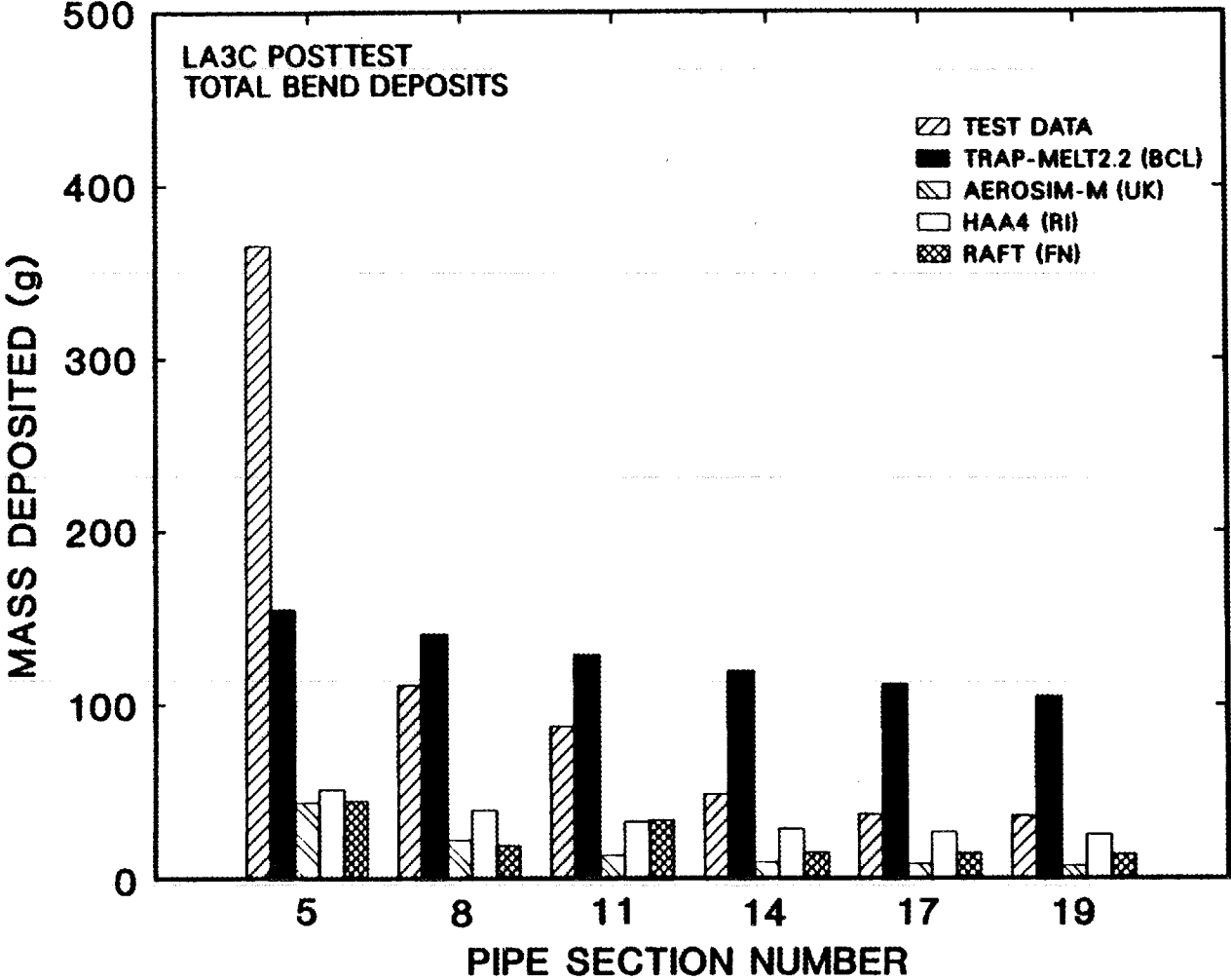


Fig. 38. LA3C posttest results: total (CsOH + MnO) aerosol deposition in pipe bends at end of test (3,600 s).

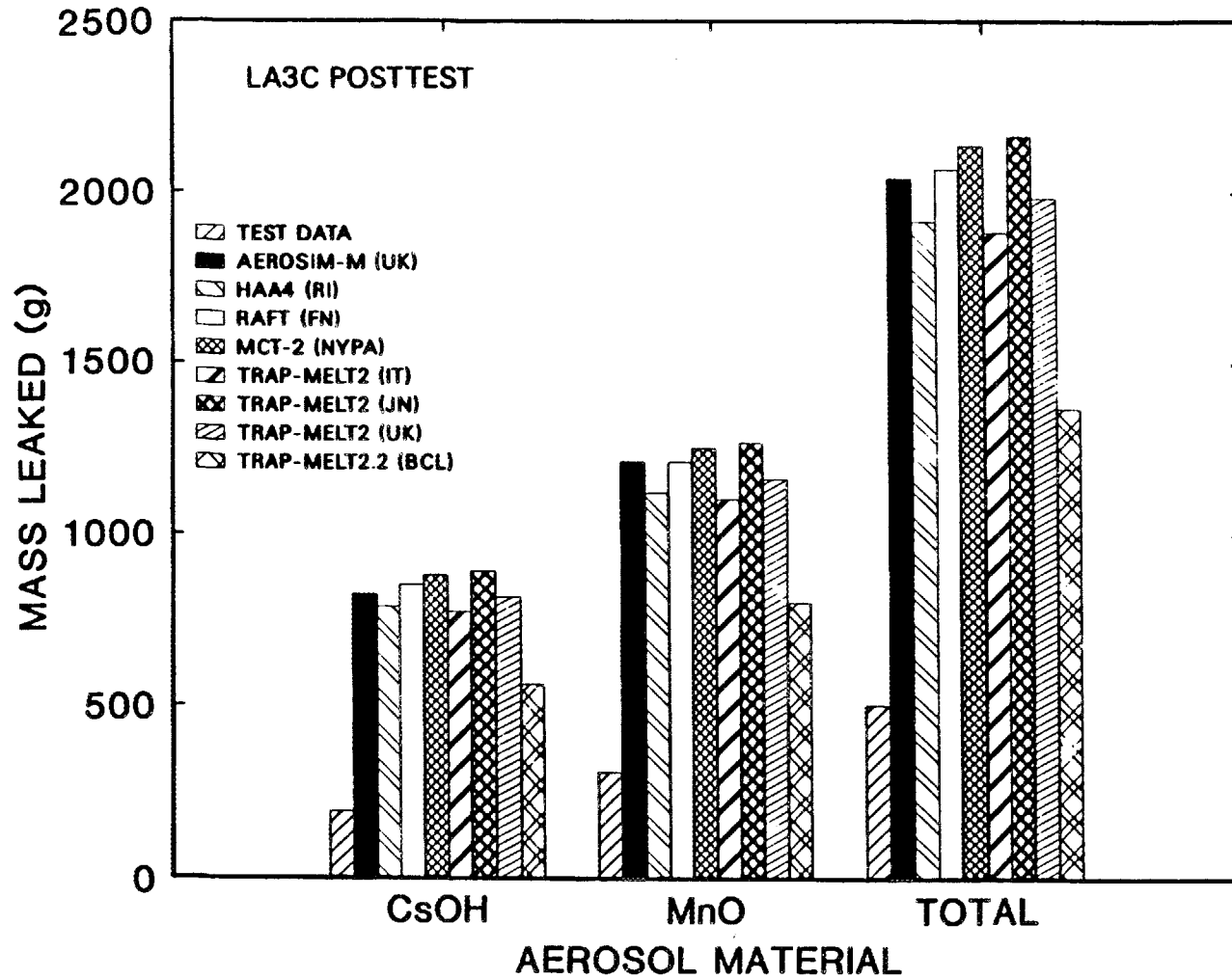


Fig. 39. LA3C posttest results: aerosol transport out of pipe at end of test (3,600 s).

Table 23. Comparisons of measured and calculated aerosol transport from pipe for test LA3C^a

Method	Total CsOH transported (g)	Total MnO transported (g)	Total aerosol transported (g)
TEST DATA	194.6	310.5	505.1
AEROSIM-M (UK)	826.2	1213.5	2039.7
HAA4 (RI)	790.6	1122.8	2066.7
RAFT (FN)	854.2	1212.5	2135.1
MCT-2 (NYPA)	882.5	1252.7	2135.1
TRAP-MELT2 (IT)	777.3	1104.6	1881.9
TRAP-MELT2 (JN)	894.4	1268.4	2162.8
TRAP-MELT2 (UK):			
time-averaged source size	819.3	1163.1	1982.5
time-dependent source size	820.6	1164.9	1985.5
TRAP-MELT2.2 (BCL)	565.1	803.9	1369.0

^aIn test LA3C, 87.8% of the Cs and 85.6% of the Mn input to the test equipment was recovered. This suggests that the uncertainties in the measured LA3C aerosol transport data were ~12% for Cs and ~14% for Mn.

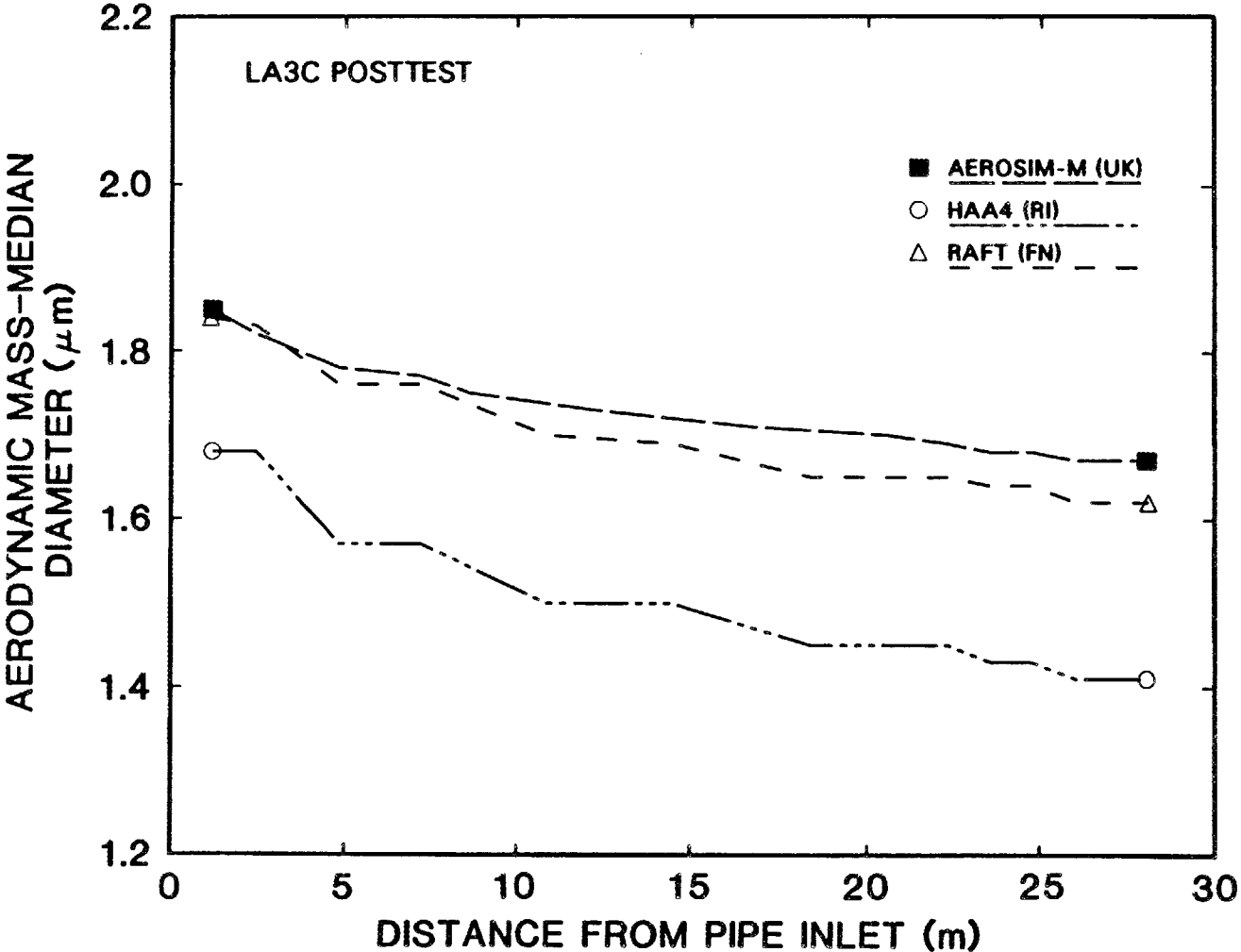


Fig. 40. LA3C posttest results: calculated aerodynamic mass-median diameter (AMMD) vs distance from pipe inlet at end of test (3,600 s), for codes that do not include TRAP-MELT modeling.

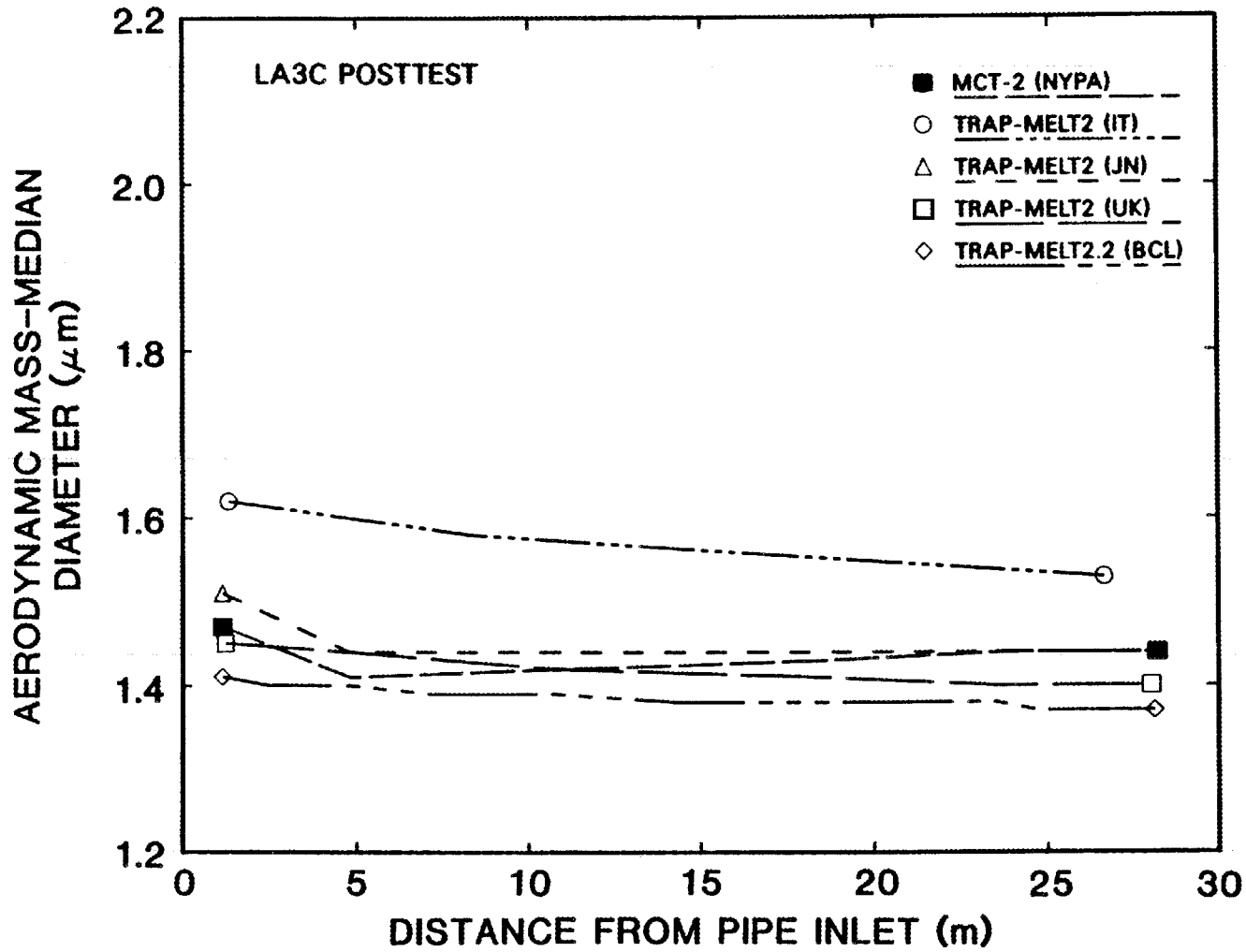


Fig. 41. LA3C posttest results: calculated aerodynamic mass-median diameter (AMMD) vs distance from pipe inlet at end of test (3,600 s), for codes that do include TRAP-MELT modeling.

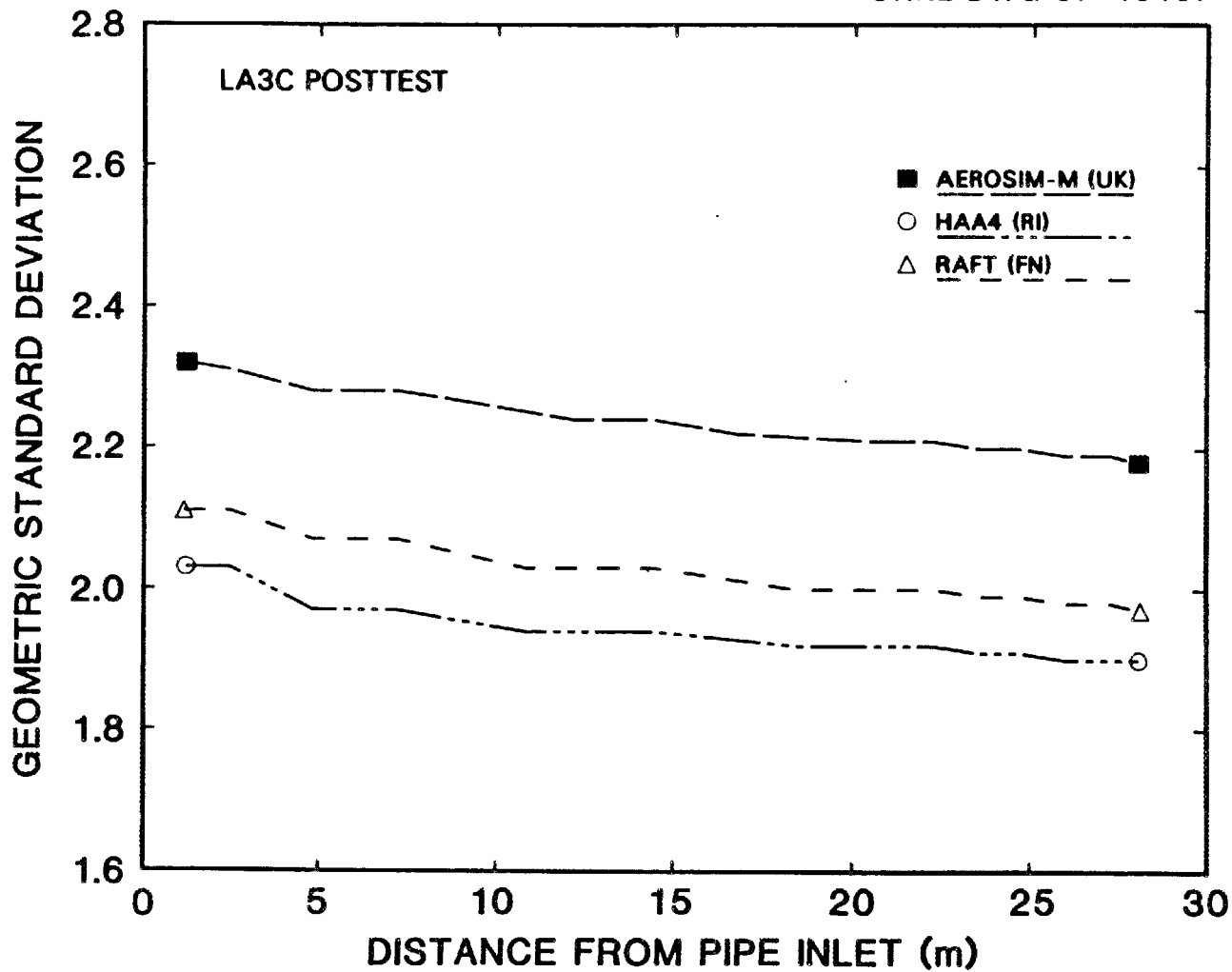


Fig. 42. LA3C posttest results: calculated geometric standard deviation (GSD) vs distance from pipe inlet at end of test (3,600 s), for codes that do not include TRAP-MELT modeling.

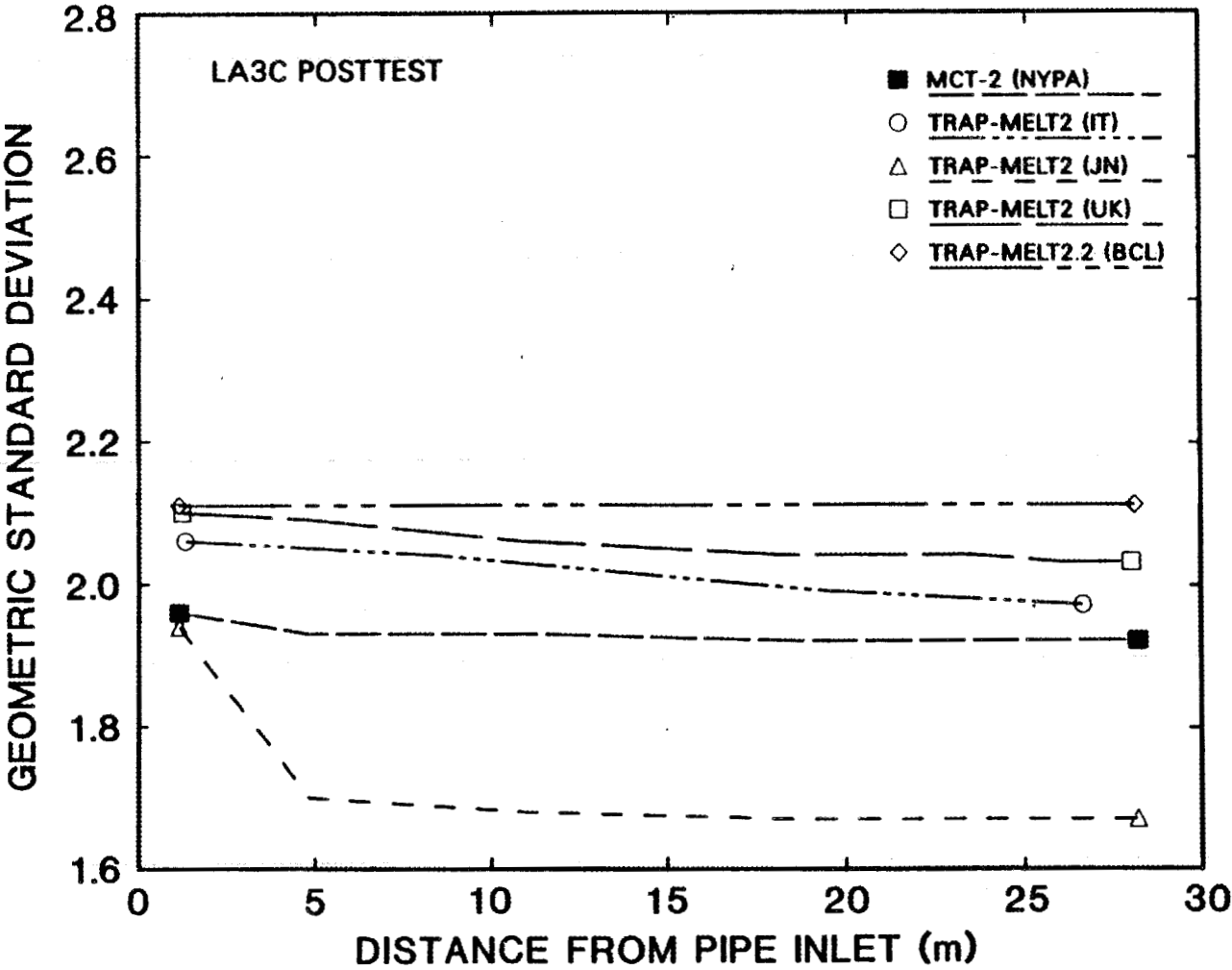


Fig. 43. LA3C posttest results: calculated geometric standard deviation (GSD) vs distance from pipe inlet at end of test (3,600 s), for codes that do include TRAP-MELT modeling.

4. DISCUSSION OF LA3 CODE-EXPERIMENT COMPARISON RESULTS

In this section, we will discuss the test results and the results of the code comparisons for each of the LA3 experiments.

4.1 TEST LA3A

As was noted in Sect. 2, this test was performed with a gas flow velocity of ~ 77 m/s and had an overall MnO/CsOH aerosol source mass ratio of ~ 5.0 . As was discussed in the LA3 test data report,² the test mass balance was good since 87.6% of the Cs, and 98.9% of the Mn input to the test equipment was recovered.

From the results presented in Table 12, we find that (1) 18.0% of the CsOH, 23.9% of the MnO, and 23.0% of the total aerosol recovered (pipe sections 4 through 21 and transport out of the pipe) was transported out of the pipe, (2) 46.5% of the CsOH, 44.3% of the MnO, and 44.7% of the total aerosol deposition in the pipe occurred in the pipe bends. These numbers illustrate that bend deposition was a major contributor to deposition in LA3A; and, on the basis of the overall deposition and transport results, the CsOH-MnO aerosol seemed to act largely as a mixed, coagglomerated aerosol in its transport through the test pipe.

Figure 44 is a plot of the measured aerosol deposit MnO/CsOH mass ratio, for each of the LA3A pipe sections (from the data presented in Table 12). In contrast to the total deposition results, variability in deposit mass ratio in different pipe sections suggests that the LA3A aerosol mixture did not act as a coagglomerated aerosol, and that perhaps the two species behaved, to some extent, as independent aerosol populations with different their size distributions. We in particular note that there was a slight enhancement of the deposition MnO/CsOH mass ratio for pipe bend sections 11, 14, 17, and 19.

The measured pipe-inlet and pipe-outlet aerosol size parameters for test LA3A (Table 15 in Sect. 3) illustrate the following interesting results:

1. For the CsOH aerosol component, at three-of-four of the sampling times, the measured outlet AMMD was less than the

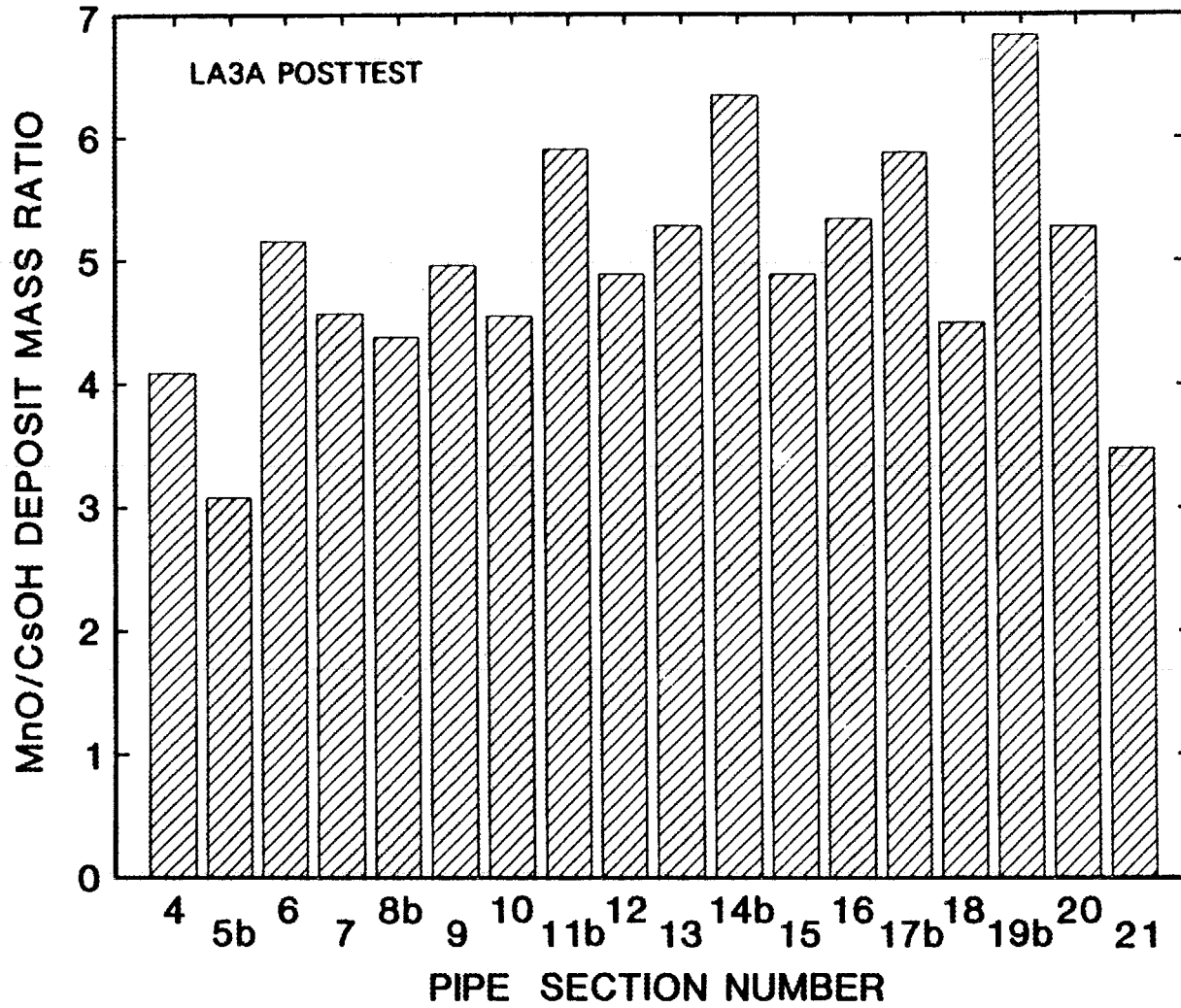


Fig. 44. Measured MnO/CsOH aerosol deposit mass ratio in each of the pipe sections for test LA3A.

measured inlet AMMD. This would be expected if no resuspension occurred, since turbulent inertial aerosol deposition and deposition in pipe bends is, based on available models, more effective for larger aerosol sizes.

However, for the MnO aerosol component, at three-of-four of the aerosol sampling times, the measured outlet AMMD was greater than that measured at the pipe inlet. An explanation for this observed difference in the MnO and CsOH behavior is that resuspension of MnO deposits occurred more readily than for the CsOH component, and that the resuspended MnO was larger in size than the material that initially deposited. This result is interesting and unexpected.

2. For both the CsOH and MnO aerosol components, the results in Table 15 show that the measured outlet GSD was larger than that at the pipe inlet. Stated another way, the aerosol at the pipe outlet was more polydisperse than the aerosol at the pipe inlet. This behavior could also have occurred as a result of aerosol resuspension in LA3A.

Before discussing the comparisons of the test and code results, it is instructive to investigate the models used in the codes to calculate turbulent-inertial deposition (the major turbulent deposition mechanism under the flow conditions in the LA3 test series) and to calculate aerosol deposition in pipe bends. Table 24 presents a summary of the sources of the models used in the various codes; they are documented in refs. 5 to 13.

The turbulent-inertial deposition models used in the TRAP-MELT2, TRAP-MELT2.2, MCT-2, and HAA4 codes were described in detail and compared against each other for LA3 test conditions in the LA3 pretest report.¹⁴ The model used in AEROSIM-M for the LA3 posttest calculations and the RAFT turbulent deposition model were not described previously so they will be presented here.

Table 24. Comparisons of modeling assumptions used in LA3 posttest pipe calculations

Code	Number of control volumes	Turbulent deposition model used	Bend deposition model used
AEROSIM-M (UK)	16	Correlation to Liu-Agarwal test data ^{5,6}	Modified turbulent deposition, for bend pressure loss ⁶
HAA4 (RI)	8	Correlation to Liu-Agarwal test data ^{5,7}	Transport efficiency equation in HAA4 manual ⁷
MCT-2 (NYPA)	8	Friedlander and Johnstone, ⁸ with Battelle modification ⁹	none
RAFT (FN)	13	Simplified Im-Chung, ¹⁰ from RAFT manual ¹¹	From equation presented in RAFT manual ¹¹
TRAP-MELT2 (IT)	5	Friedlander and Johnstone, ⁸ with Battelle modification ⁹	none
TRAP-MELT2 (JN)	8	Friedlander and Johnstone, ⁸ with Battelle modification ⁹	none
TRAP-MELT2 (UK)	8	Friedlander and Johnstone, ⁸ with Battelle modification ⁹	none
TRAP-MELT2.2 (BCL)	8	Wood, ^{12,13} using a surface roughness of 1.5 μm	Modified Wood turbulent deposition, for bend pressure loss ¹³

The turbulent deposition correlation used in AEROSIM-M⁶ is a new correlation to the Liu-Agarwal data; it has the following form:

$$V_{ASM} = 1.96 \cdot 10^{-5} \cdot \tau_+^2 \cdot u^* \quad \text{for } 0 < \tau_+ < 40, \quad (1)$$

$$V_{ASM} = -(6.27 \cdot 10^{-6} \cdot \tau_+^2 - 1.47 \cdot 10^{-3} \cdot \tau_+ + 0.01741) \cdot u^* \quad (2)$$

for $40 < \tau_+ < 120$,

$$V_{ASM} = -(7.46 \cdot 10^{-6} \cdot \tau_+ - 0.0696) \cdot u^* \quad \text{for } 120 < \tau_+ < 4000, \quad (3)$$

$$V_{ASM} = \text{AEROSIM-M turbulent-inertial deposition velocity,}$$

where

$$\tau_+ = \rho_p \rho_g d^2 C (u^*)^2 / (18 \mu^2 \chi), \quad (4)$$

τ_+ = dimensionless relaxation time,

ρ_p = gas density,

ρ_g = particle density,

d = particle diameter,

C = Cunningham slip-correction factor,

u^* = friction velocity = $U(f/2)^{0.5}$,

f = Darcy friction factor,

U = gas flow velocity through pipe,

μ = gas dynamic viscosity, and

χ = aerosol particle dynamic shape factor.

The Darcy fluid friction factor is calculated using a correlation by Swamee and Jain¹⁵ which is accurate for smooth and rough tubes:

$$f = 0.25 [\log_{10}(h/(3.7D) + 5.74/Re^{0.9})]^{-2}, \quad (5)$$

where

h = equivalent sand roughness height of pipe,
value of $1.5 \mu\text{m}$ used in calculations,

D = pipe diameter, and

Re = flow Reynolds number.

Note that this friction factor is roughly a factor of 4 larger than the typical Fanning friction factor used by most other codes to calculate u^* .

The turbulent deposition velocity correlation in the version of RAFT used for the LA3 posttest calculations has the following form: ^{10,11}

$$V_{RF} = v_a / (1 + v_a / v_f). \quad (6)$$

$$v_a = v_r' (1 / Sc_p)^{0.5} \quad (7)$$

$$v_r' = 0.9 u^*, \quad (8)$$

$$Sc_p = (\tau_f + \tau_p) / \tau_f, \quad (9)$$

$$v_f = 0.4 \cdot u^* / [Sc_p \cdot \{0.9 \cdot \ln(b_+ / S_+) + 13 \cdot (1/S_+ + 1/b_+) + 365 \cdot (1/S_+^2 - 1/b_+^2)\}], \quad (10)$$

$$\tau_p = \rho_p d^2 C / (18 \mu), \quad (11)$$

$$\tau_f = 2 \cdot b / (3 \cdot u^*), \quad (12)$$

$$S = v_a \cdot \tau_p, \quad S_+ = S / (\nu / u^*), \quad (13)$$

$$b = 100 \cdot \nu / u^*, \quad b_+ = b / (\nu / u^*) = 100, \quad (14)$$

where

V_{RF} = RAFT turbulent-inertial deposition velocity,

v_a = rms radial particle velocity at S,

v_r' = rms radial component of turbulence velocity,

u^* = friction velocity (based on Fanning friction factor),

Sc_p = particle Schmidt number,

τ_f = turbulent integral time scale,

τ_p = particle relaxation time,

S = stopping distance,

S_+ = dimensionless stopping distance,

b = buffer layer thickness,

b_+ = dimensionless buffer layer thickness, and

ν = gas kinematic viscosity.

These correlations were (as was done in the LA3 pretest report) compared with the deposition velocities measured in the Liu-Agarwal experiments,⁵ which were smooth-pipe experiments. For conditions simulating those in the LA3 experiments, deposition velocities calculated with the AEROSIM-M and RAFT models compared quite well with the Liu-Agarwal data.

Essentially, two different approaches were taken by the codes to calculate aerosol deposition in bends. The first approach was that taken by the modelers using the AEROSIM-M and TRAP-MELT2.2 codes. The bend models in these codes basically assume that enhanced aerosol deposition in bends occurs due to enhanced turbulent-inertial deposition. In AEROSIM-M, the bend pressure drop was calculated and from that an equivalent length of straight smooth pipe for which that bend pressure drop would occur was calculated. The bend deposition velocity was then assumed to be equal to the calculated turbulent deposition velocity multiplied by the ratio of the equivalent bend pressure-drop length to the actual bend length. In TRAP-MELT2.2, the pressure drop in the bend was also calculated using a correlation appropriate for smooth-wall pipe bends.¹⁶ The friction factor obtained from this calculation was then used to calculate, using a rough-pipe correlation,¹⁷ an "equivalent sand roughness" for the pipe wall that would give the same friction factor. This equivalent roughness was then used as input to the Wood turbulent deposition model¹² to calculate enhanced deposition in the bend.

A different approach to calculating deposition in bends was used in the HAA4 and RAFT calculations. These codes assumed that bend deposition was only due to inertial impaction on the upstream wall of the pipe bend. The aerosol parameter that is typically used to correlate bend deposition due to impaction is the Stokes number, which is defined as:

$$St = \rho_p d^2 C U / (9 \mu D), \quad (15)$$

where

- ρ_p = particle density,
- d = particle diameter,
- C = Cunningham slip-correction factor,
- U = mean gas-flow velocity through pipe,
- μ = gas dynamic viscosity, and
- D = pipe diameter.

In the HAA4 code, the efficiency of aerosol transport through bends was calculated using the following formula:⁷

$$E_{tb} = 1 - E_{db} = \exp[-(4/\pi) \cdot St \cdot (\theta/2)], \quad (16)$$

where

E_{tb} = aerosol transport efficiency through bend,

E_{db} = aerosol deposition efficiency in bend,

St = Stokes number defined in Eq. (15), and

θ = bend angle, in radians.

Another equation that is often used to calculate aerosol deposition in bends is the one derived in the paper by Crane and Evans:¹⁸

$$E_{tb} = 1 - E_{db} = 1 - St \cdot (\theta/2). \quad (17)$$

It can be noted that Eqs. (16) and (17) have the same functional form; in fact, for small values of the exponent in Eq. (16), the equation for E_{tb} becomes $E_{tb} = [1 - (4/\pi) \cdot St \cdot (\theta/2)]$, which is similar to Eq. (17). For a 90° bend and values of $St < 0.5$, Eq. (16) calculates slightly more bend deposition than does Eq. (17). However, for a 90° bend and for $St > 0.5$, the Crane-Evans equation (Eq. (17)) calculates more deposition in the bend. The differences, however, are not great; for example, for $St = 1$, Eq. (16) calculates 63% deposition in the bend while Eq. (17) calculates 79% deposition in the bend. The equation used in the RAFT code¹¹ is similar in form to Eq. (16):

$$E_{tb} = 1 - E_{db} = 1 - St_H \cdot (\theta), \quad (18)$$

where St_H is the particle Stokes number based on the bend height rather than the pipe diameter of the bend. Note that for bend heights $H > 2D$, where D is the pipe diameter, that Eq. (18) would calculate less deposition than Eq. (17), the Crane-Evans equation.

The results from the LA3A blind code comparisons were presented in Sect. 3 in Figs. 2 through 15 and Tables 18 and 19. A few initial comments on the code calculations are in order. First of all, the AEROSIM-M (UK) and TRAP-MELT2 (JN) calculations were performed with a time-averaged aerosol source; all other calculations were performed with the time-dependent aerosol source defined in Tables 3. The TRAP-MELT2 (IT) and TRAP-MELT2 (UK) calculations were performed with a time-dependent aerosol source size, while all other calculations were performed using the mean

source size defined in Table 6. In fact, two TRAP-MELT2 (UK) calculations were performed: one with time-independent and one with time-dependent source data (only the time-independent source size results for TRAP-MELT2 (UK) are shown in the plots). Finally, the comparison results shown are for $t=3,600$ s, the end of the aerosol source period. Results from the MCT-2 (NYPA) calculation were extrapolated results from a calculation time of 150 s, and the TRAP-MELT2 (JN) results were an extrapolation from results at 660 s; all other calculations were performed for the total 3,600 s source time.

It should be mentioned that, in the process of performing the TRAP-MELT2 (UK) calculations using a time-dependent aerosol source, the UK investigator discovered an error in the reference version of the TRAP-MELT2 code.¹⁹ It was discovered that the code did not appropriately use the time-dependent aerosol source size data provided to it as input. This coding error was corrected in all TRAP-MELT2 and in the MCT-2 calculations.

The overall aerosol deposition comparison results, in terms of the cumulative amounts of aerosol deposited as a function of distance from the pipe inlet, are presented in Figs. 2 to 7. Note that (for each aerosol species) the codes including a bend deposition model were included on one plot, and the codes without bend models were on a separate plot. Bar charts illustrating comparisons of aerosol deposition in the pipe bends are presented in Figs. 8 to 10. Comments on the data in these figures are presented below:

1. For each aerosol species, the first two bends made the major contribution to the total bend deposition. For example, 76% of the CsOH measured bend deposition and 65% of the MnO measured bend deposition occurred in the first two bends. The codes including bend models predicted a similar trend of larger deposition in the upstream bends. This would be expected, since all of the bend models would predict greater deposition of the larger particles.

2. All of the predicted deposition curves and the measured deposition curves tend to have an "exponential" shape, if one ignores the influence of the bends on the aerosol deposition patterns.
3. The curves illustrate that the TRAP-MELT2.2 (BCL) and the AEROSIM-M (UK) calculations seem to do the best job of predicting the overall aerosol deposition patterns in LA3A. Surprisingly, AEROSIM-M (UK) predicted the CsOH deposition pattern best (Fig. 2), while the TRAP-MELT2.2 (BCL) calculation did best at predicting the MnO deposition pattern (Fig. 4). We should recall that these two codes included similar types of bend deposition models.

A major reason why AEROSIM-M (UK) predicted the CsOH deposition well in LA3A is that the predicted CsOH deposition in the first pipe section was at least twice that predicted by the other codes. AEROSIM-M (UK) did not predict similar enhanced deposition in the first pipe section for the MnO aerosol.

4. The aerosol deposition patterns predicted by HAA4 (RI) were not significantly different from those predicted by the codes that did not include bend models; this situation occurred because HAA4 (RI) did not predict much bend deposition for LA3A test conditions.
5. The RAFT (FN) calculation did the least satisfactory job of predicting the measured aerosol deposition pattern. However, as was discussed earlier in this section, the turbulent-inertial deposition correlation used in RAFT calculates similar deposition velocities compared to correlations used in other codes. At present, we cannot explain why the RAFT calculation for LA3A predicted less deposition than the others.
6. All of the codes that did not include a bend deposition model were versions of TRAP-MELT2. All of these calculations predicted very similar aerosol deposition patterns. This suggests that these four investigators applied TRAP-MELT2 in very similar ways to predict the LA3A results.

7. The bend deposition results summarized in Figs. 8 to 10 illustrate that, for LA3A conditions, the bend models in HAA4 and RAFT consistently predict less bend deposition than the models in TRAP-MELT2.2 and AEROSIM-M. With the exception of the TRAP-MELT2.2 model, all of the bend models tended to underpredict deposition in bends. For the last three bends, the TRAP-MELT2.2 model over-estimated the amount of aerosol that was deposited in the bends.

Table 18 summarizes overall measured and calculated aerosol deposition results for LA3A. The data in this table show that most codes did a reasonable job of calculating the total deposition in test LA3A (even though many codes did not model bend deposition). For CsOH deposition in LA3A, the AEROSIM-M (UK) calculation underestimated deposition by a factor of 1.15, the RAFT (FN) calculation underestimated deposition by 3.8, and all other calculations underpredicted deposition by factors ranging from 1.3 to 2.0. For MnO deposition, the TRAP-MELT2.2 (BCL) calculation underpredicted deposition by a factor of 1.12, the RAFT (FN) calculation by 3.4, and all other calculations underestimated deposition by factors ranging from 1.5 to 1.8.

Because deposition in bends and turbulent-inertial deposition were both significant in test LA3A, it becomes difficult to assess with certainty how well the various turbulent-inertial models calculated the LA3A results. However, we should recall that roughly 40% of the measured aerosol deposition occurred in bends in LA3A. Noting that most of the codes that did not include bend models under-predicted measured aerosol deposition by about a factor of 2 or less suggests, then, that the turbulent inertial models did a reasonable job of calculating the deposition that occurred in the straight pipe segments in LA3A.

The overall deposition results for the TRAP-MELT2 (UK) calculation shown in Table 18 illustrate that, for LA3A conditions, using a time-dependent or time-averaged aerosol source had no major influence on the calculated overall deposition; in fact, the differences in these results was less than 1%.

Calculated LA3A overall aerosol leakage results are illustrated in Fig. 11 and Table 19. All codes calculated more aerosol transport from the pipe than was measured in LA3A. For CsoH transport, AEROSIM-M (UK) overpredicted leakage by a factor of 1.9, RAFT (FN) by a factor of 4.4, and all other calculations overestimated CsoH transport by factors ranging from 2.3 to 3.0. For MnO transport, the TRAP-MELT2.2 (BCL) calculation overestimated leakage by a factor of 1.7, the RAFT (FN) by 3.3, and all other calculations overpredicted MnO transport by factors ranging from 2.1 to 2.4.

Calculated aerosol size-distribution parameters for test LA3A are illustrated in Figs. 11 to 15. All results in the figures, except the ones from the TRAP-MELT2 (IT) calculation, were based on calculations performed with mean aerosol-source-size parameters. For LA3A, we recall from Table 15 that measured mean inlet and outlet aerosol size parameters were: $AMMD_{in} = 1.37 \mu m$, $AMMD_{out} = 1.05 \mu m$, $GSD_{in} = 1.97$, and $GSD_{out} = 3.14$. Comments on the aerosol size results include the following:

1. All of the AMMD results in Figs. 11 and 12, except those from the RAFT (FN), MCT-2 (NYPA), and TRAP-MELT2 (IT) calculations fall in a similar band. The fact that the predicted RAFT sizes were greater than those calculated with the other codes is consistent with the fact that RAFT calculated the least amount of aerosol deposition in the pipe. At present we cannot explain why the MCT-2 AMMD results should be slightly higher than those from the other TRAP-MELT2 calculations, although we note from Table 18 that MCT-2 calculated less overall deposition than the other TRAP-MELT-like codes.

The TRAP-MELT2 (IT) AMMD results were slightly lower than all of the other ones presented. However, this may be explainable by the fact that this calculation was done with a variable source size, and that the source AMMD measured at 53 min (Table 15) was less than the mean source-size value.

2. Calculated AMMD values at the pipe outlet ranged from 0.75 to $1.3 \mu m$. These values are reasonably close to the measured mean

outlet AMMD of 1.05 μm . Note that six of the eight calculations predicted outlet AMMD values in the range of 0.75 to 0.85 μm , a fairly narrow range.

3. The most interesting size-comparison result is that none of the code calculations predicted the measured increase in GSD from test LA3A. All codes predicted a decreased GSD for the aerosol that transported through the pipe. Predicted pipe-outlet GSD values ranged from 1.66 to 2.07.
4. The predicted values of GSD from the TRAP-MELT2 (IT) calculation were higher than calculated by the other codes. Again, however, we believe that this was the result of using a variable source size in this calculation.

4.2 TEST LA3B:

As was noted in Sect. 2, this test was performed with a gas flow velocity of ~ 25 m/s and had an overall MnO/CsOH aerosol source mass ratio of ~ 7.5 . As for LA3A and as was discussed in the LA3 test data report,² the test mass balance was good: 93.8% of the Cs and 89.7% of the Mn input to the test equipment was recovered.

From the results presented in Table 13, we find that (1) 44.7% of the CsOH, 49.9% of the MnO, and 49.3% of the total aerosol recovered was transported out of the pipe, (2) 84.3% of the CsOH, 92.1% of the MnO, and 91.2% of the total aerosol deposition in the pipe occurred in the pipe bends. The bend deposition in LA3B as a fraction of the total deposition, was even larger than in test LA3A, and accounted for almost all of the aerosol deposition that occurred.

As in LA3A, the overall deposition results suggest that the aerosol existed largely as a mixed co-agglomerated aerosol in its transport through the test pipe. However, the measured aerosol deposit MnO/CsOH mass ratio results presented in Fig. 45 suggest that the LA3B aerosol may not have been fully coagglomerated. These results show that in all of the straight pipe sections except section 18, the measured MnO/CsOH deposit ratio was significantly less than the average aerosol-source value of

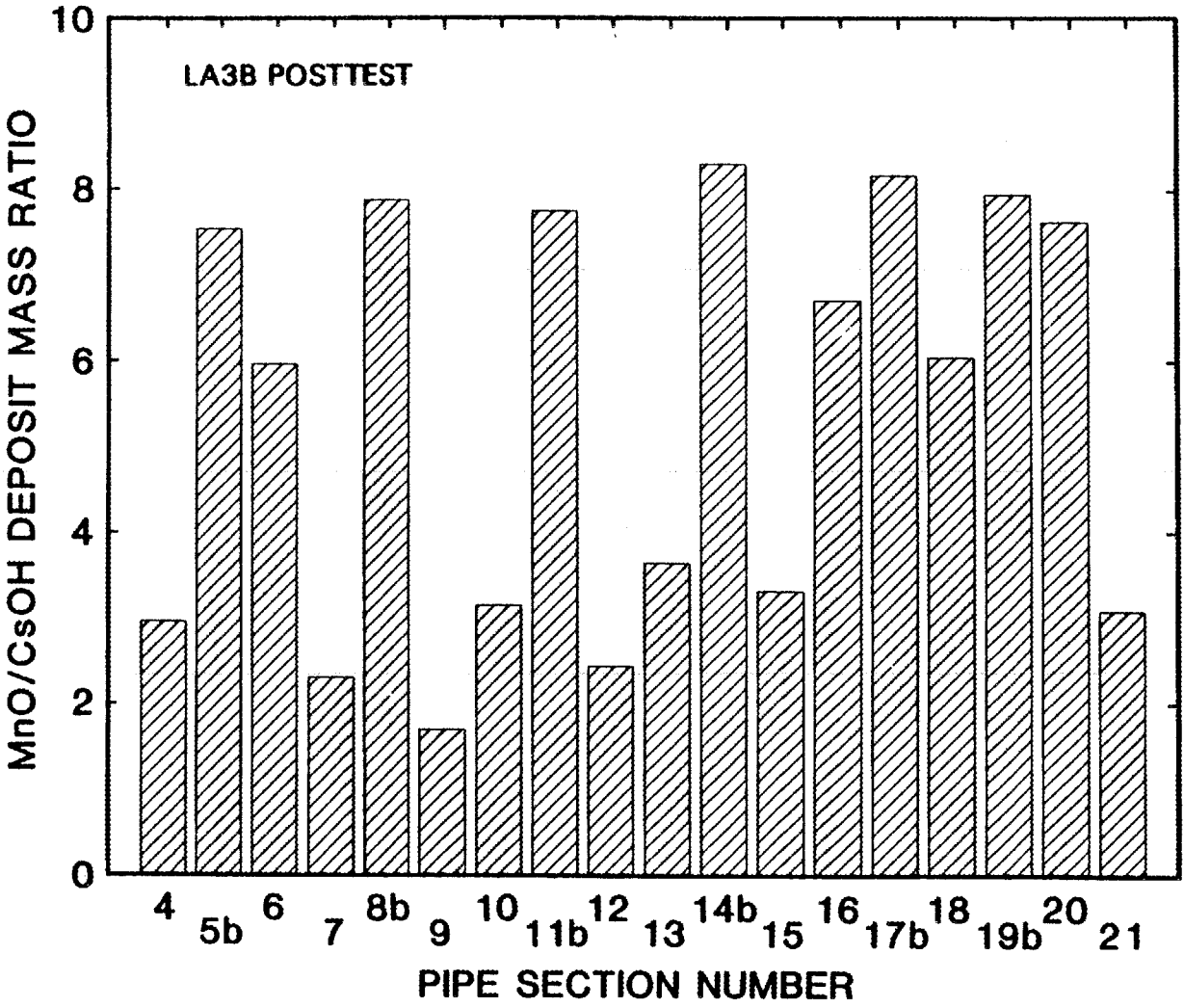


Fig. 45. Measured MnO/CsOH aerosol deposit mass ratio in each of the pipe sections for test LA3B.

7.5. This result either suggests that the MnO deposited in straight sections was easier to resuspend than the CsOH aerosol, or that the aerosol was not co-agglomerated and that MnO deposited less efficiently, due to a different particle size distribution, in the straight pipe sections.

The measured pipe-inlet and pipe-outlet aerosol size parameters for test LA3B are presented in Table 16 in Sect. 3. In contrast to the aerosol-size results for test LA3A (Table 15), the LA3B results were "as expected" in that, for both the CsOH and MnO components, the measured outlet AMMD values were less than those measured at the pipe inlet. For some of the sampling times, the outlet GSD was slightly larger than the inlet one; however, the differences in the inlet and outlet values for these times were well within expected 25% uncertainty in the GSD measurement.² For the most part, it can be stated that for LA3B the outlet GSD values were less than measured at the pipe inlet.

The results from the LA3B blind code comparisons were presented in Sect. 3 in Figs. 16 through 29 and Tables 20 and 21. For the most part, the way that all LA3B calculations were performed was similar to the way that LA3A calculations were performed. The comparison results shown are for $t=3,600$ s, the end of the aerosol source period. Results from the MCT-2 (NYPA) calculation were extrapolated results from a calculation time of 576 s; all other codes calculated the full 3,600 s of the experiment.

The overall aerosol deposition comparison results, in terms of the cumulative amounts of aerosol deposited as a function of distance from the pipe inlet, are presented in Figs. 16 to 21. For each aerosol species, the codes including a bend deposition model were included on one plot, and the codes without bend models were on a separate plot. Bar charts illustrating comparisons of aerosol deposition in the pipe bends are presented in Figs. 22 to 24. Comments on the data in these figures are presented below:

1. The most striking result from the LA3B test is the amount of aerosol deposition that occurred in the pipe bends. Roughly 90% of the LA3B deposition occurred in bends.

2. Another major result from the LA3B test comparison is the excellent agreement between the TRAP-MELT2.2 (BCL) results and the test results. This, however, is partly due to the fact that underprediction of bend deposition is compensated for by overprediction of deposition in straight sections. The comparisons of bend deposition in Figs. 22 to 24 do however, illustrate the good agreement in predicted LA3B bend deposition by TRAP-MELT2.2. These results suggest that there is some merit to the bend-modeling approach used in TRAP-MELT2.2.
3. The deposition patterns predicted by all of the other codes, neglecting the small amounts of bend deposition predicted by the codes including bend models, were quite similar. With the exception of the TRAP-MELT2.2 calculation, none of the codes was able to satisfactorily predict the deposition pattern observed in the LA3B test.
4. If we look at the results from the "TRAP-MELT-like" calculations where bend modeling was not included, we see that the TRAP-MELT2 (UK) and TRAP-MELT2 (IT) deposition patterns were similar to each other, while the TRAP-MELT2 (JN) and MCT-2 (NYPA) results were similar to each other but not to the other TRAP-MELT2 results. For these TRAP-MELT2 LA3B calculations, turbulent-inertial deposition was the major deposition mechanism. The similarities and differences in these results can be explained solely by looking at the differences in calculated turbulent-inertial deposition velocities; these ranges were: (1) for TRAP-MELT2 (UK): 0.93 to 0.33 cm/s, (2) TRAP-MELT2 (IT): 0.90 to 0.27 cm/s, (3) TRAP-MELT2 (JN): 0.30 to 0.10 cm/s, and (4) MCT-2 (NYPA): 0.35 to 0.10 cm/s. We cannot, however, presently explain why the different TRAP-MELT calculations produced different results for calculated turbulent-inertial deposition velocities.
5. A close look at the comparison results presented in Figs. 16 to 21 shows that many of the codes - particularly those codes that did not include a bend deposition model - predicted more

deposition in the straight sections of pipe than was measured in test LA3B. The graphical results illustrate that, even in the upstream sections of pipe, the measured deposition profiles in the straight sections were nearly flat. This result is indicated more clearly in Table 13, where we see that the maximum amount of aerosol (CsOH + MnO) deposited in any of the straight sections of pipe was less than 20 g. Even for the TRAP-MELT2.2 (BCL) calculation, where significant bend deposition was predicted, the deposition in the straight pipe sections was over-estimated.

A major reason for this comparison result is that most calculations significantly under-estimated bend deposition, so there was a greater driving force for deposition (due to higher airborne concentrations) in the straight pipe sections. Another possible explanation, however, is that aerosols initially deposited in straight sections could have been resuspended from these sections and carried downstream.

6. The comparisons of the calculated bend-deposition by the various models (Figs. 22 to 24) produced somewhat different conclusions than for LA3A. As discussed previously, the TRAP-MELT2.2 (BCL) calculation did an excellent job of predicting the LA3B bend deposition. However, for LA3B, the Stokes-number impaction models in HAA4 and RAFT predicted more bend deposition than did the turbulence-effect model in the AEROSIM-M (UK) calculation. This differs from the LA3A result, where the AEROSIM-M (UK) model predicted more bend deposition.

Table 20 summarizes overall measured and calculated aerosol deposition results for LA3B. Even though bend deposition was relatively more important in LA3B than in LA3A, the uncertainties in the total calculated amounts of aerosol deposition for LA3B were similar to those for LA3A. For CsOH deposition in LA3B, the TRAP-MELT2.2 (BCL) calculation underestimated deposition by only a factor of 1.01, the MCT-2 (NYPA) calculation underestimated deposition by 3.2, and all other calculations underpredicted deposition by factors ranging from 1.7 to 3.2. For MnO

deposition, the TRAP-MELT2.2 (BCL) calculation overpredicted deposition by only a factor of 1.05, the MCT-2 (NYPA) calculation underpredicted deposition by a factor of 3.0, and all other calculations underestimated deposition by factors ranging from 1.5 to 2.9.

The overall deposition results for the TRAP-MELT2 (UK) calculation shown in Table 20 illustrate that, as in the LA3A calculations, using a time-dependent or time-averaged aerosol source had no major influence on the calculated overall deposition; the differences in these results were less than 4% (compared to 1% for LA3A).

Calculated LA3B overall aerosol leakage results are illustrated in Fig. 25 and Table 21. As for LA3A, all codes calculated more aerosol transport from the pipe than was measured in test LA3B. For CsOH transport, TRAP-MELT2.2 (BCL) overpredicted leakage by a factor of 1.24, MCT-2 (NYPA) and TRAP-MELT2 (JN) by a factor of 2.0, and all other calculations overestimated CsOH transport by factors ranging from 1.7 to 1.9. For MnO transport, the TRAP-MELT2.2 (BCL) calculation overestimated leakage by a factor of 1.07, the MCT-2 (NYPA) calculation by 1.7, and all other calculations overpredicted MnO transport by factors ranging from 1.5 to 1.7. The agreement in leaked-mass calculations is better for LA3B than for LA3A because a larger fraction of the aerosol source mass was transported out of the pipe in LA3B.

Calculated aerosol size-distribution parameters for test LA3B are illustrated in Figs. 26 to 29. All results in the figures except the ones from the TRAP-MELT2 (IT) calculation were based on calculations performed with mean aerosol-source size parameters. For LA3B, we recall from Table 16 that measured mean inlet- and outlet- aerosol size parameters were: $AMMD_{in} = 2.42 \mu m$, $AMMD_{out} = 1.77 \mu m$, $GSD_{in} = 2.01$, and $GSD_{out} = 1.82$. Comments on the aerosol size results include the following:

1. There were significant differences among the AMMD profiles calculated by different versions of the TRAP-MELT code and by the other codes (RAFT, AEROSIM-M, and HAA4). The results in Figs. 26 and 27 show that, for all of the TRAP-MELT

calculations, the calculated AMMD in the first pipe section modeled was between 2.03 and 1.78 μm , a significant drop from the aerosol-source value of 2.42 μm . The AMMD calculated by HAA4 in the first section was roughly 2.15 μm , but the values calculated by AEROSIM-M and RAFT were greater than 2.3 μm . Another difference is that the AMMD profiles calculated by the different TRAP-MELT versions tended to be "flatter" - less change in AMMD from the first pipe section modeled to the last - than the profiles calculated by the other codes.

We believe that this difference is caused largely by, as was discussed in the LA3 pretest report,¹⁴ the fact that the TRAP-MELT code incorrectly calculates the aerosol AMMD and, in fact, tends to under-estimate it. Appendix A presents a letter that was sent to us by the UKAEA Winfrith staff; it discusses modifications that they have made to TRAP-MELT AMMD calculations. As for the LA3A calculations, the TRAP-MELT2 (IT) calculation was performed with a variable source size. However, the source size used for times near 3,600 s was about 2.5 μm , significantly greater than the value of 1.78 μm calculated for the first pipe section.

2. There were also differences among the profiles calculated by the RAFT, AEROSIM-M, and HAA4 codes. In addition, the downward slope of the AMMD curve calculated by HAA4 was slightly greater than that calculated by AEROSIM-M and RAFT. We believe that these differences can partially be explained by the fact that, for LA3B, the RAFT (FN) calculation predicted less deposition in the first pipe section and for the whole pipe than was predicted by HAA4 and AEROSIM-M; therefore, we would expect less change in the RAFT aerosol size. In addition, the observed differences may also be the result of the fact that the HAA4 calculation does not model aerosol agglomeration whereas the other calculations do include agglomeration.

3. The outlet AMMD values predicted by the various TRAP-MELT and HAA4 calculations were closer to the measured mean value of 1.77 μm than were the results from the RAFT and AEROSIM-M calculations. However, this comparison is probably not meaningful since the TRAP-MELT versions incorrectly calculate the AMMD.
4. All codes, except the TRAP-MELT2 (IT), calculated that the aerosol GSD at the pipe outlet was less than the inlet value which is consistent with the measured mean values for test LA3B. Calculated outlet GSD values - excluding the TRAP-MELT2 (IT) one - ranged from 2.0 to 1.8 which compared well to the measured mean outlet value of 1.82.

In the TRAP-MELT2 (IT) calculation, the GSD decreased from 2.34 in pipe sections 4 and 5 to 2.24 in sections 11 to 16; however, the GSD then increased to a value of 2.65 in pipe sections 17 to 21. This does not make physical sense in terms of the modeling approach used in TRAP-MELT2 and suggests a numerical instability in the TRAP-MELT2 (IT) calculation. Correspondence with the code analysts confirmed that this was the cause of the problem.

5. The AEROSIM-M (UK), RAFT (FN), TRAP-MELT2 (UK), and TRAP-MELT2.2 (BCL) calculations predicted an insignificant change in the airborne GSD as the aerosol was transported through the pipe. However, all other calculations [except for the TRAP-MELT2 (JN), HAA4 (RI), and TRAP-MELT2 (IT) calculations], predicted a drop in GSD as the aerosol passed from the pipe inlet to the first modeled-pipe-control volume and then little change in GSD as the aerosol was transported through the pipe. At present, we do not have an overall explanation for these observed differences in the calculate GSD profiles. The HAA4 (RI) and TRAP-MELT2 (JN) GSD profiles showed more change in calculated GSD from the first pipe section to the outlet section than the others. The fact that HAA4 does not model agglomeration probably accounts for the HAA4 results; the

slight difference between TRAP-MELT2 (JN) GSD results and those calculated by other TRAP-MELT2 versions cannot presently be explained.

4.3 TEST LA3C:

As was noted in Sect. 2, test LA3C was performed with a gas flow velocity of ~ 24 m/s, and it had an overall MnO/CsOH aerosol source mass ratio of ~ 1.4 . As for the other two tests and as was discussed in the LA3 test data report,² the test mass balance was good: 87.8% of the Cs and 85.6% of the Mn input to the test equipment was recovered.

From the results presented in Table 14, we find that (1) 19.8% of the CsOH, 22.2% of the MnO, and 21.2% of the total aerosol recovered was transported out of the pipe, (2) 34.8% of the CsOH, 45.8% of the MnO, and 41.1% of the total aerosol deposition in the pipe occurred in the pipe bends. The fraction of the total aerosol deposition due to bend deposition in LA3C was similar to that in LA3A, even though the gas velocity in LA3C was $\sim 30\%$ that in LA3A.

As for tests LA3A and LA3B, the overall deposition and transport results again suggest that a mixed, co-agglomerated aerosol flowed through the pipe, although for LA3C the amount of MnO bend deposition was significantly larger than that for CsOH. However, the measured deposit MnO/CsOH mass ratio results presented in Fig. 46 again show, as for test LA3B, that the LA3C aerosol may have not been fully coagglomerated. The LA3C results indicate enhancement of MnO aerosol deposition in the pipe bends, although this result was not as pronounced as observed in test LA3B.

Test LA3C data were unique compared to those from the other two tests in that a significant amount of aerosol deposition occurred in pipe section 4, a 2.26-m length vertical section (the first pipe section modeled). In that pipe section, 46.1% of the CsOH, 36.4% of the MnO, and 40.6% of the total aerosol deposition occurred. In comparison, in LA3A, 16.3% of the total aerosol deposition occurred in section 4, while in LA3B, 1.4% of the total aerosol deposition occurred in section 4. If

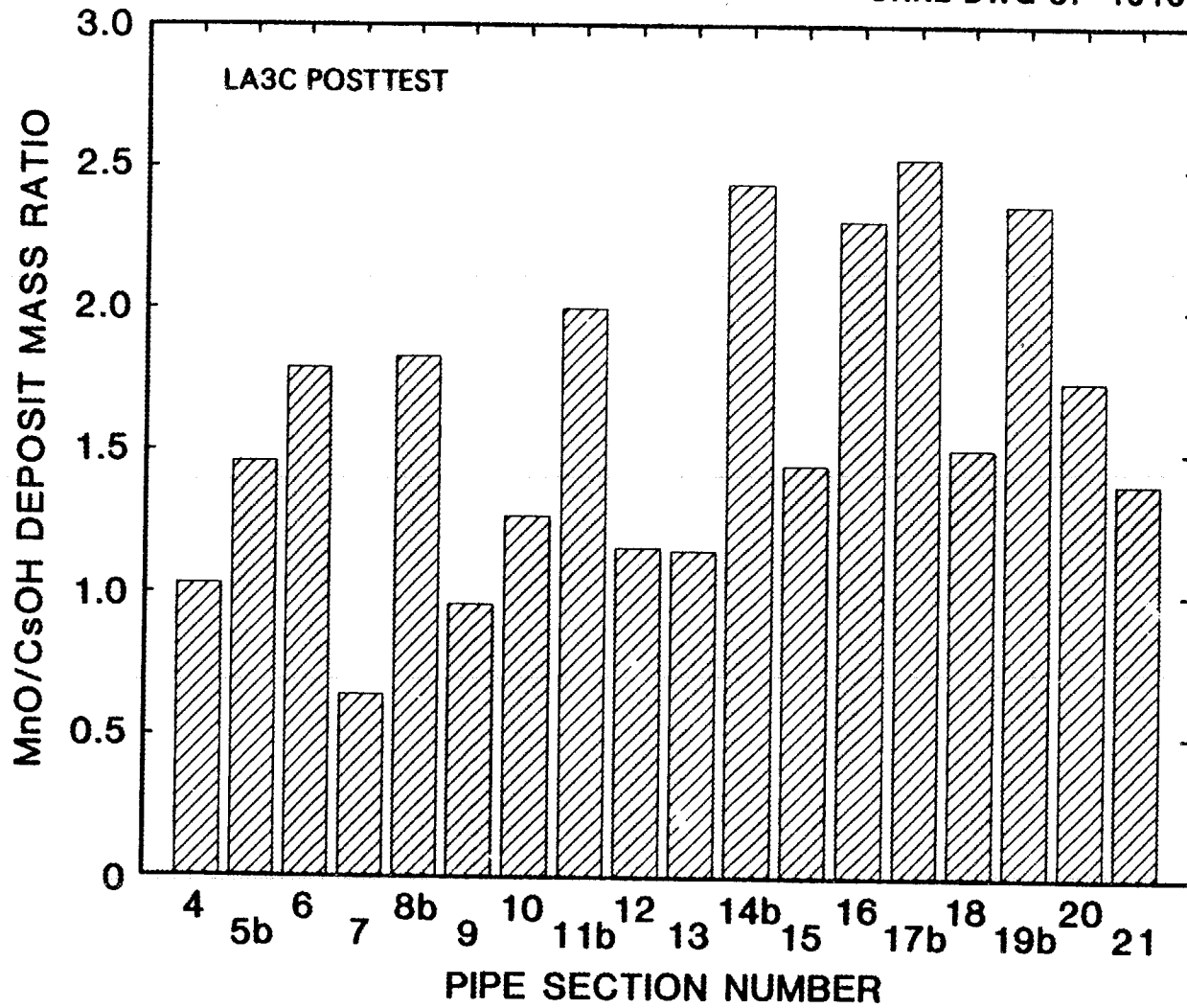


Fig. 46. Measured MnO/CsOH aerosol deposit mass ratio in each of the pipe sections for test LA3C.

we, in addition; combine the deposition that occurred in section 4 with that from the first pipe bend, we see that 62.4% of the CsOH, 59.3% of the MnO, and 62.5% of the total aerosol deposition occurred in the first two pipe sections in LA3C. One possible explanation for the higher deposition for LA3C in pipe section 4 is that the LA3C aerosol was "stickier" than that in tests LA3A and LA3B. Test LA3C had a higher proportion of CsOH aerosol than did the other two tests; the CsOH mass fraction in LA3C was greater than that in LA3A and LA3B by more than a factor of 3. It may be, then, that some of the aerosol that initially deposited in section 4 in LA3A and LA3B was resuspended and transported to downstream pipe sections.

The measured pipe-inlet and pipe-outlet aerosol size parameters for test LA3C are presented in Table 17 in Sect. 3. Interesting observations related to these results are as follows:

1. At all sampling times, the measured outlet AMMD values were less than measured at the pipe inlet. In comparing the LA3B and LA3C size results, we see that the change in aerosol size due to transport through the pipe for test LA3C was significantly greater than for test LA3B.
2. For the CsOH and MnO aerosol, the measured outlet GSD was less than the pipe-inlet value at each sampling time.

The results from the LA3C blind code comparisons were presented in Sect. 3 in Figs. 30 through 43 and Tables 22 and 23. For the most part, the way that all LA3C calculations were performed was similar to the way that LA3A and LA3B calculations were performed. The comparison results shown are for $t=3,600$ s, the end of the aerosol source period. Results from the MCT-2 (NYPA) calculation were extrapolated results from a calculation time of 570 s, and TRAP-MELT2 (JN) results were extrapolated from a calculational time of 3,000 s; all other codes calculated the full 3,600 s of the experiment.

The overall aerosol deposition comparison results, in terms of the cumulative amounts of aerosol deposited as a function of distance from the pipe inlet, are presented in Figs. 30 to 35. For each aerosol species, the codes including a bend deposition model were included on one

plot, and the codes without bend models were given on a separate plot. Bar charts illustrating comparisons of aerosol deposition in the pipe bends are given in Figs. 36 to 38. Comments on the data in these figures are listed below:

1. None of the LA3C calculations were able to predict the measured aerosol deposition in vertical pipe section 4. All of the codes underestimated the aerosol deposition in pipe section 4 by more than a factor of 8, some more than a factor of 20. Since the aerosol deposition in section 4 accounted for as much as 40% the total deposition in LA3C, this meant that none of the codes could adequately calculate the deposition pattern observed in LA3C.

We can only speculate at this time as to the reason for the high deposition in pipe section 4 in LA3C. Presently, we think that this was possibly the result of the higher CsOH aerosol-source fraction in LA3C. Since the LA3C aerosol would be expected to be "stickier" than that in LA3A and LA3B, there could have been less likelihood of aerosol resuspension or relocation from the surface of pipe section 4. Also, we should note that the upstream end of section 3 of the LA3C pipe was nearly plugged;² it is possible that this near-plugging had an influence on the flow patterns and resulting aerosol deposition patterns in pipe section 4.

2. The calculation that came the closest to predicting the total amount of aerosol deposition that occurred in LA3C was the TRAP-MELT2.2 (BCL) calculation. All of the other calculations predicted fairly similar amounts of total aerosol deposition. However, that result is somewhat deceiving, and the reason is illustrated in the bend deposition comparisons in Figs. 36 to 38. Although the TRAP-MELT2.2 (BCL) calculation underestimated the amount of aerosol deposition that occurred in the first pipe bend, it overestimated the deposition in the other bends by more than a factor of 2 in some cases. The overestimation

of the bend deposition in all but the first bend is largely responsible for TRAP-MELT2.2 predicting greater deposition than the other codes (more about this later).

3. If we again look at the results from the "TRAP-MELT-like" calculations where bend modeling was not included, we again see that the TRAP-MELT2 (UK) and TRAP-MELT2 (IT) deposition patterns were similar, and the TRAP-MELT2 (JN) and MCT-2 (NYPA) results were similar but not to the other TRAP-MELT2 results. For LA3B, the similarities and differences in these results can be explained solely by looking at the differences in calculated turbulent-inertial deposition velocities. These ranges were: (1) for TRAP-MELT2 (UK): 0.30 to 0.17 cm/s, (2) TRAP-MELT2 (IT): 0.32 to 0.18 cm/s, (3) TRAP-MELT2 (JN): 0.11 to 0.07 cm/s, and (4) MCT-2 (NYPA): 0.23 to 0.07 cm/s. As for the LA3B results, we cannot presently explain why the different TRAP-MELT calculations produced different results for calculated turbulent-inertial deposition velocities.

We find it interesting to note that, although LA3B and LA3C were performed with similar flow velocities, the ranges of deposition velocities mentioned above for the TRAP-MELT calculations were about a factor of 3 less than those calculated for test LA3B. We believe that this is purely due to the fact that the LA3B source aerosol was larger than that for test LA3C (Tables 16 and 17).

4. The comparisons of the calculated bend deposition by the different models for LA3C (Figs. 36 to 38) lead to conclusions similar to those reached in evaluating LA3B bend results. As was mentioned previously, the TRAP-MELT2.2 (BCL) calculation overestimated bend deposition for all but the first bend. All other calculations, as before, underpredicted deposition in all of the bends. For the LA3B results, the Stokes-impaction models in RAFT and HAA4 calculated more deposition than did the turbulence-enhanced model in AEROSIM-M.

For the first three bends, the TRAP-MELT2.2 bend model did the best job of predicting the bend results; however, for the last three pipe sections, the results in fact suggest that the Stokes-impaction models did the best job of modeling the LA3C results. However, all of these comparisons are influenced by the fact that none of the codes could predict the measured deposition in pipe section 4. If the TRAP-MELT2.2 (BCL) calculation had been able to predict the section 4 deposition, it is likely that it would also have done a much-improved job of predicting the overall bend deposition results. On the other hand, if the other bend codes had predicted the section 4 deposition, they would have predicted even less deposition in the pipe bends than they did (due to the decreased airborne aerosol concentration that would have been available for bend deposition).

Table 22 summarizes overall measured and calculated aerosol deposition results for LA3C. All codes had a more difficult time of predicting the overall deposition results for LA3C than for the other two tests. For CsOH deposition in LA3C, the TRAP-MELT2.2 (BCL) calculation underestimated deposition by a factor of 1.7, the TRAP-MELT2 (JN) calculation underestimated deposition by a factor of 8.4, and all other calculations underpredicted deposition by factors ranging from 3.6 to 5.7. For MnO deposition, the TRAP-MELT2.2 (BCL) calculation underpredicted deposition by a factor of 1.6, the TRAP-MELT2 (JN) calculation underpredicted deposition by a factor of 7.6, and all other calculations underestimated deposition by factors ranging from 3.3 to 5.5.

The overall deposition results for the TRAP-MELT2 (UK) calculation shown in Table 22 illustrate that, as in the LA3A and LA3B calculations, using a time-dependent or time-averaged aerosol source had no major influence on the calculated overall deposition; the differences in these results were less than 1%.

Calculated LA3C overall aerosol leakage results are illustrated in Fig. 39 and Table 23. As for LA3A and LA3B, all codes calculated more aerosol transport from the pipe than was measured in test LA3C. For CsOH

transport, TRAP-MELT2.2 (BCL) overpredicted leakage by a factor of 2.9, TRAP-MELT2 (JN) by a factor of 4.6, and all other calculations overestimated CsOH transport by factors ranging from 4.0 to 4.5. For MnO transport, the TRAP-MELT2.2 (BCL) calculation overestimated leakage by a factor of 2.6, the TRAP-MELT2 (JN) calculation by 4.1, and all other calculations overpredicted MnO transport by factors ranging from 3.6 to 4.0. The agreement in leaked-mass calculations was worse for LA3C than for LA3B, even though these two tests were performed under the same flow conditions. We believe the larger uncertainty in LA3C leaked-mass results is largely due to the inability of the codes to predict the high amount of deposition that occurred in pipe section 4.

Calculated aerosol size-distribution parameters for test LA3C are illustrated in Figs. 40 to 43. All results in the figures, except the ones from the TRAP-MELT2 (IT) calculations, were based on calculations performed with mean aerosol-source size parameters. For LA3C, we recall from Table 17 that measured mean inlet- and outlet- aerosol size parameters were: $AMMD_{in} = 1.90 \mu m$, $AMMD_{out} = 0.64 \mu m$, $GSD_{in} = 2.13$, and $GSD_{out} = 1.77$. Comments on the aerosol size results include the following:

1. The major LA3C aerosol-size comparison result is that none of the codes was able to predict the large drop in outlet AMMD compared to the measured inlet AMMD value. The lowest outlet AMMD value predicted by the codes was about $1.4 \mu m$; this is more than a factor of 2 greater than the measured mean outlet AMMD value of $0.64 \mu m$. We believe, however, that this difference in calculated and measured outlet size was largely due to the fact that none of the codes was capable of calculating the LA3C aerosol deposition pattern correctly, particularly the large deposition in pipe section 4.
2. As for the LA3B calculations, there were significant differences in the AMMD profiles calculated by different versions of the TRAP-MELT code and by the other codes (RAFT, AEROSIM-M, and HAA4). These differences were larger for LA3C than for LA3B. We believe that these differences were again due to the fact that the TRAP-MELT code incorrectly calculates the AMMD.

3. As for the LA3B calculations, there were differences in the RAFT, AEROSIM-M, and HAA4 AMMD results. However, for LA3C the RAFT and AEROSIM-M results were similar to each other but different from the HAA4 results. This suggests that the observed LA3C differences may be largely due to the fact that the HAA4 (RI) calculation does not include aerosol agglomeration effects.
4. There were large differences in the pipe-outlet GSD values predicted by the various codes. These ranged from an upper value of 2.18 (by AEROSIM-M (UK)) to a lower value of 1.78 (by TRAP-MELT2 (JN)). This variation was partially the result of the fact that the GSD values predicted by the AEROSIM-M (UK) calculation for the first pipe section was slightly greater than the mean mixed aerosol-source value provided in the calculations.

We believe that the AEROSIM-M (UK) GSD profile results occurred because of the way aerosol sources are input to the AEROSIM-M (UK) calculation. AEROSIM-M uses source GSD values for each of the aerosol species, rather than for the mixed aerosol; these mean values for LA3C calculations were (Table 17) 1.95 for the C₅H₈ aerosol and 2.30 for the MnO aerosol. Combination of these two size distributions, we believe, produced a distribution with a mixed GSD source value slightly greater than 2.3.

5. The TRAP-MELT2 (JN) calculation predicted a large drop in GSD - from 1.94 to 1.70 - as the aerosol was transported from pipe section 4 to sections 5 to 8, and then only a slight change in GSD for the remainder of transport through the pipe. This behavior was not predicted by the other TRAP-MELT codes and cannot presently be explained.

5. SUMMARY AND CONCLUSIONS

A series of blind posttest calculations were performed to model the aerosol deposition and transport results from the LACE LA3 test series. The main test parameters for the LA3 experiments were the gas flow velocity through the 0.063-m-diam, 28.8-m-long test pipe, and the MnO/CsOH aerosol mass ratio input to the test pipe; approximate values of these parameters for the LA3 tests were:²

<u>Experiment</u>	<u>v(m/s)</u>	<u>MnO/CsOH mass ratio</u>
LA3A	77	5.0
LA3B	25	7.5
LA3C	24	1.4

Section 3 of this report presented the experimental and calculated results from the LA3A, LA3B, and LA3C experiments, and Sect. 4 of this report presented a discussion of the comparison results for these tests.

Before summarizing the overall code-comparison results, it is useful to summarize a number of the major experimental results from the LA3 test series:

1. Aerosol deposition in the LA3 test section pipe bends was a major mechanism for deposition in these experiments. Bend deposition accounted for the following fractions of deposition in the experiments:

LA3A: 44.7% of the total deposition

LA3B: 91.2% of the total deposition

LA3C: 41.1% of the total deposition

Two comments on the above bend results are of note: (1) the fraction of total deposition in bends was similar for tests LA3A and LA3C, even though these two experiments were performed with significantly different gas flow velocities, and (2) the fraction of total aerosol deposition in bends for tests LA3B and LA3C differed significantly, even though these two tests were performed with similar gas flow velocities. Variations in aerosol source particle sizes probably account for some of these observed differences, but they are probably also

associated with differences in the aerosol source MnO/CsOH mass ratio and the "stickiness" of the aerosol in each test. Another important comment relates to comparison of these results with those from test LA1. Looking at the bend deposition results from that test,²⁰ we see that only 8% of the total aerosol deposition occurred in the 6 pipe bends in the LA1 test section. However, this result may have occurred either because bend deposition was not important in LA1, or because resuspension removed a significant fraction of aerosols deposited in bends in LA1.

2. The deposition results from test LA3C were unique in that a significant amount of aerosol deposition occurred in the first pipe section (section 4, a vertical pipe section). In LA3C, deposition in pipe section 4 accounted for 40.6% of the total aerosol deposition; this compares to 16.2% deposition in section 4 for test LA3A and 1.4% in section 4 for test LA3B.

Unless this result was due to other factors in the LA3C test that were different from those in LA3A and LA3B (for example, the near plugging of pipe section 3 in LA3C), it suggests that the low MnO/CsOH aerosol source ratio in LA3C led to enhanced sticking of the deposited aerosol on the section 4 surface.

3. The overall aerosol transport results from the LA3 test series can be summarized as follows:

LA3A: 23.0% total aerosol transport

LA3B: 49.3% total aerosol transport

LA3C: 21.2% total aerosol transport

The enhanced transport in LA3B compared to LA3A would be expected, since turbulent-inertial deposition is less effective for reduced gas flow velocities. The decreased transport for LA3C compared to LA3B probably resulted from the significant aerosol deposition in pipe section 4 for test LA3C.

4. Test results provide conflicting evidence as to whether the MnO-CsOH aerosol in the LA3 tests was totally coagglomerated. The overall deposition and transport results for each test seem

to suggest that the MnO-CsOH aerosol was coagglomerated. However, test LA3B aerosol deposit ratio results (Fig. 45) showed reduced MnO deposition in straight pipe sections, while LA3A and LA3C deposit ratio results (Figs. 44 and 46, respectively) showed significant variations in deposit ratios in different pipe sections. Information in a recently published AEE Winfrith Report,²¹ based on analyses of aerosol samples collected from the LA3 tests, indicated that aerosol deposits from test LA3A and LA3B were "relatively homogeneous and amorphous," while there were greater inhomogeneities in samples from LA3C. Putting all of this information together does not lead to any firm conclusions on the degree of aerosol coagglomeration in the LA3 tests.

5. Evaluations of measured pipe inlet- and outlet- aerosol size distribution parameters produced some interesting results, most notably a measured increase in MnO AMMD and mixed-aerosol GSD for aerosol transport through the pipe in test LA3A. We would not expect the aerosol transport codes, with the present models in them, to predict these results.
6. A number of the results from the LA3 test series suggest that aerosol resuspension or relocation was an important factor in the experiments. These include: (1) the varied MnO-CsOH deposit ratio results in LA3B and LA3C, (2) the measured aerosol size results discussed above, (3) as discussed in Sect. 4.2, the low amounts of aerosol deposition in straight pipe sections in test LA3B, and (4) the large difference in aerosol deposition in pipe section 4 for tests LA3B and LA3C, which may have been due to the "stickier" nature of the LA3C aerosol.

Eight calculations were performed for each of the LA3 tests. Three of these calculations used versions of the TRAP-MELT2 code, one used the MCT-2 code (which uses TRAP-MELT2 as a module), and the other calculations were performed with the TRAP-MELT2.2, AEROSIM-M, HAA4, and RAFT codes. In these codes, six different models for turbulent-inertial deposition were used. Four of the codes - AEROSIM-M, HAA4, RAFT, and TRAP-MELT2.2 - included models for aerosol deposition in pipe bends. The HAA4 code was

the only log-normal code used in the study; the other codes used were discrete size-distribution codes.

An important conclusion from the LA3 comparisons is that, to adequately predict the deposition patterns that were observed in the tests, modeling of aerosol deposition in pipe bends was required. Codes that did not include a bend model always underpredicted the measured aerosol deposition. Even when bend models were included, in only two cases - calculations performed with the TRAP-MELT2.2 (BCL) code for tests LA3A and LA3B, and calculations performed with AEROSIM-M (UK) for test LA3A - did the results of calculations come close to matching the experimentally measured deposition patterns.

The results from the LA3 code comparisons indicate that the bend model used in the TRAP-MELT2.2 (BCL) calculations came the closest to matching the measured bend deposition results. The overall comparison results with the TRAP-MELT2.2 bend model were quite encouraging. This model: (1) underpredicted bend deposition in the first two bends and overpredicted bend deposition in the last four bends for LA3A, (2) did a good job of predicting the LA3B bend deposition, and (3) underpredicted bend deposition in the first bend and overpredicted bend deposition (sometimes significantly) in the remaining bends in test LA3C (however, we believe that this occurred because the code significantly underestimated aerosol deposition in pipe section 4 in LA3C). All of the other bend models, for the most part, significantly underpredicted the measured bend deposition in the LA3 tests. For these three models, the AEROSIM-M (UK) did a better job of predicting the LA3A results, but the RAFT (FN) and HAA4 (RI) models more satisfactorily predicted the LA3B and LA3C results.

Because of the competing effects that were important in the LA3 tests - turbulent-inertial deposition, deposition in bends, and perhaps aerosol resuspension from surfaces being the dominant ones - it is difficult to use the test results to make any definitive statements related to the validation of the turbulent-inertial deposition models used in the codes. The only summary statements that we can presently make in regards to the turbulent-inertial deposition models are (1) as was discussed in Sect. 4.1, if we ignore the contribution of bend

deposition to total deposition in LA3A, we note that most of the turbulent deposition models seemed to do a reasonable job of calculating the LA3A deposition pattern, and (2) none of the turbulent deposition models adequately calculated aerosol deposition in pipe section 4 in test LA3C.

For the LA3 calculations, two sets of TRAP-MELT2 (UK) calculations were performed for each test: one with time-dependent aerosol source parameters and one with time-independent parameters. An interesting result from this study is that these results, in terms of calculated total aerosol deposition, were essentially the same: variations in the two calculations were never greater than 4%. This suggests (but we do not necessarily believe in all cases) that there is no advantage to using the time-dependent source parameters to model the LA3 tests.

One measure by which the overall ability of the codes to calculate deposition and transport for the LA3 tests can be characterized is the ratio of measured-to-calculated total aerosol deposition and calculated-to-measured total aerosol transport for each of the codes applied to the LA3 tests. The ranges of these calculated ratios were presented in Sect. 4, and are summarized again in Tables 25 and 26 for the CsOH and MnO aerosol species. With only one exception (MnO deposition in test LA3B), all codes underpredicted total aerosol deposition and overpredicted total aerosol transport in the LA3 test series. The codes predictions of overall deposition in LA3A and LA3B were similar, while code predictions of LA3C were in error by the largest amount (up to a factor of 8). In terms of aerosol leakage, predictions of overall results for LA3A and LA3C were similar (because these tests had similar amounts of fractional leaked mass), and the predictions of leaked mass for LA3B were the most satisfactory (since LA3B had the most leaked mass, and all codes overpredicted leaked mass). Overall, the LA3 test series leaked-mass results illustrate that all codes were able to calculate total leaked mass from the tests within a factor of 4.6.

However, had the codes included models for resuspension they might actually have done a worse job of calculating the deposition and transport results from the LA3 tests. That is because (1) none of the codes

Table 25. Summary of overall aerosol deposition results for the LA3 test series

Aerosol material	Total aerosol deposition test/code values: ^a		
	Low	High	Remaining range ^b
	<u>Test LA3A:</u>		
CsOH	1.15	3.8	1.3 to 2.0
MnO	1.12	3.4	1.5 to 1.8
	<u>Test LA3B:</u>		
CsOH	1.01	3.2	1.7 to 3.2
MnO	0.95	3.0	1.5 to 2.9
	<u>Test LA3C:</u>		
CsOH	1.7	8.4	3.6 to 5.7
MnO	1.6	7.6	3.3 to 5.5

^a"Test/code" defined as the ratio of the measured total aerosol deposition for a test divided by the total aerosol deposition calculated by a code.

^b"Remaining range" is the range of test/code values for codes other than those that calculated the low and high values.

Table 26. Summary of overall aerosol transport results for the LA3 test series

Aerosol material	Total aerosol transport code/test values: ^a		
	Low	High	Remaining range ^b
	<u>Test LA3A:</u>		
CsOH	1.9	4.4	2.3 to 3.0
MnO	1.7	3.3	2.1 to 2.4
	<u>Test LA3B:</u>		
CsOH	1.2	2.0	1.7 to 1.9
MnO	1.07	1.7	1.5 to 1.7
	<u>Test LA3C:</u>		
CsOH	2.9	4.6	4.0 to 4.5
MnO	2.6	4.1	3.6 to 4.0

^a"Code/test" defined as the ratio of the total aerosol transport from the pipe calculated by a code divided by the measured total aerosol transport from the pipe for that test.

^b"Remaining range" is the range of code/test values for codes other than those that calculated the low and high values.

overpredicted LA3 deposition, (2) if resuspension was modeled and the resuspended particle sizes were less than those originally deposited, then codes with resuspension models would predict even less deposition than when resuspension was not accounted for. This at least suggests that the possibility that the turbulent deposition models are not as valid (within a factor of 2?) as we might believe them to be.

We believe that only qualitative comparisons of the measured and calculated aerosol size parameters from the LA3 tests can be made, for two reasons: (1) most codes used only mean values of aerosol source parameters in their calculations, (2) the aerosol deposition patterns in the experiments, in particular the bend deposition, had a major influence on the calculated aerosol size distributions. The more important observations related to the AMMD and GSD comparisons for the LA3 tests include the following:

1. In all calculations but one, the codes predicted that the airborne mixed-aerosol AMMD and GSD decreased as the aerosol was transported through the test pipe; that is the result we would expect from the calculations. However, in test LA3A the measured mean pipe-outlet GSD was greater than that determined at the pipe inlet. This result suggests that a mechanism not included in the codes (perhaps resuspension) led to the observed change in size distribution.
2. For each of the tests, there were observed differences in the AMMD profiles calculated by the codes. We believe that these can largely be attributed to the following causes: (1) differences in the amounts of deposition calculated by the codes, (2) errors in the coding used to calculate the AMMD in the TRAP-MELT code.¹⁴
3. For LA3A and LA3B, most codes did a reasonable job of predicting the measured mean values of AMMD and GSD at the pipe outlet. However, for test LA3C, all codes overestimated the outlet AMMD by more than a factor of 2. We believe this was due to the uncertainties in predicting the LA3C aerosol deposition.

Our major overall conclusions from the LA3 posttest blind code-comparison study are:

1. Accident analysis codes should include models for aerosol deposition in bends. Although the codes used in this study that did not include bend models sometimes calculated the observed aerosol deposition within factors of 2 to 3, including valid bend deposition models will greatly enhance the predictive capabilities of the codes.
2. The LA3 test series illustrates that the nature (or perhaps "stickiness") of the airborne aerosol influences the behavior of the aerosol transport through the pipe. None of the aerosol transport codes include models for this phenomena.

6. ACKNOWLEDGMENTS

We would like to thank the code analysts who participated in this study for their efforts and cooperation. We would also like to thank the HEDL staff, and in particular Dean Dickinson, for their cooperation in providing us with the experimental data from the LA3 test series.

7. REFERENCES

1. D. R. Dickinson, Test Plan, LWR Aerosol Containment Experiment (LACE) Test LA3, Containment Bypass Conditions, Westinghouse Hanford Company, March 17, 1986.
2. D. R. Dickinson, et al., Aerosol Behavior in LWR Containment Bypass Piping--Results of LACE Test LA3, Westinghouse Hanford Company, LACE TR-011 (to be published).
3. A. L. Wright, "Instructions for LA3 Blind Posttest Aerosol Calculations," letter to LACE program participants, Oak Ridge National Laboratory, January 16, 1987.
4. A. L. Wright, "Corrections to Aerosol Source Rate Data for LA3 Blind Posttest Calculations," letter to LACE program participants, Oak Ridge National Laboratory, March 3, 1987.
5. B. Y. H. Liu and J. K. Agarwal, "Experimental Observation of Aerosol Deposition in Turbulent Flow," J. Aerosol Sci. 5, 145-155 (1974).

6. M. P. Kissane, "Using a Containment Aerosol Code in a 'Lagrangian Mode' to Model Aerosol Processes in Pipe Flows," presented at the Workshop on Water Cooled Reactor Code Evaluation and Uncertainty Assessment, Brussels, Belgium, Sept. 9-11, 1987 (proceedings to be published).
7. J. M. Otter and E. U. Vaughan, HAA4 Code Description and User Manual, AI-DOE-13528, December 1986.
8. S. K. Friedlander and H. F. Johnstone, "Deposition of Suspended Particles From Turbulent Gas Streams," Ind. Eng. Chem. 49, 1151-1156 (1957).
9. J. A. Gieseke, K. W. Lee, and M. A. Goldenberg, Measurement of Aerosol Deposition Rates in Turbulent Flows, NUREG/CR-1264, BMI-2041, Battelle-Columbus Laboratories, January 1980.
10. K. H. Im and P. M. Chung, "Particulate Deposition from Turbulent Parallel Streams," AIChE Journal 29, No. 3, 498-505 (1983).
11. K. H. Im, R. K. Ahluwalia, and H. C. Lin, "Formation and Transport of Fission Product and Structural Material Aerosols in the Primary Systems of Light Water Reactors Undergoing Hypothetical Severely Degraded Core Accidents," Argonne National Laboratory (to be published).
12. N. B. Wood, "A Simple Method for the Calculation of Turbulent Deposition to Smooth and Rough Surfaces," J. Aerosol Sci. 3, 275-290 (1981).
13. M. R. Kuhlman, V. Kogan, and P. M. Schumacher, TRAP-MELT2 Code: Development and Improvement of Transport Modeling, NUREG/CR-4677, BMI-2141, Battelle-Columbus Laboratories, July 1986.
14. A. L. Wright and P. C. Arwood, Summary of Pretest Aerosol Code Comparisons for LWR Aerosol Containment Experiment (LACE) LA3, LACE TR-023, ORNL/M-352, Oak Ridge National Laboratory, December 1987.
15. P. K. Swamee and A. K. Jain, "Explicit Solutions for Pipe Flow Problems," ASCE, J. of Hydraulics Div. 102, No. HY5 (May 1976).
16. C. M. White, "Fluid Friction and Its Relation to Heat Transfer," Inst. Chem. Eng. 10, 66 (1932).
17. C. F. Colebrook, "Turbulent Flow in Pipes with Particular Reference to the Transition Region Between the Smooth and Rough Pipe Laws," J. Inst. Civil Eng. 12, No. 4, 133-156 (1939).

18. R. I. Crane and R. L. Evans, "Inertial Deposition of Particles in a Bent Pipe," J. Aerosol Sci. 8, 161-170 (1977).
19. Personal communication, D. K. Williams, United Kingdom Atomic Energy Authority, May 1987.
20. A. L. Wright, P. C. Arwood, and J. H. Wilson, Summary of Posttest Aerosol Code Comparisons for LWR Aerosol Containment Experiment (LACE) LA1, LACE TR-022, ORNL/M-365, Oak Ridge National Laboratory, December 1987.
21. B. R. Bowsher, G. R. Brown, A. L. Nichols, Analysis of Samples from Tests LA3A, B, and C of the LACE Project, United Kingdom Atomic Energy Authority, Winfrith, AEEW-M 2409 (December 1986).

APPENDIX A
THE MODIFICATION OF THE TRAP-MELT MASS
MEDIAN DIAMETER CALCULATION

N. M. CHOWN
AEE Winfrith

1. INTRODUCTION

The TRAP-MELT2 computer code¹ was designed to model the transport of aerosols and fission products through the primary circuit of a LWR under severe accident conditions. In a recent code comparison² between TRAP-MELT2 and VICTORIA³ it was found that TRAP-MELT2 consistently underpredicted the value of the aerosol mass median diameter.

This note outlines the reason for the underprediction and also the correction which has been made to improve the accuracy of the calculated value of the mass median diameter.

2. TREATMENT OF AEROSOLS IN TRAP-MELT2

The discretization of the aerosol particle size distribution in TRAP-MELT2 is taken from the QUICK aerosol code.⁴ The aerosol size distribution is discretised into a number of classes, and the volume per particle (and thus, the radius) of these classes is fixed throughout a calculation. Any particles falling between these discrete values of radii, known as the representative particle class radii, are distributed between the adjacent in such a way as to preserve particle mass and number, where possible. Calculation of the mass median diameter of the discretised size distribution may only be achieved by interpolation between the size classes.

3. THE EXISTING SCHEME

At present, TRAP-MELT2 calculates the mass median diameter of a size distribution as follows. The aerosol mass in the particle classes are summed, starting with the class containing the smallest particles, and the first particle class which results in a cumulative mass greater than half the total aerosol mass is determined. Defining the representative volume per particle of this class to be $X(I)$, the cumulative aerosol mass up to, and including this class to be $CM(I)$, and M_{50} to be equal to half the total aerosol mass, then the mass median diameter (MMD) is given by:

$$MMD = 2\left(\frac{3}{4\pi} XMM\right)^{1/3}$$

where

$$XMM = X(I-1) + [X(I)-X(I-1)] \frac{M_{50} - CM(I-1)}{CM(I) - CM(I-1)}$$

TRAP-MELT3 calculates mass median diameter in a similar way. Rather than interpolating between the representative volume per particle of the classes these values are converted to radii. The interpolation is then performed between these representative class radii. Thus, if

$$R(I) = \left[\frac{3}{4\pi} X(I) \right]^{1/3}$$

then,

$$MMD = 2 \cdot RMM$$

where

$$RMM = R(I-1) + [R(I)-R(I-1)] \frac{M_{50} - CM(I-1)}{CM(I) - CM(I-1)}$$

The most important point to note from these equations is that the interpolation is carried out between the representative values of volume per particle of the classes or the representative radii of the particles classes.

4. THE NEED FOR REVISION

The inadequacy of the TRAP-MELT2 method for calculating the mass median diameter of a particle size distribution is clearly demonstrated in Figure A.1, where the approximate value of the mass median diameter is marked as point A. This should be compared to the value given by the existing TRAP-MELT2 calculation, point B. Since the current TRAP-MELT schemes interpolate between either X(J-1) and X(J) or R(J-1) and R(J) it is not possible to obtain the correct value.

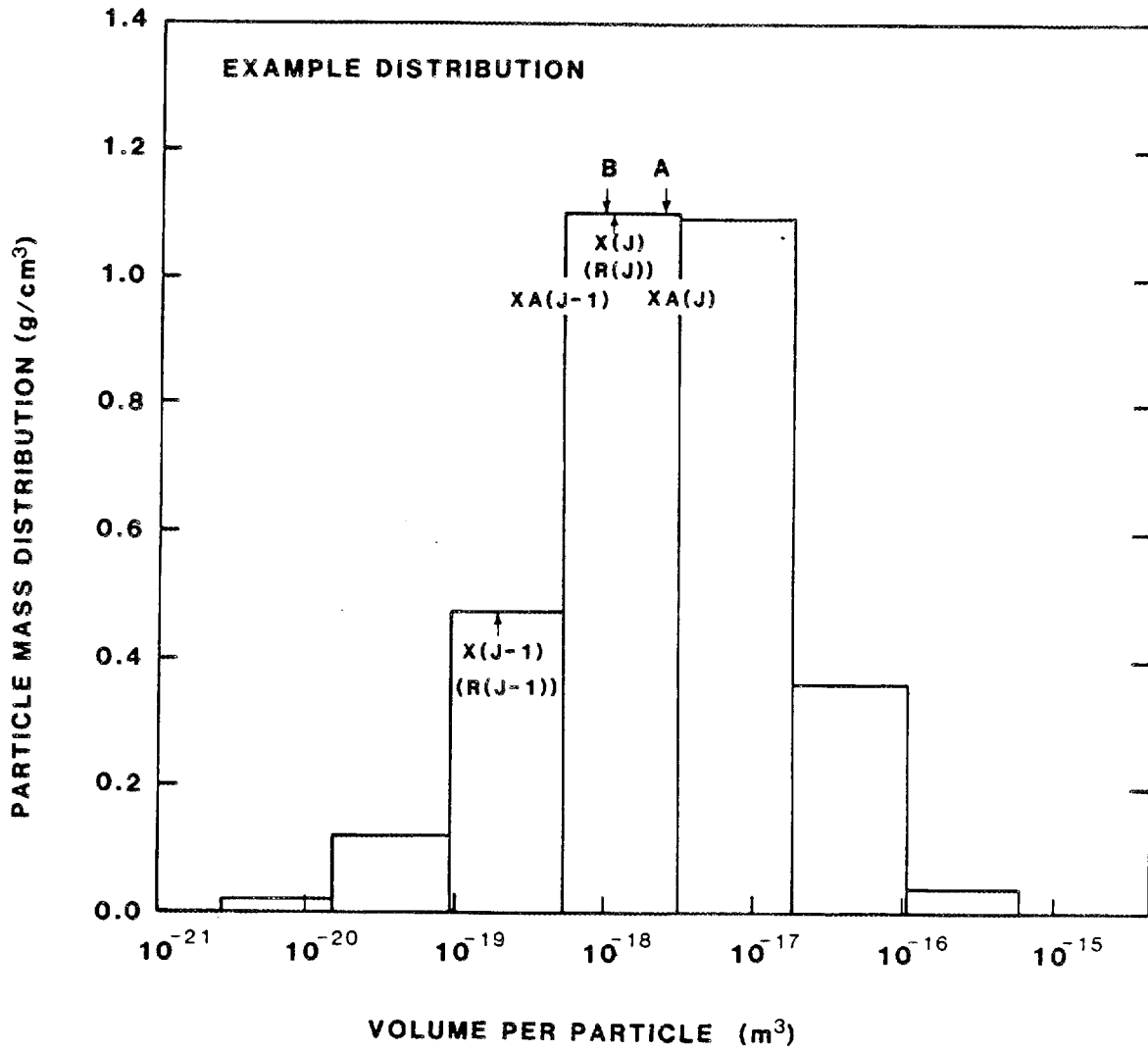


Fig. A.1. Mass distribution.

5. THE REVISED SCHEME

The revised method makes use of the values calculated in TRAP-MELT for the maximum radius of each individual particle class. These values are indicated by the width of the histogram blocks in Figure A.1, and the representative particle class radii are the geometric mean of these values. The revised calculation of mass median diameter assumes that the cumulative mass is the mass below the maximum volume per particle of the class, $XA(I)$, and not below the representative volume per particle of the class $X(I)$. The interpolation is therefore carried out between the maxima of adjacent particle classes. The mass median diameter is calculated by

$$MMD = 2 \left[\frac{3}{4\pi} XMM \right]^{1/3}$$

where

$$XMM = XA(I-1) + [XA(I) - XA(I-1)] \frac{M_{50} - CM(I-1)}{CM(I) - CM(I-1)}$$

In Fig. A.1 this means the interpolation is performed between $XA(J-1)$ and $XA(J)$, producing a value for mass median diameter at point A, the approximate value expected by observation.

This correction can also be implemented after a calculation has been performed. The representative particle class radii are the geometric mean of the adjacent maximum particle class radii and remain fixed throughout a calculation. Therefore, multiplying the value of mass median diameter, calculated by the existing method, by the factor shown below simulates the interpolation between maximum class radii rather than between the representative class radii. This factor, K , is the sixth root of the fractional change in maximum or representative volume per particle of the classes. That is

$$K = \left[\frac{XA(I+1)}{XA(I)} \right]^{1/6} = \left[\frac{X(I+1)}{X(I)} \right]^{1/6}$$

6. CONCLUSIONS

The calculation of mass median diameter in TRAP-MELT2 has been modified. The same interpolation method is used, but it is performed between the maximum volume per particle of the classes rather than the representative volume per particle of the classes. This arises from the assumption that the particles in a given class are spread over the whole width of the class and not concentrated solely at the representative particle class radius. The same value can be obtained after a calculation has been performed using the existing method by multiplying the calculated mass median diameter by a factor K, shown above.

REFERENCES

1. Jordan, M., Gieseke, J. A., Baybutt, P., TRAP-MELT Users' Manual, NUREG/CR-0632 (February 1979).
2. Johns, N. A., A Comparison of TRAP-MELT and VICTORIA, PWP/SAMAS/P(88)67, (December 1987):
3. Camp, W. J., Nucl. Sci. and Technol. 5, No. 6, (1984).
4. Jordan, H., Schumacher, P. M., Gieseke, J. A., Quick Users' Manual, NUREG/CR-2105 (May 1981).

DISTRIBUTION

- 1-3. P. C. Arwood
4. R. K. Genung
5. J. R. Hightower, Jr.
6. E. K. Johnson
7. T. S. Kress
8. A. P. Malinauskas
9. J. R. Merriman
10. F. M. Scheitlin
11. M. G. Stewart
12. J. H. Wilson
- 13-15. A. L. Wright
- 16-17. Office of Scientific and Technical Information Center,
Department of Energy, P.O. Box 62, Oak Ridge, TN 37831
18. Office of Assistant Manager, Energy Research and Development,
Oak Ridge Operations Office, Oak Ridge, TN 37831
19. Laboratory Records Department
20. Laboratory Records - RC
21. ORNL Patent Section
22. Central Research Library
23. Document Reference Section